UNIVERSIDADE DE LISBOA

FACULDADE DE CIÊNCIAS

DEPARTAMENTO DE FÍSICA

Ultrasound Assisted Oncolytic Virotherapy - *In Vitro* and *In Vivo* Studies

Nádia Andreia Pacheco Vilhena

Orientadores

Professor Gail Ter Haar

Prof. Dra. Raquel Cruz da Conceição

Mestrado Integrado em Engenharia Biomédica e Biofísica
Perfil em Radiações em Diagnóstico e Terapia

DISSERTAÇÃO

2015

Resumo

A ‘sonoporação’ é um processo através do qual a permeabilidade de membranas celulares é modificada. Esta alteração na membrana leva à formação de poros através dos quais pequenas moléculas conseguem passar. Nas últimas decadas, investigação na área de viroterapia mediada por ultrassons focalizados, na presença de agentes de contraste, designados por ‘micro bolhas’, provou que este tratamento poderia ser uma boa alternativa para o tratamento de tumores. As terapias em estudo incluem estratégias tais como o recurso a vírus oncolíticos que têm afinidade para tecidos inflamados e que por activação do sistema imunitário causam a sua destruição – estes vírus são conhecidos em viroterapia como ‘vírus suicidas’.

Aplicações com vírus oncolíticos encontram no processo de sonoporação uma forma de aumentar/facilitar a entrada de conteúdo viral para o interior das células cancerígenas mas existem ainda muitos problemas a ultrapassar em termos de eficiência e segurança para que estes tratamentos possam ser utilizados em meio clínico. A toxicidade da ‘terapia viral’ é um dos maiores problemas associados e com o intuito de minimizar este problema, foi desenvolvida uma nova técnica designada por ‘Isolated Limb Perfusion’ (ILP). Esta técnica tem por base o isolamento de vasos sanguíneos que irrigam a região do tumor, normalmente aplicada nos membros superiores ou inferiores, isolando o membro da circulação sistémica através de um torniquete. A técnica ILP vai ser usada neste projecto em ratos da linhagem Brown Norwegian, nos quais serão implantadas células cancerígenas (linha de células de fibrosarcoma BN175) nos membros inferiores.

Um fibrosarcoma/sarcoma é um tumor maligno dos tecidos moles que normalmente se desenvolve nos membros inferiores. Os tratamentos para este tipo de cancro incluem uma cirurgia extremamente invasiva com possibilidade de remoção do

membro para garantir a sobrevivência do doente e que é normalmente combinada com radioterapia.

Posto isto, é muito importante que se promova a investigação neste tipo de terapias de forma a tornar os tratamentos menos invasivos. Com este objectivo, este projecto é um estudo piloto com fundamento num estudo de Pencavel *et al.*, com o título "Isolated limb perfusion with melphalan, tumour necrosis factor-alpha and oncolytic vaccinia virus improves tumour targeting and prolongs survival in a rat model of advanced extremity sarcoma", publicado em 2015 em International Journal of Cancer. Assim, o propósito deste estudo é adicionar 'ultrassons focalizados' a esta terapia combinada para verificar se i) há um aumento da entrada e replicação do vírus de forma a aumentar a eficiência do tratamento e ii) se existe a possibilidade de evitar o uso de um factor de necrose tumoral (TNF-α) para reduzir a toxicidade do tratamento. Este factor, pretence a um grupo de citocinas capaz de provocar a morte de células tumorais e que possuem uma vasta gama de acções pró-inflamatórias sendo altamente tóxico quando em circulação sistémica.

A distribuição de vírus mediada por ultrassons oferece uma oportunidade para a realização de terapia direccionada não-invasiva em órgãos internos específicos. Para isto, a sonoporação envolve o uso de micro bolhas que são injectadas na corrente sanguínea em conjunto com os restantes agentes químicos e os vírus. Quando estas micro bolhas são expostas aos feixes de ultrassons focalizados, a uma dada frequência, estas expandem-se e contraem com rapidez. Se as micro bolhas estiverem próximas de uma membrana celular, a sua deformação ou fragmentação física aumenta a porosidade da membrana celular. O mecanismo exacto envolvido ainda não é completamente compreendido, mas é associado a cavitação acústica que pode ser estável ou instável. A cavitação estável ocorre quando as bolhas oscilam por sucessivas compressões e descompressões mas permanecem intactas. Por outro lado, a cavitação instável ocorre quando são usadas amplitudes de alta pressão, conduzindo ao colapso das bolhas.

Os principais objectivos deste projecto piloto são estudar a distribuição do vírus nos tumores e quantificar o número de particulas virais com capacidade de se replicarem. Isto é conseguido através de ensaios químicos como qPCR (quantitative real-time Polymerase Chain Reaction), Plaque Assay (para quantificar a presença de vírus) e Imunofluorescência. Este processo vai incluir experiências *in vitro* com a linha de células BN175, inicialmente para testar o efeito da utilização de (i) ultrassons focalizados (ii) micro bolhas e (iii) ultrassons focalizados e micro bolhas.

As experiências *in vitro* vão incluir o estudo do efeito de diferentes parâmetros físicos tais como: o valor de pressão *in situ* causado pela propagação da onda de som; a quantidade de tempo em que os ultrassons são emitidos durante um determinado tempo de exposição (Duty Cycle); a frequência de repetição do pulso de ultrassom; o tempo de exposição e a concentração de micro bolhas na solução a ser testada. O objectivo da variação destes parâmetros, que é feita com base na literatura, tem como objectivo promover a cavitação instável e ao mesmo tempo evitar que isto cause a morte das células cancerígenas para garantir que os vírus poderão vir a atravessar a membrana de células viáveis. A partir dos resultados encontrados através das experiências *in vitro*, serão escolhidos os melhores parâmetros a utilizar *in vivo* para determinar se uma terapia que combina ultrassons focalizados, Melphalan, TNF-α e Vírus da Varíola (geneticamente modicado para uma 'versão' menos infecciosa) será uma potencial forma de tratamento/cura de tumores, de forma menos invasiva.

Para realizar as experiências *in vitro*, foi realizada uma calibração dos equipamentos a utilizar, nomeadamente dos transdutores, para garantir que todos os 'outputs' são conhecidos (com uma incerteza de 10% associada). Além disto, foi realizado um estudo para perceber quais são os valores de pressão que favorecem a cavitação inercial para poder associar os resultados à presença ou ausência de cavitação inercial, de acordo com os parâmetros utilizados. Os testes *in vitro* mostraram que valores de pressão superiores a 0.9 MPa, para valores fixos de frequência de repetição do pulso de 100 Hz, um feixe com 40 ciclos e uma exposição de 0.5 s, reduzem a viabilidade das células em cerca de 80%. A variação dos restantes parâmetros parece não ter muita influência a nível da viabilidade celular. Os resultados *in vivo* não permitem concluir acerca do aumento da eficiência do tratamento pois os níveis de pressão *in situ* utilizados parecem ser nocivos ou para as partículas virais ou para as células – mais experiências serão necessárias para tirar conclusões *in vivo*.

Palavras-Chave: Sonoporação, Viroterapia, Vírus Oncolíticos, Cavitação Acústica, Ultrassons Focalizados, *Isolated Limb Perfusion*, BN175, Ratos Brown Norwegian

Abstract

The phenomenon by which ultrasound may transiently alter the structure of the cellular membrane, and thus allowing enhanced uptake of low and high molecular weight molecules into the cell is defined as Sonoporation. In gene therapy, the main goal is to increase the delivery efficiency of exogenous nucleic acid to a site-specific target. For gene transfer using sonoporation, the biophysical effects involved include cavitation, radiation pressure, and microstreaming - the shear forces present near the microbubbles. The acoustic pressures required to destroy microbubbles lie in the diagnostic range, and if these are too high or last too long, undesirable levels of cell killing will occur, resulting in poor DNA transfer.

There is the need to develop a new treatment for a soft tissue tumor defined as fibrosarcoma which is a malignant tumor that usually develops in the legs and whose treatment involves a wide excision, usually combined with radiation therapy. This project is a pilot study in which Focused Ultrasound and Microbubbles is added to a combined therapy including Melphalan, TNF-α and Vaccinia Virus to try to enhance the efficacy and reduce the toxicity of the treatment. The main goals of this pilot project are to study tumor virus distribution and then to quantify the number of viral particles in the tumors using appropriate assays (e.g. qPCR, Plaque Assay, Immunofluorescence). This involves *in vitro* experiments with BN175 rat sarcoma line, initially to test a combination therapy with the virus in the presence or absence of (i) focused ultrasound (ii) microbubble and (iii) focused ultrasound and microbubbles.

The physical parameters to be optimised are peak rarefactional focal pressures, duty cycle, pulse repetition frequency, exposure duration and microbubble concentration.

In vitro results suggest that once inertial cavitation starts, the viability of BN175

cells decreases and this effect is higher in the presence of microbubbles. *In vivo* experiments in Brown Norwegian rats should help to determine the effectiveness of the combined therapy using Focused Ultrasound in the presence of Microbubbles, Melphalan, TNF-α and Vaccinia Virus using the technique of Isolated Limb Perfusion but the results suggest that the use of Focused Ultrasound and Microbubbles might be killing the virus. Although, the results from qPCR analysis and viral plaque assays are not enough to confirm this theory and the histochemical analysis failed.

Keywords: Sonoporation, Virotherapy, Oncolytic Viruses, Cavitation, Focused Ultrasound, Isolated Limb Perfusion, BN175 cell line, Brown Norwegian rats

Acknowledgements

The last five years of my life have been full of moments of learning – learning about life, learning about people, learning about me. I could not have done this by myself and fortunately I had (and have) people that gave me support and allways believed in me. I must show how grateful I am to all of them.

First, I must say ‘Thank You’ and dedicate all my effort to my parents and sister that are allways by my side and supported my academic journey, allways believing that I would achieve every single goal I would be proposed to.

Then, I am grateful to Professor Gail Ter Haar for having accepted me to be part of her great team in The Institute of Cancer Research, in Sutton, UK. This allowed me to acquire unvaluable knowledge and helped me to be involved in the research environment with amazing people.

During my academic journey in the Faculty of Sciences, Professor Eduardo Ducla-Soares was of great importance because of his passionate way to talk about science and most of all for believing, supporting and encouraging his students to allways search better for more.

Finally, I am thankful to have met good people, friends for life, Célia, Francisco, Filipa and João. They have joined my journey in the best moment possible, giving me all the support I needed, trusting me and providing moments of joy and happiness. I must say a special ‘Thank You’ to Francisco and Celia because they have helped me to feel at home far away from home by their companionship while we shared a flat in London.

Contents

List of Figures

List of Tables

List of Acronyms

FUS: Focused Ultrasound

MB: Microbubbles

ILP: Isolated Limb Perfusion

PNP: Peak Negative Pressure

PRF: Pulse Repetition Frequency

DC: Duty Cycle

DE: Duration of Exposure

US: Ultrasound

PCD: Passive Cavitation Detection

PZT: Piesoelectric

OA: Oncolytic Adenoviruses

OD: Optical Density

P1: Population 1

P2: Population 2

P3: Population 3

VPAs: Viral Plaque Assays

SD: Standard Deviation

TNF-α: Tumour Necrosis Factor-alpha

qPCR: real-time quantitative Polimerase Chain Reaction

RFP: Red Fluorescet Protein

GFP: Green Fluorescent Protein

DMEM: Dulbecco's Modified Eagle Medium

1. Introduction

1.1. Chapter by Chapter Overview

1.1.1. Chapter 1 – Introduction to Transducers Calibration

The Introductory part of this thesis is divided in sections such as i) "Motivation and Background", in which there is a brief description of the main concepts and of the project itself, ii) Hypothesis and Thesis Aim", where the hypothesis is that Focused UltraSound (FUS) in the presence of MicroBubbles (MB) enhances the activity of oncolytic virotherapy delivered during Isolated Limb Perfusion (ILP) through several mechanisms which include direct anti-tumour activity and enhancement of the activity of melphalan/TNF-α and increased intratumoural delivery of oncolytic viruses. For this, the FUS fields to be used will be characterised using well established techniques. *In vivo* experiments will be made in Brown Norwegian Rats implanted with fibrosarcoma cells (BN175 cell line) and then an overview on, iii) Virotherapy for Cancer, iv) Focused Ultrasound in Cancer Therapies, v) Basic Principles of FUS, vi) Cellular interaction mechanisms in therapies using Focused Ultrasound which will help to clarify the main concepts used along this dissertation. Finally, vii) the state of the art of combined treatments using drugs/virus and focused ultrasound that describes the last decade studies on the area of oncolytic virotherapy combined with FUS.

1.1.2. Chapter 2 – Calibration of a Focused Ultrasound Transducer and Measurement of Cavitation Thresholds under Different Frequencies

This chapter is divided into two main sections. The first section describes the ultrasound beam, its propagation and the processes involved in Transducers Calibration. There are three sub-sections for Transducers Calibration: an introduction, then the methodology used and finally the results. The second part of this chapter has to do with the Measurement of Cavitation Thresholds at three different drive frequencies. A Brief

Review on the topic is the first sub-section and this is followed by the description of the Methods and then the Results which are presented paired with the Discussion of the Results.

1.1.3. Chapter 3 - *In Vitro* Study on the Effects of Focused Ultrasound on BN175 Sarcoma Cell Line

This chapter focuses on the potential of ultrasound and microbubbles to enhance drug delivery by the process of Sonoporation, *i.e.* the formation of temporary pores in the cell membrane, as well as enhanced Endocytosis that have been reported as the main biological mechanisms involved. In general, the uptake of drugs or small molecules is attributed to ultrasound mediated transient permeabilization of the cell membrane. This transient permeabilization can occur due to stable and inertial cavitation events in the presence or absence of artificial microbubbles. To confirm this, physical parameters of ultrasound such as Peak Negative Pressure (PNP), Pulse Repetition Frequency (PRF), Duty Cycle (DC) and Duration of Exposure (DE) have been tested at different levels to see how this could affect the fibrosarcoma cell line. The Methodoly used is described and a Discussion of the Results helps to take some conclusions.

1.1.4. Chapter 4 - *In Vivo* Study on the Development of a Combined Treatment for Cancer using Virus and Focused Ultrasound

The toxicity of viral therapy is a concern and to minimize it, a novel technique known as Isolation Limb Perfusion has been developed. This is a chemotherapeutic technique using melphalan, Tumour Necrosis Factor-alpha (TNF-α), oncolytic vaccinia virus and involving the cannulation of the blood vessels feeding the tumour-bearing region and isolation of the limb from the systemic circulation by tourniquet mainly due to the severe toxicity of TNF-α. ILP is used in this project, which aims to study the combination of ILP and FUS in the presence of microbubbles to increase viral penetration of tumour bulk in Brown Norwegian rats transfected with BN175 fibrosarcoma cells. The *in vivo* work is described in Chapter 4 and this includes a short introduction, the description of methods and then the presentation of the results and its discussion.

1.1.5. Chapter 5 - Conclusions and Future Work

This chapter helps to summarize all the conclusions from the experiments of this pilot project but also, contains some important suggestions on what could have been done better and what could be done in the future.

1.2. Motivation and Background

Sonoporation is a process by which the permeability of a membrane is changed. This alteration in the membrane generates a passage through which small molecules can enter. During the last decades, research on focused ultrasound and microbubble mediated virotherapy has been carried out and proved to be a good approach to cancer treatment. The treatments under research include strategies such as viral transduction of tumour cells with 'suicide genes', using viral infection to trigger immune-mediated tumour cell death and using oncolytic viruses for their direct anti-tumour action.

For oncolytic viruses, sonoporation seems to be important to get increased viral uptake in cells but the safety and efficiency of the overall process needs to be studied for clinical use. The toxicity of viral therapy is a concern and to minimize it, a novel technique known as Isolated Limb Perfusion has been developed. This is a chemotherapeutic technique involving the cannulation of the blood vessels feeding the tumour-bearing region and isolation of the limb from the systemic circulation by tourniquet. ILP will be used in this project in Brown Norwegian rats transfected with BN175 Fibrosarcoma cells.

A Fibrosarcoma is malignant soft tissue tumor or sarcoma that usually grows in the lower extremities of the human body. Treatment for a fibrosarcoma involves a wide excision, usually combined with radiation therapy. In severe cases of fibrosarcoma, it might be necessary to remove the entire limb to guarantee the survival of the patient.

Research must be done to diminish the invasiveness of tumor therapies. This project is a pilot study based on a study of Pencavel *et al.* which is entitled as "Isolated limb perfusion with melphalan, tumour necrosis factor-alpha and oncolytic vaccinia virus improves tumour targeting and prolongs survival in a rat model of advanced extremity sarcoma" that was published in 2015 in the International Journal of Cancer. So, the aim is to add Focused Ultrasound to this combined therapy to see i) if there is an increased uptake and replication of virus for enhanced efficacy of the treatment and ii) if there is a

possibility to avoid the use of tumour necrosis factor-alpha, which is toxic when in the systemic circulation, to reduce the invasiveness of the treatment.

The main goals of this pilot project are to study tumor virus distribution and then to quantify the number of viral particles in the tumors using appropriate assays (*e.g.* qPCR, Plaque Assay, Immunofluorescence). This will involve *in vitro* experiments with the BN175 rat sarcoma line, initially to test a combination therapy with the virus in the presence or absence of (i) focused ultrasound (ii) microbubble and (iii) focused ultrasound and microbubbles.

The physical parameters to be optimised are peak negative pressures, duty cycle, pulse repetition frequency, exposure duration and microbubble concentration. Once a range of optimal parameters has been found, these will be applied in *in vivo* Brown Norwegian rats in order to determine if a combined therapy using Focused Ultrasound, Melphalan, TNF-α and Vaccinia Virus using the technique of ILP. TNF-α is a cell signaling protein (cytokine) involved in systemic inflammation that is also capable of induce fever, apoptotic cell death, and inhibit tumorigenesis and viral replication. This molecule is mortal in the concentration it is used in this therapy so it will also be studied the possibility to avoid this chemotherapeutic agent to reduce the toxicity of the treatment.

1.3. Contributions

The hypothesis to be tested was that Focused Ultrasound in the presence of microbubbles enhances the efficacy of oncolytic virotherapy delivered during Isolated Limb Perfusion through several mechanisms, which include direct anti-tumour activity, enhancement of the activity of melphalan/TNF-alpha, and increased intratumoural delivery of oncolytic viruses.

The following specific research aims were addressed:

1. Characterisation (*in vitro* and *in vivo*) of the effects of FUS and MB on standard ILP with melphalan/TNF-alpha in rat distal limb sarcoma.
2. Evaluation of FUS + MB over a range of ultrasound intensities as a means of enhancing intratumoural delivery of oncolytic virotherapy during ILP. These studies included the evaluation of viral biodistribution using viral plaque assays, quantitative PCR, analysis of gene expression and non-invasive imaging (bioluminescent and GFP/RFP imaging), – characterisation of the effects of

therapeutic FUS + MB with ILP-delivered oncolytic virotherapy. These studies involved the evaluation of the effects of treatment schedule and dose and included *in vivo* (direct measurement, imaging analysis).

The FUS fields used were characterised using well established techniques and the ultrasound parameters investigated were peak negative pressures, duty cycle, Pulse repetition frequency, and duration of exposure. These parameters were varied with the aim of identifying the conditions that gave the optimal viability for the sarcoma cell line used (BN175 cell line). These were investigated in combination with commercially available ultrasound contrast agents (i.e. MB) in an attempt to find the most effective exposure. The mechanisms for any observed effects were studied. Ultrasonic cavitation was monitored, and its influence investigated.

The therapeutic efficacy of FUS/MB-assisted oncolytic virotherapy during ILP, this was tested in immunocompetent brown Norwegian rats bearing BN175 syngeneic tumours. These models allowed evaluation of effects of the combination therapy on locoregional control.

1.4. **Virotherapy for Cancer**

The possibility of treating the underlying causes instead of solely its symptoms, and thus eliminating disease, is getting closer and closer to reality when we talk about cancer. Research is being undertaken in the field of viral based gene delivery systems and has already proved to be useful for the treatment of some tumors [1-4].

Over the last century, clinicians have already used a spectrum of wild-type viruses to treat cancer patients. However this approach was temporarily abandoned not only due to adverse biological effects of the virus and to safety of both patients and staff, but also because of enthusiasm for the advent of chemotherapy [5]. Over the past decade, research in this field has once again been taking place, with several viruses having been evaluated. Genetic engineering of viruses to target cancers safely is now a few steps away from worldwide clinical application - the first agent is about to be approved for use as a novel cancer therapy modality [6, 7].

The use of oncolytic viruses in oncology is called virotherapy, and nowadays is one of the most promising cancer therapy methods. Viral-mediated gene delivery systems consist of site-specific delivery of viruses which are modified to be replication-deficient outside the target tissue, but which can deliver DNA for expression. In this context, viruses can be used as anti-cancer agents which attack malignant cells, while healthy cells remain relatively undamaged. Different kinds of viral vector systems are used, including retrovirus, adenovirus, adeno-associated virus, herpes simpex virus or lentivirus [8]. As well as having an anti-cancer effect, oncolytic viruses are also capable of inducing an anti-tumour immune response – immunotherapy – which is thought to help in eliminating residual cancer cells or in maintaining micrometastases in a state of dormancy [9].

Adenoviral vectors are the most promising and widely used platform for gene therapy and virotherapy. However, there have been problems associated with their use [10]. The major challenges in adenovirus-mediated cancer gene therapy and virotherapy are poor transduction in human tumors, and the existence of immune responses against the adenovirus that drastically limit the vector transduction efficiency and the duration of transgene expression [11]. In order to avoid these problems, several strategies have been proposed, these include the modification of the viral particles to provide increased affinity to tumor receptors, and to facilitate binding and replication, and the use of immunosuppressive agents to eliminate a possible anti-viral immune response [10-12]. Others goals, which focus on treatment efficacy, are to obtain specificity to cancer cells (in order to avoid damaging normal cells), and improvement in the means of inducing cell death by modifying viral proteins to destroy cancer cells by promotion of viral replication in malignant cells but not in normal cells, thus enabling the targeting of metastastic cancer cells. A third goal in terms of efficiency is to improve transduction – the delivery of therapeutic genes into cancer cells. The overall efficacy of the treatment of tumors with viral particles can also be enhanced if combined with methods that help to open the membranes of cancer cells [11, 12].

There are tumor specific viral vectors which are equipped with an efficient delivery system, and are ready for immediate use in *in vivo* mouse models, and for testing in clinical trials, but still can not be used to treat patients on a regular basis. The therapy most used to treat tumours is chemotherapy. It helps to shrink tumors but this is usually reversible – the tumors can grow again and become resistant to the treatment. This resistance can be reduced if chemotherapy is combined with other treatments which rely

on different mechanisms for attacking and killing cancerous cells. The main problem of combined therapies is the toxicity – it must be reduced as much as possible - and special attention to other possible safety issues such as environmental shedding, mutation and reversion to wildtype virus is necessary [7].

One novel cancer therapy technique under investigation is Isolated Limb Perfusion using melphalan, tumour necrosis factor-alpha and oncolytic vaccinia virus. Improved tumour targeting has been reported by Pencavel *et al* [13]in terms of transduction route and prolonged survival in a rat model with advanced extremity sarcoma . Standard *in vitro* assays were used to characterise the single and combined effect of melphalan, Tumour Necrosis Factor-alpha (TNF-α) and Lister strain vaccinia virus (GLV-1h68), which is an attenuated recombinant vaccinia virus (VACV) that selectively colonizes established human xenografts, thus inducing their complete regression, in BN175 rat sarcoma cells. An orthotopic model of advanced extremity sarcoma (a model in which the tumor is localised in the place in the body where it belongs) was used to evaluate the survival of animals after receiving ILP with this triple Melphalan, TNF-α and Vaccinia Virus therapy . Successful pre-clinical results, in terms of reduced tumor growth and increased rat survival, have highlighted the need to develop a treatment with increased viral uptake in which invasiveness can be reduced, and where post-treatment surgery is not needed. In addressing this goal, this project focuses on the study of the combination of ILP and FUS in the presence of microbubbles to increase viral penetration efficiency of tumour bulk in Brown Norwegian rats transfected with BN175 fibrosarcoma cells.

1.5. Focused Ultrasound in Cancer Therapies

A method of improving the specificity and efficiency of any treatment is crucially needed. The difficulty of getting molecules across membranes to reach the cell nucleus, for tumour treatment, may potentially be overcome using Focused Ultrasound. It can be used to facilitate the transport of molecules into cells by altering their membrane permeability.

Therapeutic ultrasound is a continuously expanding field and new clinical applications are constantly being developed. The term ‘Ultrasound’ (US) is used to

describe sound waves with frequency above the upper limit of the human hearing range (>20 kHz). Applications of medical ultrasound can be divided into focused and unfocused therapies with devices operating at frequencies from 20 kHz to 5MHz [14, 15]. The energy produced by these devices propagates in soft tissue as longitudinal pressure waves, interacting with tissue through reflection, scatter and absorption [16, 17].

Major advances have been made in some fields of medical US and one of major interest is Focused Ultrasound surgery. In clinical focused ultrasound treatments, US energy of frequencies in the range 0.5 – 5 MHz is concentrated into a focal spot of millimetric dimensions. The biophysical effects of ultrasound are traditionally separated into those of thermal and non-thermal (acoustic streaming and acoustic cavitation) origin [18, 19]. However, it may not be completely correct to assume that there is no rise in temperature when considering non-thermal effects, because the interaction between tissue and ultrasound usually results in energy absorption, and therefore a temperature rise [18]. Conversely, acoustic fields which aim to cause heating can also give rise to non-thermal effects.

Non-thermal mechanisms include: Acoustic Streaming which arises from the loss of momentum when the ultrasound hits a target, and provides a driving force capable of displacing ions and small molecules; Acoustic cavitation, defined as the interaction between sound waves and microscopic gas bubbles within a fluid. The compression and rarefaction present in the ultrasound field lead to bubble compression and expansion [20].

Focused ultrasound can be used to enhance the ability of a virus to infect cells upon arrival at a target, in part, because of the increased blood flow which is the body's biological response to the temperature rise at the focus, but mainly because it can cause a temporary change in cell membrane permeability. Acoustic Cavitation plays an important role in this process.

1.5.1. Acoustic Cavitation

Acoustic cavitation helps to concentrate acoustic energy into small volumes. Inertial cavitation can lead to a local rise in temperature of thousands of kelvin, pressures of GPa, high local accelerations and shockwaves. Acoustic cavitation thus constitutes a

complex multidisciplinary problem, involving a wide range of temporal and spatial scales, and is difficult to measure, control, predict, and to scale up.

Two types of acoustic cavitation are defined: stable and inertial. Stable cavitation occurs when a bubble oscillates steadily in an ultrasonic field, intercepting and re-radiating energy to the surrounding tissue, causing microstreaming, which can, in turn, leads to shear stresses which can damage cells. This form of cavitation is characterised by the emission of harmonics and ultra-harmonics of the drive frequency, which can be monitored. Above a certain pressure amplitude threshold, oscillation becomes non-linear and the bubbles expand and collapse vigorously resulting in localised acoustic pressures of several thousand atmospheres that cause damage to cells in their immediate vicinity- this is known as inertial cavitation and is characterized by broadband acoustic emissions in addition to the harmonics and ultraharmonics of stable cavitation.

Inertial cavitation occurring near a cell boundary can cause transient membrane rupture due to shock waves and jetting during microbubble collapse [21]. This effect, also known as "sonoporation" , is thought to be a major contributor towards improving intracellular drug and gene delivery [22, 23] – see Figure 1.1. Sonoporation is of special interest due to its non-invasive nature, and its potential for treating tissues located several centimetres deep within the body.

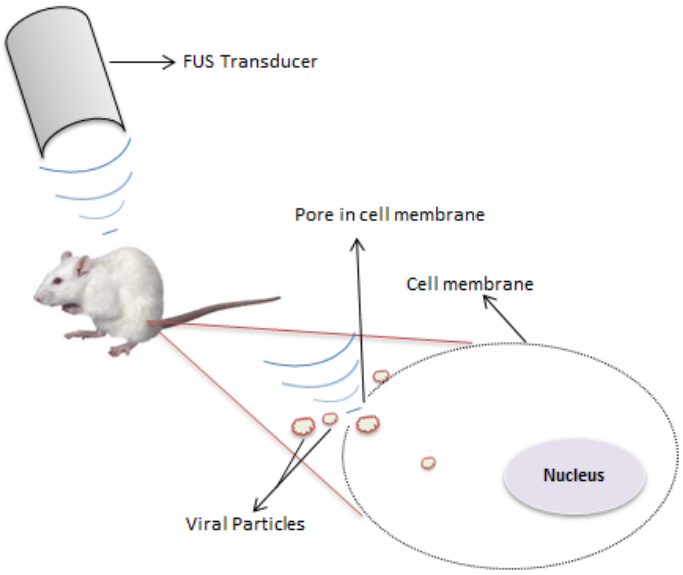

Figure 1.1. Schematic of the Focused Ultrasound - mediated viral particles delivery by sonoporation

An ultrasound exposure may be carried out on its own [24] or in the presence of gas microbubbles [25]. Microbubbles are stabilised gas bubbles used to increase scatter to provide ultrasound imaging contrast, but which can also serve as nuclei for acoustic cavitation. The gas filling the bubble provides elasticity to the bubble which in turn opposes the resistance to any compression or expansion imposed by the liquid motion. This force may put the liquid into motion, so that the bubble constitutes a mass–spring system [26]. When excited at large amplitudes, the bubble oscillations can exhibit a non-linear behaviour. When the ratio of the linear resonance frequency and the driving frequency – f0/f - approaches a rational number n/m, a non-linear resonance can occur and the amplitude of the bubble oscillations increases. The 1/1 peak corresponds to the linear resonance frequency. Following the accepted terminology, the resonances n/1 are called harmonic, the resonances 1/m are sub-harmonic, while the rational ratio n/m gives ultra-harmonic resonances [26].

In gene therapy, the combination of gas microbubbles with ultrasound can result in greater delivery efficiency than when no microbubbles are present [25, 27] and there are differences in the effects produced in the cells when in high or low *in situ* ultrasound pressures are used. The probability of cavitation increases with increasing pressure and decreasing frequency. This has been extensively investigated with ultrasound contrast agents and microbubbles have been shown to lower the threshold of cavitation [28].

1.5.2. High Intensity Focused Ultrasound Therapy

The potential of focused ultrasound to produce localised destruction of deep tissue structures has been known since the early 1950s [15]. Focused Ultrasound at intensities in the range 10^2–10^4W/cm^2 is known as High Intensity Focused Ultrasound (HIFU) [29]. In medical HIFU treatments, US energy is focused into a millimeter or even a sub millimeter sized focal spot to heat and destroy the targeted tissue, while ideally not damaging tissue outside the focal region. When the ultrasonic energy absorption in a focal volume is sufficient to raise the temperature above 55ºC for 1s or longer, proteins are denaturated, causing immediate cell death – the volume of dead cells being referred to as "lesion" [15, 29]. The two mechanisms believed to be most important for tissue destruction are heating and acoustic cavitation [29].

HIFU was first developed for localised tissue destruction in the brain by Fry *et al.* [30, 31]. Burov, in 1956 [32], was the first to suggest its use for cancer therapy. Early use was made of HIFU in the treatment of Parkinson's disease and for a number of ophthalmological problems (including the treatment of glaucoma and retinal tears) [15].

The possibility of non-invasive targeting of subcutaneous tissue volumes has made HIFU a potential substitute for surgery for liver, bladder, prostate and kidney tumors. Hepatocellular carcinoma is one of the most common malignancies worldwide and hepatic metastases are a common cause of death in cancer patients [14]. This technique may not require surgery, anaesthesia or adjuvant cytotoxic drugs, and thus the likely side effects are minimal.

The preceding description of High Intensity Focused Ultrasound indicates that this technique as a powerful tool for fighting malignant cells, but not that it is a means of enhancing therapeutic efficiency for drug/viral delivery. However, a combination of differents levels of intensity can be used to advantage for this.

1.5.3. Low Intensity Focused Ultrasound Therapy

Low Intensity Focused Ultrasound is associated with intensities below approximately $10^2 W/cm^2$ [29], and its main applications are in bone healing, sonothrombolysis, ultrasonic enhancement of drug uptake by sonophoresis and sonoporation and gene therapy [15].

The way in which bone repair may be accelerated by ultrasound is still not fully understood. Mechanisms that have been proposed are signal transduction, enhancement of gene expression, blood flow changes, tissue modelling effects or micro-mechanical stresses. In sonothrombolysis, the dissolution of blood clots is mediated by ultrasound, both in the absence and in the presence of microbubbles, and the responsible mechanisms are suggested to be acoustic cavitation, streaming, and mechanical interaction that affect the fibrin mesh, thus allowing disruption and better access for drugs [15].

The applications of most interest for this project are the ultrasonic enhancement of drug uptake and gene therapy, although this is an area of study that is still poorly understood. Sonoporation and gene therapy have similarities since both involve an

alteration in membranes to facilitate the entrance of therapeutic vectors. Sonoporation is the term used for the phenomenon by which ultrasound may transiently alter the structure of the cellular membrane, and thus allowing enhanced uptake of low and high molecular weight molecules into the cell. In gene therapy the main goal is to increase the delivery efficiency of exogenous nucleic acid to a site-specific target – the main vehicles being studied are viral and non-viral vectors. [15].

For gene transfer using sonoporation, the biophysical effects involved include cavitation, radiation pressure, and microstreaming - the shear forces present near the microbubbles. [16]. The acoustic pressures required to destroy microbubbles lie in the diagnostic range, and if these are too high or last too long, undesirable levels of cell killing will occur, resulting in poor DNA transfer [34].

Microbubbles may be added to the blood circulation to aid drug delivery. These lower the threshold for acoustic cavitation and can also be manipulated to be drug carriers.

It is possible to encapsulate drugs within the bubbles, they may be incorporated either into the shell or inside it in some way, for example using ligands embedded into the lipid membrane. It is also possible to construct microbubbles with a multilayered shell containing drug [15, 23, 25]. The loaded microbubbles, can be metabolized and accumulated within the target volume. Low intensity ultrasound can then destroy them locally, releasing the drug. The spatial localisation relies on the ability to confine the ultrasound beam to the required target volume [15].

There are allways bio-effects associated with ultrasound, but their significance depends on the intensity and duration of the exposure. At low intensities, any effect seen is likely to be reversible and/or beneficial. On the other hand, at high intensities it is possible to destroy tissue by protein denaturation, and this may be really useful in oncology [15]. The diagnostic and therapeutic ability of ultrasound turns it into a very interesting tool for research and optimisation in the medical field.

1.6. Basic Principles of Focused Ultrasound

Ultrasound is known for its routine use in imaging, and research in this area allowed the discovery of powerful potential for therapeutic applications. A range of

biological effects can be induced by ultrasound, each depending on a wide variety of physical parameters that may be varied.

Focused Ultrasound is gaining rapid clinical acceptance as a treatment modality which enables non-invasive tissue heating and ablation for numerous applications. One of the greatest advantages of this technique is the possibility of non-invasivetargeting the ultrasound focus deep in the tissue . Focused beams can be used at high power, with the source placed either outside the body (for treatment of tumours of, for example, the abdomen, breast, uterus, and bone, either for surgery or for enhanced uptake of drugs/virus) or in the rectum (for treatment of the prostate), and are designed to treat thetarget tissue volume, while leaving tissue in the ultrasound propagation path relatively unaffected. A brief description of the principles of operation and physics associated with focused ultrasound will be addressed in this chapter.

A wave capable of travelling through multiple tissue layers until it reaches the target is produced from an ultrasound transducer. At each tissue interface, part of the energy carried by the sound wave will be reflected, with the remaining energy being transmitted. The amount of transmission at the interface depends primarily on the difference in acoustic impedance, Z (defined as the product of density and speed of sound, between the two tissue layers) [35]. At interfaces where there is little difference in acoustic properties, the transmission coefficient is close to unity. With the exception of fat, air and bone, most tissues in the human body have acoustic properties similar to those of water. Aqueous media are therefore optimal for coupling ultrasound energy from the transducer into the body, and reflections at tissue interfaces are generally weak [35].

Within a tissue layer, an ultrasound beam consists of pressure fluctuations which result in frictional heating. Part of the mechanical energy carried by the incident wave is thus converted into heat by this viscous absorption, which constitutes the primary mechanism for ultrasound-induced hyperthermia [35, 36]. In an inhomogenous medium, regions with different acoustic properties will scatter the incident wave in various directions, causing a loss of acoustic intensity in the direction of sound propagation.

The loss in incident acoustic energy in a medium is characterised by its attenuation coefficient, μ, given by the sum of the absorption coefficient μ_a and the scattering coefficient μ_s. Following propagation through a distance x in a medium of attenuation coefficient μ, the ultrasound intensity, I, is given by $I = I_0 e^{-\mu x}$ where I_0 is the incident

ultrasound intensity at the origin (x=0). For most tissues, the attenuation coefficient is related to the ultrasound frequency, f, by a power law of the form $\alpha = af^b$ where a and b are constants specific for each tissue [35].

It is this dependency of attenuation on frequency that makes ultrasound particularly useful to non-invasive therapies, but which causes some significant challenges in optimising the overall treatment procedure. Higher ultrasound frequencies give a power-dependent increase of both the absorption and attenuation coefficient. This implies a trade off between penetration, associated with low frequencies, and absorption, paired with high frequencies. Therefore, the optimal choice of therapeutic ultrasound frequency is application-specific, and represents a compromise between treatment depth and the desired rate of heating [36].

When a large-amplitude single-frequency sound wave propagates through a nonlinear medium there is a leakage of energy from the fundamental frequency into its higher harmonics. The extent to which such leakage occurs depends on the amplitude of the incident wave, on the nonlinearity of the medium and on the distance travelled by the wave into the medium. The nonlinear effects become increasingly significant as the depth of treatment is increased, or if a region of high intensity happens to be coincident with a layer of tissue with significantly different acoustic impedance [35].

Acoustic cavitation, previously discussed in chapter 1.3.1., and classified into stable and inertial behaviour, depends on the bubble size compared to the linear resonance size at the frequency of insonation, the ultrasound exposure parameters, and on the relative contribution of vapour and gas pressures to the total pressure inside the bubbles [35]. The presence of bubbles results in a change in the acoustic impedance of the tissue volume, yielding larger reflection coefficients at the boundaries of the cavitating region. In any given medium, the relative increase in any of these coefficients will depend primarily on the bubble number density, the range of bubble sizes and the type of cavitation activity being excited [37]. At a given pressure level, the relative contribution of nonlinear effects and cavitation depends on the threshold pressure at which cavitation occurs, the tissue temperature and the distance over which ultrasound has propagated [35].

Most clinical applications of Focused Ultrasound make use these effects occurring during the propagation of ultrasound waves. Negative acoustic pressures (~1 to 5 MPa)

and high temperatures caused by HIFU exposures contribute to the formation of gas cavities. Cavitation detection can be performed acoustically by detection of subharmonics, harmonics, superharmonics or broadband signals emitted, using e.g, a Passive Cavitation Detector (PCD). It is possible to infer the existence of cavitation by looking at the images acquired by the imaging device associated with a FUS system, since bright spots occurred because of a greater amount of reflected energy. Cavitation can be quantified in terms of number of events, or by the amount of released energy (in mV) - see figure 1.2.

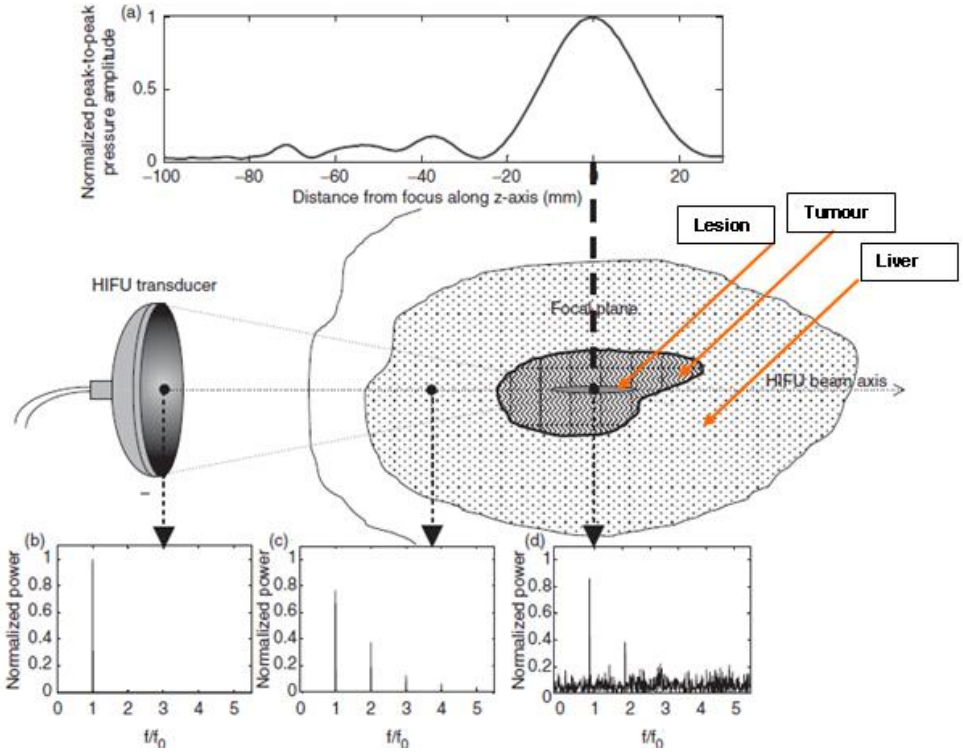

Figure 1.2. Superposition of an illustration of the principle of HIFU (centre), a typical axial HIFU pressure profile and a diagrammatic representation of the frequency-content, f, of the HIFU wave (b-d) as it propagates through tissue. HIFU delivers energy onto a small region deep within tissue. Thermal necrosis occurs within the focal volume but the surrounding tissues remains unaffected. In (a) the large peak defines the focal region of the HIFU transducer, within which thermal damage is expected to occur. Pre-focal peaks are due to pre-focal heating in the different tissue layers. In (b), the peak represents, f_0, the frequency of the monochromatic wave generated by the transducer. As this wave travels through a nonlinear medium, superharmonics leakage occurs (c) and the energy of these harmonics is rapidly absorbed and converted to heat. Finally, (c) the detection of cavitation results in broadband noise emissions that are readily absorbed and converted into heat *(ter Haar, G., 2007).*

1.7. Cellular interaction mechanisms on therapies using Focused Ultrasound

There is a lack of knowledge about the cellular and molecular biological effects of Focused Ultrasound exposures. The cellular and molecular biology of tissues can be dramatically altered by mechanical force and stress. As the use of FUS increases in clinical applications, there is a need for a better understanding of the cellular and molecular consequences of depositing this form of energy in tissues, and of how to harness this non-invasive technique for novel therapies.

FUS is generally considered to be noninvasive, Some studies have provided some insight into the mechanism of action of FUS at sub-cellular and molecular levels. Two types of mechanisms of action are involved in FUS: thermal and mechanical in origin – as discussed previously in section 1.4.

At high intensities, coagulative necrosis is the main mechanism for cell death but others, such as apoptosis or cell lysis, may also take place [38]. When there is cell death, one particularly interesting effect is the increase in the systemic immune response due to exposure by ultrasound. A response to this inflammatory process can result in the increase of CD3+ and CD4+ cells – the denditric cells responsible for a systemic immune response [39].

In contrast to HIFU, where the biological outcome is typically instant cell death, low-intensity ultrasound may induce numerous short- and long-term outcomes that may be suppressive or proliferative depending on the acoustic exposure parameters [38, 40]. Temporary membrane poration may readily be achieved at low intensities (often refered to as sonoporation), and it has been tipped as an emerging paradigm for drug/gene delivery.

In particular, sonoporated cells have been found to exhibit membrane shrinkage and intracellular lipid accumulation. Also, compared to normal cells, their DNA synthesis kinetics were found to be significantly slowed, and the onset of cell-cycle arrest was evident. In some instances, programmed cell death (i.e. apoptosis) may even take place. This highlights the need to refine and optimize sonoporation for drug/gene delivery purposes in order to maintain cellular viability. On the other hand, this may represent a way of inducing cell death that is different to HIFU-based thermal ablation [40].

1.8. State of the Art of Combined Treatments using Drugs/Virus and Focused Ultrasound

Viral agents replicate and induce cell death through mechanisms other than apoptosis, e.g. by eliminating cancer stem cells or by being engineered to carry a wide variety of transgenes which induce cell death in a number of different ways. These vectors may be used safely with other treatment modalities and have a synergistic anti-cancer effect which can also be achieved through specific immunological reactions [41]. They can increase the potency of multi-modality treatment regimes in an amplified site-specific manner which can induce additional specific anti-tumour effects, and thus have the potential to target metastases through immunological strategies [41].

There have been several approaches to gene or viral ultrasound-facilitated therapy over the last few decades, as the mechanism by which ultrasound enhances gene delivery is still not completely understood. Experiments on the effects of ultrasound on *in vitro* gene delivery have been extensively used to determine optimal conditions for use when exposing *in vivo*. Some of the studies in this field, published over the last ten years, are described below.

Focused Ultrasound is attractive because of its potential in non-invasive surgery to provide tumor thermal ablation selectively in the focal volume, leaving surrounding healthy tissue unharmed. The whole process can be guided using ultrasound or magnetic resonance imaging. Non-thermal effects such as acoustic cavitation must also be considered when talking about focused ultrasound therapy. Lithotripsy was one of the first applications of focused ultrasound to be considered. Here, shock waves are used to break kidney stones into fragments which the body is able to expel through the urinary tract [42]. In lithotripsy treatment, cavitation is thought to be the explanation for the side effects, such as haemorrhage, seen in soft tissue. The cavitation threshold has been estimated to be in the range of 1.5 to 3.5 MPa when treating human tissue with 0.2 MHz pulsed ultrasound [43]. Cavitation thresholds are thought to be higher *in vivo* because tissues and blood circulation in the path traveled by the ultrasound beam cause increased sound absorption or scattering [44]. Ways of enhancing cavitation *in vivo* [45] and *in vitro* [46] by introducing gas bubbles have been studied, and have led to the identification of the process of sonoporation which, when combined with shock wave ablation of tumors has resulted in DNA transfer [45, 47-49]. However, the use of lithotripsy to achieve DNA

transfer proved to be unsafe due to the potential for enhanced metastasis of malignant tumors. Lithotripter shockwaves can enhance metastasis from tumors, and this effect is attributable to the cavitation mechanism [50, 51].

The drawbacks of lithotripsy for cancer therapy needed overcoming, and so FUS started to be considered as a less harmful technique, which has the same objectives, since it provides a means of easily adjusting parameters to promote either thermal or non-thermal effects. These parameters include transducer frequency, exposure duration, pulse length, peak negative pressures in the focal volume, duty cycle and pulse repetition frequency. Huber and Pfisterer [34] used focused ultrasound to perform experiments on *in vivo* transfection with plasmid DNA at 1 MPa pressure amplitude. The authors found no evidence of increased incidence of metastasis.

A study by Miller and Song [52] was designed to investigate the potential for simultaneous gene transfer and tumor ablation with cavitation-enhanced FUS using a 1.55MHz transducer and US image guidance to treat mouse renal carcinoma tumors in the presence of microbubbles. Tumors were exposed for up to 0.4 seconds using a range of Peak Rarefactional Pressure Amplitudes (PRPA) of 2MPa to 8MPa. Tests were performed to assess the influence of the microbubble injection route, burst duration and pressure amplitude by reducing exposure duration and using multiple pulses. Evaluated both in terms of the subsequent tumor growth and gene transfer, the expression of marker plasmids injected into the tumors indicated that tumor growth reduction and gene transfer can be achieved with cavitation-enhanced FUS treatment, and that gene transfer tended to decrease with increasing exposure duration, or PRPA. The decrease in gene transfer might be due to a decrease in cell viability, (the ability of cells to maintain or recover viability), which was not investigated. The way by which cavitation enhanced gene delivery is still not clear.

Challenged to get closer to an ideal vector system, thus allowing an efficient and safer transfection of virus into a target tissue, Meier-Humbert *et al*. [53] based their research on the assumption that DNA is transferred into cells across the plasma membrane via ultrasound-induced pores. The authors tried to figure out the size of the pores created by ultrasound application and the duration of pore opening. A 2.25 MHz focused ultrasound transducer operating at 570kPa was used to expose rat mammary carcinoma cells. Good DNA transfection on cells was achieved with a 10s exposure, duty cycle of 20% and Pulse Repetition Frequency of 100Hz with cell viability assays showing more

than 70% cell survival. The experimental conditions used gave results which showed that macromolecules of up to 37 nm were delivered into cells; pores at least as large as 75 nm were formed with the opening lasting milliseconds to seconds.

The *in vitro* studies of Rahim *et al*. [54, 55] investigated individual exposure parameters using a system designed to minimise experimental artefacts, and to allow the control of many parameters of the US field. They evaluated the targeting ability and spatial distribution of gene delivery using focused ultrasound by performing dosimetry in the focal plane and in the homogeneous near-field. To study the influence of physical parameters [55], a 1MHz-transducer was used and a sinusoidal pulse was generated with amplifier input amplitude up to 100 mV, pulse length up to 80 cycles, pulse repetition frequency up to 2.5 kHz, duration of exposure up to 60s and microbubble concentration varying from 0 to 16% by volume. Both cell viability and gene delivery were tested, and the authors concluded that the optimal conditions for gene delivery with minimal impact on cell viability were 0.25 MPa peak negative pressure at focus, PRF 1 kHz, 10s exposure, 40 cycle pulse length and 4% microbubble concentration. In terms of spatial and acoustic pressure dependence [54] exposures were performed at optimal conditions in terms of PRF, exposure time, pulse length and microbubble concentration, in a range of amplitudes from 0.35 to 1.4 MPa peak to peak pressure at the focus.

Analysis of gene delivery, cell viability and spatial distribution showed that delivery in the focal plane was concentrated around the ultrasound beam axis and that transfection efficiency increased as acoustic pressure increased towards the focus, reaching a maximum above 1 MPa. Delivery was microbubble dependent, and the cell viability was about 80% for the higher spatial average peak to peak pressure (0.88 MPa). Based on these results and exposure conditions, and with the aim of evaluating the potential for ultrasound/microbubble-mediated retroviral gene delivery, Taylor *et al*. [56] achieved good transfection results at peak-negative acoustic pressure amplitudes of 1.0 to 1.2 MPa (60 to 80 mV) using an exposure time of 5s and the pulse length of ten cycles per pulse.

Other *in vitro* studies have looked at the effect of ultrasound on viral content transfection and have been undertaken since, for the success of oncolytic virotherapy of solid tumors, it is the efficiency of infection that is important [57, 58]. Clinical trials have also been carried out using many viral vectors [59-62] to evaluate the factors that can affect infection since solid tumors contain a heterogeneous mixture of tumor and healthy

cells within an extracellular matrix supported by a tortuous vascular network [63]. Leaky vasculature and variable blood flow in tumors, lead to poor delivery of nutrients and impaired clearance of metabolic breakdown products from the tumor [64], and also make drug delivery difficult, because of the limited blood supply compared to normally vascularized tissues. Many solid tumors develop regions of hypoxia, which may lead to up-regulation of genes that predispose subjects to a more malignant phenotype [65, 66].

A different approach has addressed the question of which transduction route, i.e. the path by which DNA is introduced into another cell via a viral vector, would be best for plasmid and adenoviral delivery [67]. In their study, Agrawal *et al*., tested topical, intraflap and *in vivo* intravascular gene delivery using rat Superficial Inferior Epigastric (SIE) flaps. The extent of viral transduction through SIE flaps and its duration was assessed by non-invasive imaging of luciferase. Intravascular transduced flaps yielded the most even distribution of virus but the presence of microbubbles did not result in a higher expression of viral vector. Exposure conditions were fixed as follows: frequency 1MHz, exposure duration 30s, duty cycle approximately 66.7%, PRF of 1 kHz, each pulse consisting of 40 cycles of pressure amplitude 1.4 MPa (peak to peak) at the transducer focus.

Eisenberg *et al*. [68] completed a study relating hyperthermia and viral killing of pancreatic cancer through a heat shock protein pathway, in which a recombinant Herpes Simplex virus (NV1066) was cultured with pancreatic cancer cells (Hs700). Cell survival and viral growth proved that heating the virus NV1066 with the cell line Hs700 up to 42℃, for 4 hours, increased cell destruction by 80%. Increased viral efficacy was due to the presence of a protein (Heat-shock protein 72, Hsp72) which is regulated by thermal stimuli and lends cellular protection by inhibiting apoptosis. This protein helps to increase viral replication and tumor cell destruction.

Quantification of drug distribution is important in order to determine the ability of a drug to penetrate tissue within solid tumors. Both *in vitro* and *in vivo* techniques have been used for quantifying drug distribution. *In vitro* studies involving cell culture are a good way of obtaining optimal parameters for virus infection. Another *in vitro* study involving virus was performed by Shintani *et al*. [57] using Herpes Simplex virus to infect a mixed solution of normal and malignant cells. The effect of ultrasound and microbubbles was tested in experiments on different groups (Virus infection only, virus infection and microbubbles/ultrasound, and then virus infection with both ultrasound and

microbubbles) in which exposure conditions with a 1 MHz ultrasound transducer were varied in terms of ultrasound intensity (up to 2 W/cm2), duty cycle (up to 50%) and exposure time (up to 40s). This study gave optimal conditions in terms of maintenance of cell viability (0.5 W/cm2; 20% duty cycle and 10 s exposure) and showed a decrease of around 40% in cell viability for the extreme conditions tested, with exposure time being the parameter that most affected cell survival and transfection.

In vitro cell exposure is not the most effective way of obtaining the conditions that will be valid for *in vivo* exposures. In *in vitro* cell exposures there is no absorbing medium, and the shear stresses created by microstreaming in a fluid cause cell movement inside a solution. Bazan-Peregrino *et al*. [58] developed an *in vitro* model using a porous gel in a two-sided cylindrical container with acoustically transparent windows, and used a metal rod to create a flow-through vessel of diameter 1.6 mm. The attenuation of this gel was approximately that of water.

The studies presented so far in this document, show a lack of cavitation control which seems to be crucial for understanding transfection of particles into a cell by ultrasound and microbubbles. In Bazan-Peregrino *et al*. [58], cavitation is accounted for and ultrasonic pressures were chosen to maximize either broadband emissions, associated with inertial cavitation, or ultraharmonic emissions, associated with stable cavitation, while varying duty cycle to keep the total acoustic energy delivered constant, in order to allow comparison across exposures. A Passive Cavitation Detector (PCD) consisting of a 15 MHz spherically focused Piezoelectric Transducer (PZT), was coaxially and confocally aligned with a 0.5 MHz FUS transducer. The raw signal from the PZT transducer was amplified 25-fold, high pass filtered at 1 MHz (to reject reflections from the drive frequency), and data was recorded at a sampling rate of 20 MHz with an 8-bit digitizer. The optimal acoustic parameters were those used by Arvanitis *et al* [69] – the acoustic parameters in this study were specific to inducing inertial and stable cavitation. In the presence of ultrasound and microbubbles, a peak rarefactional focal pressure (PRFP) of 360 kPa, a duty cycle of 90% and a pulse repetition frequency (PRF) of 10 Hz were chosen to achieve stable cavitation. Conversely, PRFPs of 1250 kPa or 2400 kPa and duty cycle of 6% and 2%, respectively, were used with a PRF of 10 Hz to achieve inertial cavitation. For ultrasound only exposures, as stable cavitation could not be sustained, inertial cavitation was applied with a PRFP of 2400 kPa, 2% duty cycle and PRF of 10 Hz. All the exposures were set to 5 minutes and temperature was monitored

using a T-type fine-needle thermocouple at the FUS focus (the rise never exceeded 0.2°C so no biologically significant US induced heating occurred). Luciferase activity indicated successful infection to exposures involving both ultrasound and microbubbles, and, in terms of cell viability, the best results, in terms of the percentage of viable cells after exposure, were achieved with a PRFP of 1250 kPa and 6.5% duty cycle.

A more recent publication by Bazan-Peregrino *et al*. [70] tried to identify the key parameters needed to optimize the combined use of oncolytic adenoviruses (OA) and focused ultrasound. This optimization relies on the principle that ultrasound exposure parameters may be optimized as a function of tumor reperfusion time to sustain inertial cavitation throughout the exposure. Exposure conditions, in terms of PRFP and duty cycle, similar to their previous study were maintained [58], and PRF and exposure duration were changed to 0.5 Hz and 4 minutes, respectively. Intratumoral and intravenous injection protocols were applied using a modified adenovirus to express luciferase. Passive cavitation detection of acoustic emissions, during the *in vivo* treatment, indicated inertial cavitation as the mechanism responsible for enhanced delivery and enabled real-time monitoring of successful viral therapy. 3-fold, 12-fold and 50-fold increases in uptake have been found in 50, 30 and 20% of the tumors under inertial cavitation inducing conditions.

Another *in vivo* approach to the field of virotherapy was undertaken by Carlisle *et al*. [71] who considered that almost all the publications with solid conclusions are based on intratumoral release of virus [6] and assume that the limitations of the technique are due to poor intravenous delivery. Of particular interest is the fact that systemic deliveries of treatments for metastatic cancer still require improved circulation kinetics, extravasation from the blood-stream into the tumor, and intratumoral penetration.

Additionally the intratumoral distribution of viral content remains exclusively perivascular, without deep penetration into the tumor [72]. As a result, the therapeutic effect is restricted to a small proportion of a tumor's mass. The factors described led to research on the development of a virus coating polymer that enhances circulation and also allows triggered uncoating and reactivation of Adenoviruses within tumors. The exposures, again, were based on the findings of Bazan-Peregrino *et al*. [70] – they used a 0.5 MHz transducer at peak rarefactional pressure of 1.2 MPa at PRF of 0.5 Hz but this time the intention was to produce inertial cavitation monitored in real-time. The remaining exposure parameters were 100 ms pulse length, and 240 s exposure time. A

30-fold enhancement in tumor infection was obtained when exposing polymer coated adenovirus in the presence of microbubbles.

The last study to be discussed here, and one of the more recent ones, is that of Graham *et al*. [73] and addresses the same problem as that in the previously discussed study – namely that the clinical efficiency of stable liposomal delivery still has poor penetration into non-vascularised tumor regions and poor release of payload within the tumor. These liposomes are used to deliver powerful chemotherapeutics, which can cause severe adverse effects in non-target tissues. Although the liposomal delivery is thought to be more stable, an improved formulation is desired during the intravenous delivery phase, following arrival within the tumor, so that the drug in its free form can provide greater and more widespread effects in tissues [73]. Here, the importance of ultrasound is addressed - inertial cavitation can be used to trigger intratumoral release of drug from intravenously delivered liposomes non-invasively, and, simultaneously, inertial cavitation can be monitored through resulting acoustic emissions.

Graham *et al*. [73] used a 0.5 MHz focused ultrasound transducer, and cavitation detection has been achieved using a 7.5 MHz passive cavitation detector, which was placed in the centre of the transducer, and both were confocally and coaxially aligned. This study includes *in vitro* and *in vivo* experiments and for the former, exposure conditions varied in terms of peak rarefactional focal pressures (from 0.14 to 1.5 MPa) with fixed pulse length of 100 ms, 5% duty cycle and 30s exposure duration. Temperature was recorded using a thermocouple placed within the phantom. In terms of *in vivo* experiments for Graham *et al*. study, conditions were chosen on the basis of the work by Bazan-Peregrino *et al*. [70] (1.2 MPa of PRFP, 6% duty cycle and 0.5Hz PRF) but with some changes – total exposure time was 12 minutes and after every 90 seconds of exposure microbubbles were injected, with the focal volume being repositioned every 3 minutes. Despite the variability in intratumoral inertial cavitation levels and location, sufficient events associated with luciferin content occurred to instigate substantial and highly significant increases in payload release. The study of Graham's group is the first demonstration that such clinically applicable US parameters can be used to improve intratumoral payload release from an intravenously injected liposomal delivery agent.

The combination of ultrasound and virus seems to be a potentially useful tool for improving cancer treatment efficacy. The application of ultrasound can directly change the structure or physiology of tissues, or can induce changes in a drug or vehicle in order

to enhance payload delivery. Uptake of virus has been proven to be increased by ultrasound but a lot of work is still required to make this combined therapy clinically safe. As presented by Bourke *et al*. [41], there are some features that turn a viral vector into an "ideal virotherapy agent". These are i) a specificity to cancer cells and consequent tumour destruction, ii) the capacity for replication within neoplastic cells (which, in the best case, can be exclusive to these cells), iii) an ability to cause only mild, self-limited or no human disease, iv) the possibility of control and elimination of remaining viral particles after treatment, v) to be genetically stable; and, finally, vi) to show zero recombination events while in use.

For the purpose of this thesis, a pilot project on a combined treatment using Focused Ultrasound, Vaccinia Virus, Melphalan and TNF-α in the presence of microbubbles is expected to contribute to advances to cancer therapies. This project starts with the equipment preparation and the calibration necessary to know accurately the outputs of the equipment used and determination of the best equipment to use, then *in vitro* experiments used to help "pre-vizualise" the effects that one will get *in vivo* and finally, *in vivo* experiments that allow the testing of whether Focused Ultrasound in the presence of microbubbles enhances the activity of oncolytic virotherapy delivered during Isolated Limb Perfusion. Several mechanisms, including direct anti-tumour activity, enhancement of the activity of melphalan/TNF-alpha and increased intratumoural delivery of oncolytic viruses were considered.

2. Calibration of a Focused Ultrasound Transducer and Measurement of Cavitation Thresholds under Different Frequencies

2.1. Transducers Calibration

2.1.1. Introduction

The ultrasound beam generated by a plane transducer propagates as a longitudinal wave in soft tissue and has two distinct regions: near field (Fresnel zone) and far field (Fraunhofer zone). A focused ultrasound transducer produces a cylindrical beam that is narrowest in the focal zone, some distance from the transducer face. This US beam has side lobes due to diffraction. For therapeutic medical applications of ultrasound, beams with little lateral dispersion of energy are usually preferred and so the ultrasound beam is often focused.

There is a wide variety of FUS transducers, reported in literature and in clinical use, both in terms of geometry and drive frequency (fairly limited for FUS to the range of 0.5 to 4 MHz). It is important to design the transducer for its use and the following issues must be considered [74]:

1. The location, accessibility and size of the target.
2. The ability to deliver sufficient power to the required treatment depth, in order to provide an effective treatment. This influenced by the focal length and outer diameter of the transducer which determine the total power producing area and the focusing strength, and the frequency used which affects how much energy is absorbed at the target and lost in the overlying tissues. Lower frequencies are associated with lower attenuation losses in the overlying path and higher frequencies are favourable for greater absorption at the focus.
3. The size of the transducers matters when the available range of motion of the transducer is crucial for a specific application.

4. There must be a coupling medium between the transducer and the target and this is usually achieved with water baths in which either the transducer and the target are submerged, or one water bag is placed in between the transducer and the target.
5. If diagnostic ultrasound imaging guidance is necessary, the ultrasound transducer can be designed to incorporate an ultrasound imaging probe, preferably at its centre, enabling imaging along the therapy beam axis.

In terms of the properties of the ultrasound beam, some concepts are key to the need for calibration of the acoustic field of ultrasound beams. In any application, the intensity in the FUS beam must be known and one must not forget that [74]:

→ In the focal plane, the power is not entirely contained within the focal region, with some power being in side-lobe rings around the focal region. These are of lower intensity than the focus, and normally are of little consequence in clinical treatments using short exposures.

→ In the pre-focal beam the maximum intensity generally increases moving towards the focal plane; however, the intensity distribution is not homogeneous and there are localised regions of high and low intensity.

A quantitative characterization of the acoustic field of a FUS transducer can be made using a hydrophone - a device which provides a localised measure of the acoustic pressure. This quantitative characterization can include studies on the spatial variation (with beamplots) and/or variation of peak pressure(s) by changing the drive setting. Measurements are usually performed in degassed water, in which the ultrasound beam propagates through a non-attenuating medium, in the absence of scattering structures and cavitation nuclei.

The choice of hydrophone is dependent on a number of factors, the main considerations being: robustness, the measurement environment (e.g. degassed water, deionized water, coupling gel), sensor size, temporal stability, and flatness of the frequency response. In terms of the sensor size, both the size of the sensitive area and the size of the whole sensor because the first determines beamplot resolution and the other may affect whether the sensor fits into a system at all. Robustness is a critical factor in HIFU characterisation, since the hydrophone sensor is likely to be exposed to large peak negative pressures, and there is thus an associated risk of hydrophone damage from acoustic cavitation at its front face [74].

For this study, in order to minimise the risk of hydrophone damage, the water used for coupling medium is very well degassed (ideally less than 2 mg/l of dissolved oxygen), the water is also filtered to remove particles bigger than 5 microns, so that there are fewer cavitation nucleation surfaces available and (iii) short pulses of ~40 cycles are used so that we reach peak pressure, but reduce the number of cycles and therefore risk of cavitation.

Hydrophones, like ultrasound sources, are usually piezoelectric materials (they convert sound pressure to a voltage and *vice versa*). If a hydrophone is placed in an acoustic pressure field it produces an electrical output signal in response to the surface integral of the acoustic pressure received over its active element. Hydrophone calibration provides a value for the sensitivity of the hydrophone (expressed in mV/Pa) as a function of frequency.

For a waveform propagating linearly, the voltage values measured on an oscilloscope, V(t), can be converted to pressure, *p(t)*, using the hydrophone sensitivity, *s(f)* using the relationship $p(t) = \frac{V(t)}{s(f)}$ (3)

To decide on the best transducer to use in the present study, two transducers were calibrated in terms of acoustic power measurements, at different frequencies – one at 1.08 MHz and 1.34 MHz, and a second at 1.66 MHz. The transducers and methods are described in the next section.

2.1.2. Methods to Transducers Calibration

The calibration was performed using an automated beam plotting system (Ultrasonic Measurement System (UMS), Precision Acoustics, UK) – see figure 2.1. The ultrasonic measurement system is controlled by the Host PC by means of dedicated LabVIEW™ based software. This application controls all aspects of the operation of the system including:

- Communication with a LeCroy 64xi digital oscilloscope for acquistion of averaged waveforms
- Positioning in 3 orthogonal directions, via actuation of the stepper motors
- Waveform acquisition by the oscilloscope and subsequent transfer of data to the host computer
- Archival and post-processing of acquired data.

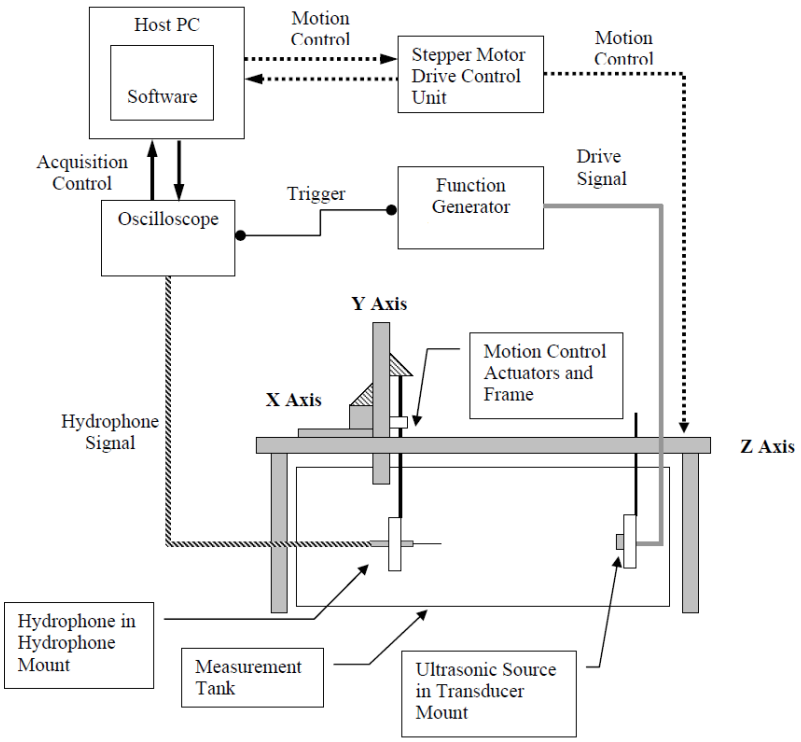

Figure 2.1. Schematic diagram of the beam plotting system

Calibration was used to find which function generator drive levels (in mV) gave free-field peak negative pressures from 0.3 to 1.8 MPa in increments of 0.3 MPa, knowing that the sensitivity of the hydrophone HGL-0200 (ONDA, USA) was approximately 45 nV/Pa for the frequencies used. The range of peak negative pressures used was based on previous publications on the subject of enhanced uptake of virus with the use of focused ultrasound.

A synchronisation signal was taken from a signal generator (the Function Generator in Figure 2.1) and used to trigger the oscilloscope. The FUS transducer was held in a fixed position perpendicular to the hydrophone, with both beam axes aligned parallel to each other, and was at first centred by visual inspection. The focus was then located by finding the maximum amplitude signal on the oscilloscope, while moving the gantry manually, being careful to ensure that the peak that had been found was not a side lobe.

After finding the focal peak position using spatial increments of 0.5 mm, relatively coarse one-dimensional scans were set up to record the pressure distribution along x, y and z, - see Figure 2.2 - to check the symmetry of the profile. The peak positive and peak negative voltages were measured at each position from a waveform averaged 100 times.

The root mean square voltage was calculated in Matlab (The MathWorks, Inc.), then converted to the root mean square pressure – see equation 3.

Pressure measurements were performed at the focal peak of the FUS field over a range of signal generator voltage settings at the three different frequencies (for the two different transducers) and at increments of 0.25 mm, over a distance of 4 mm around the focus in two directions, X and Y. The water inside the UMS tank was filtered and degassed to reduce the dissolved oxygen level (<2mg/l) to decrease the possibility of cavitation and UV light exposed to keep it clean.

The series of files, each of which contained the voltage waveform acquired from the hydrophone at each measurement location, was post-processed using Matlab code designed for the purpose (although UMS software could have been used). Linear scans of the pressure (in MPa) as a function of the distance from the focus (in mm) at each drive level were produced at the three different frequencies and then Pressure (in MPa) was plotted as a function of the Drive Level (in mV). Peak negative pressure values will be considered for further applications because inertial cavitation is more likely to happen due to the growth of a bubble during one cycle of tension (during the negative phase of acoustic cycle).

In the next section, transducer calibration results are shown for measurements at 1.08 MHz only, since similar results were found at the other two frequencies. The main difference is that the focus is narrower at higher frequencies. The focal dimension at 1.08 MHz is (considering a planar oval shaped figure) ~13 mm height and ~1.79 mm width, at 1.34 MHz, it is about ~13 mm height and and ~1.42 mm width and at 1.66 MHz it is ~10 mm height and 1.21 mm width.

In terms of the error of the experiments, the National Physics Laboratory (NPL) which is the UK's National Measurement Institute - a world-leading centre of excellence in developing and applying the most accurate measurement standards, science and technology - specifies the error of the hydrophone detection to 7% of the measured value. However, a value an error of 10% of in each measurement was considered to avoid any underestimation. This applies throughout the experiments in this dissertation.

2.1.3. Results from Transducers Calibration

The Acoustic Calibration Results at 1.08 MHz in the Y axis are shown in Figure 2.2.

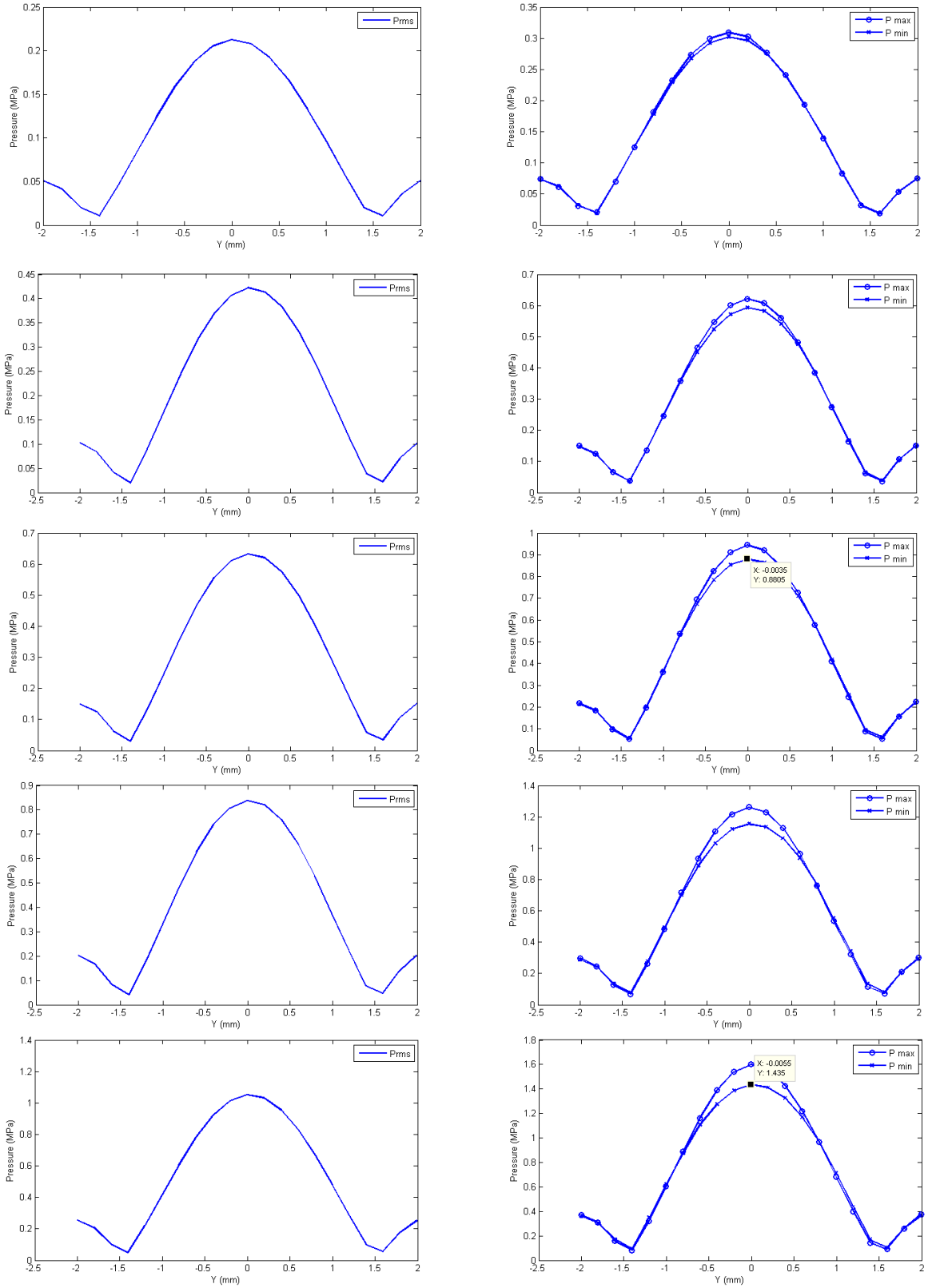

Figure 2.2. Ultrasound pressure profiles in Y (in MPa) as a function of Distance from focus (in mm) at drive levels of 166.7, 333.3, 500, 666.7 and 833.4 mV (from top to bottom). Prms corresponds to the RMS pressure, P max and P min correspond to peak positive and peak negative pressures, respectively. Nonlinearity can be seen at the highest drive levels where Pmax > Pmin

The Acoustic Calibration Results at 1.08 MHz in the X axis are shown in Figure 2.3

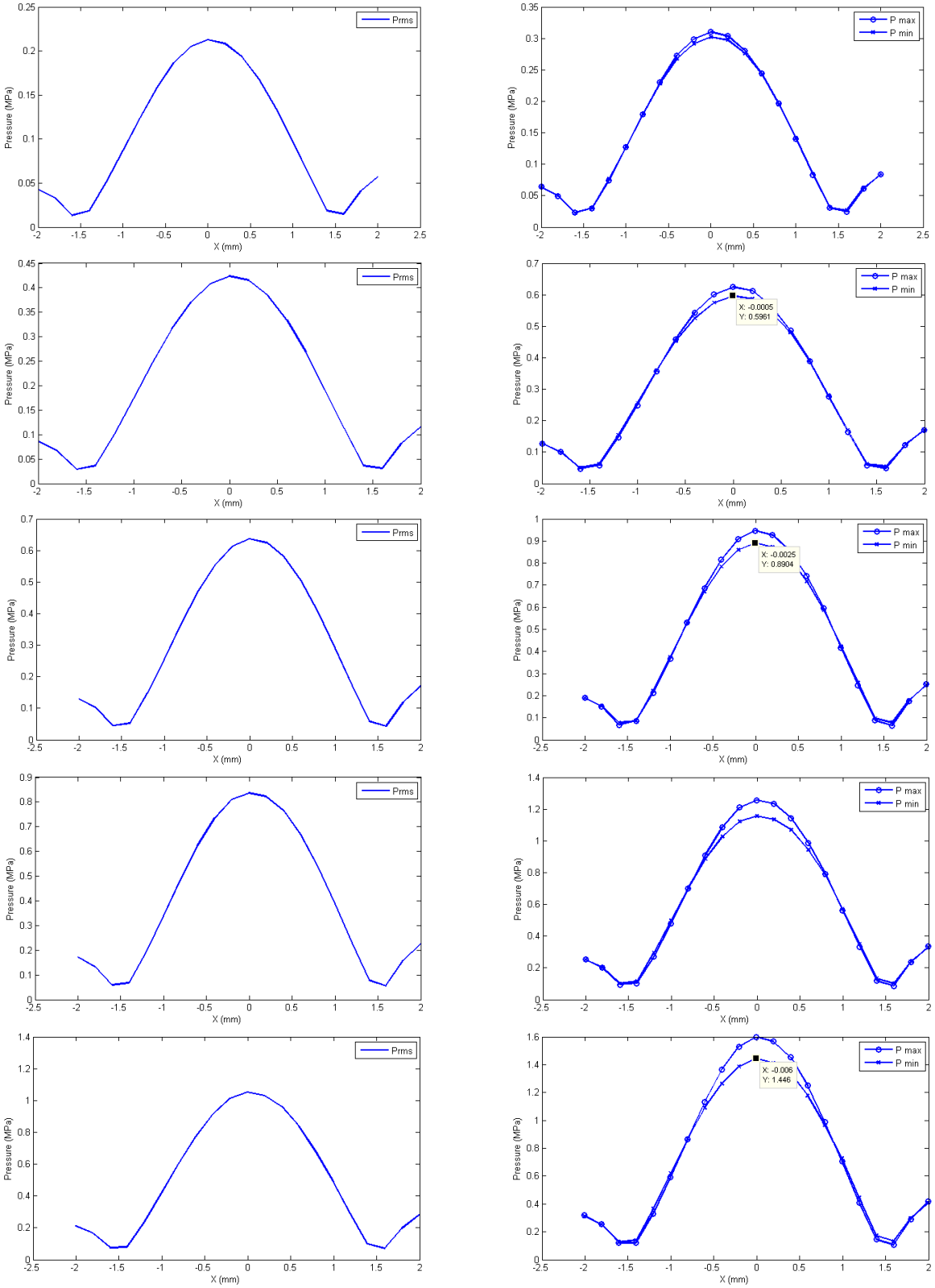

Figure 2.3. Ultrasound beam profiles in X as the Pressure (in MPa) as the function of Distance from focus (in mm) at the drive levels of 166.7, 333.3, 500, 666.7 and 833.4 mV (from top to bottom). Prms corresponds to the RMS pressure, P max and P min correspond to peak positive and peak negative pressures, respectively. Nonlinearity can be seen at the highest drive levels where Pmax > Pmin

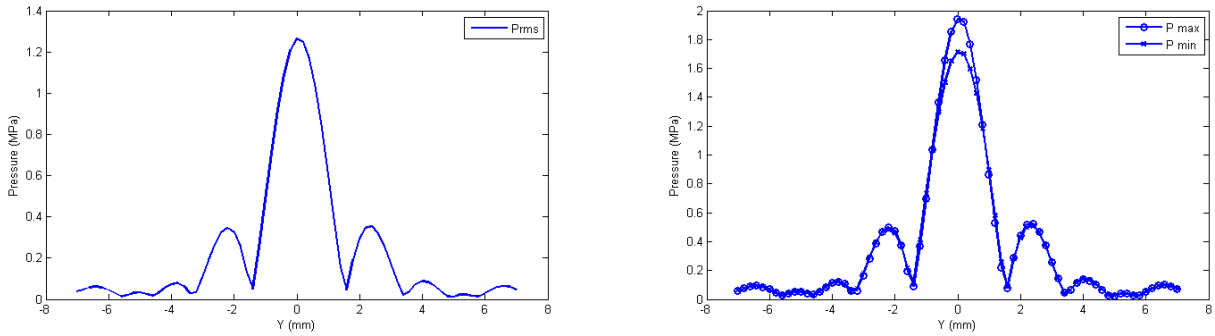

*Figure 2.4. More extensive ultrasound beam plot in **Y axis** at the drive level of 1V and drive frequency of 1.08 MHz to check if the main lobe and the side lobes imediately after the main lobe would be inside the well-plates used for in vitro experiments, to be sure that at least 80% of the energy of the beam would be used.*

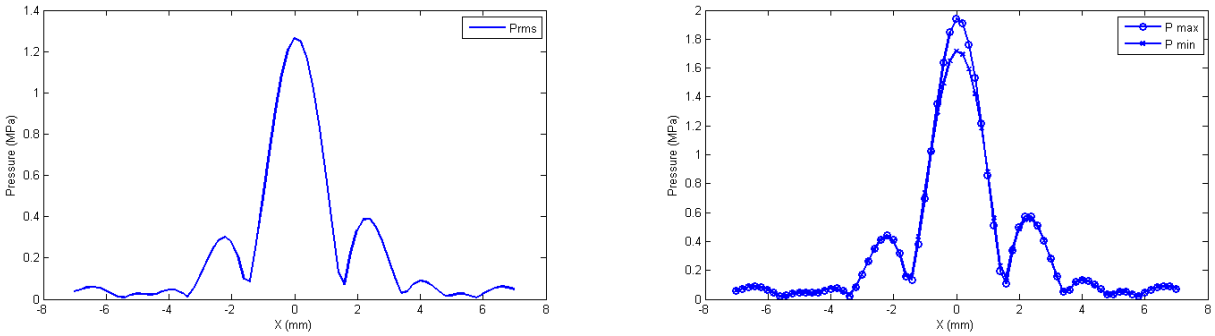

*Figure 2.5. Longer ultrasound beam plot in **X axis** at the drive level of 1V and drive frequency of 1.08 MHz to check if the main lobe and the side lobes imediately after the main lobe would be inside the well-plates used for in vitro experiments, to be sure that at least 80% of the energy of the beam would be used.*

The Acoustic Calibration as a function of signal generator drive voltage at 1.08 MHz is shown in Figure 2.6.

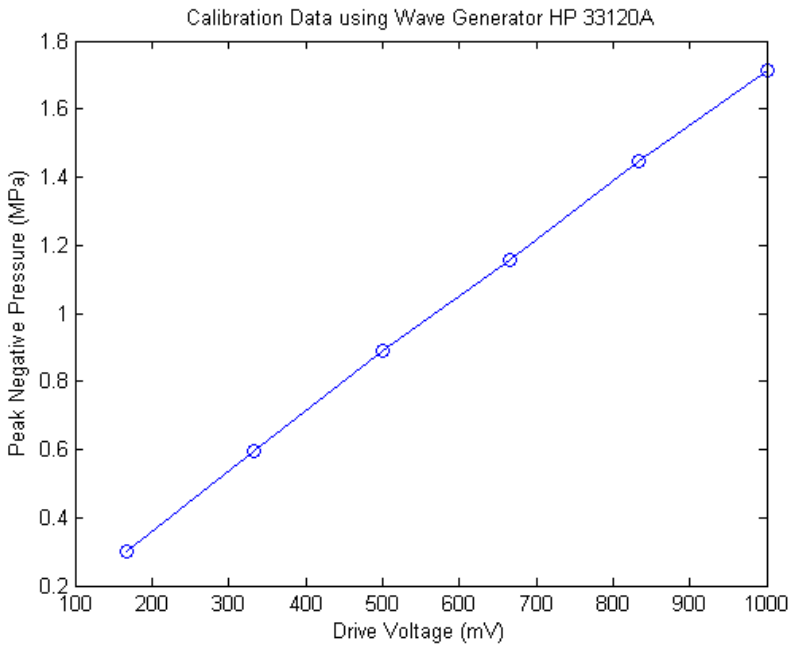

Figure 2.6. Pressure (in MPa) plotted as a function of the Drive Level (in mV) at 1.08 MHz.

The Acoustic Calibration Curve as a function of signal generator drive voltage at 1.34 MHz is shown in Figure 2.7

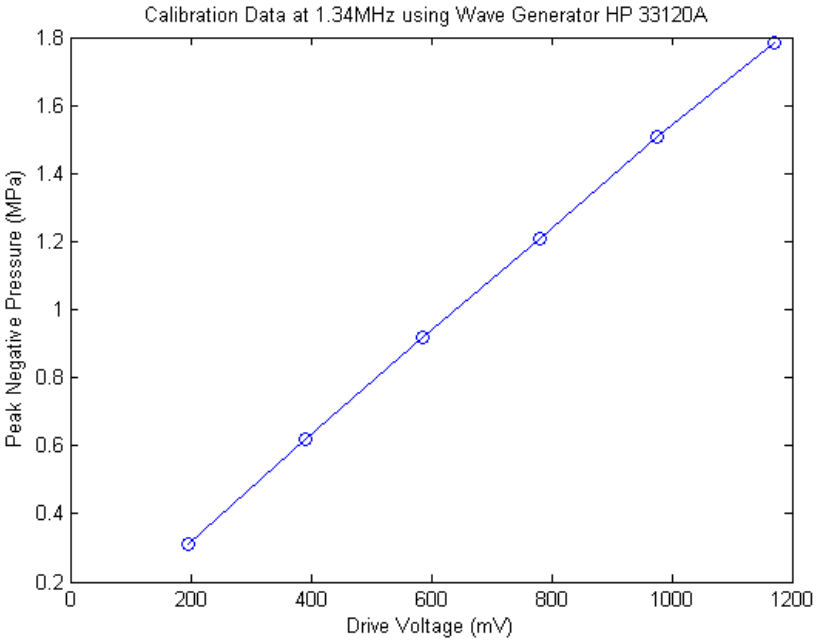

Figure 2.7. Pressure (in MPa) plotted as a function of the Drive Level (in mV) at 1.34 MHz.

The Acoustic Calibration Curve as a function of signal generator drive voltage at 1.66 MHz is shown in Figure 2.8

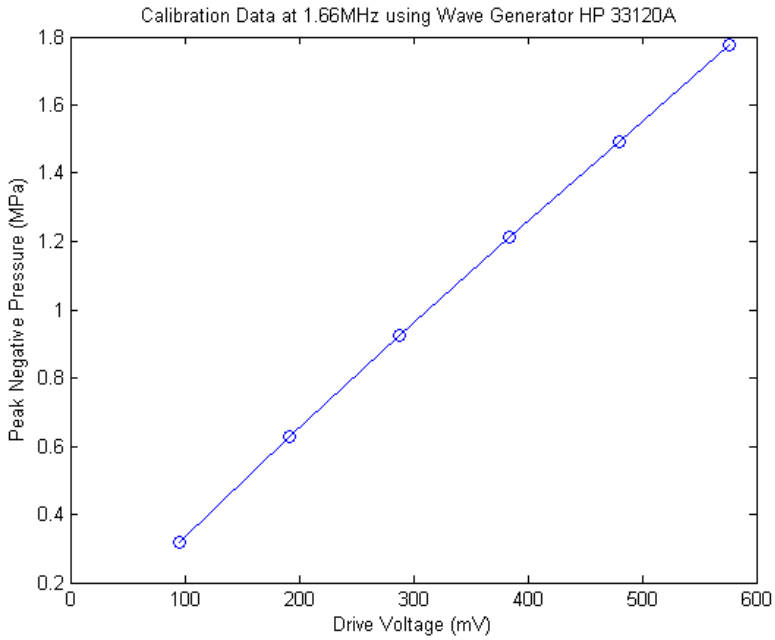

Figure 2.8. Pressure (in MPa) plotted as a function of the Drive Level (in mV) at 1.66 MHz.

2.2. Measurement of Cavitation Thresholds

2.2.1. Brief Review on Cavitation Thresholds Measurement

One of the first approaches to cavitation detection was reported in the early 90s. Huber *et al.* [75] built a hydrophone based on the system designed by Staudenraus and Eisenmenger [76] which detects changes in refractive index in the surrounding medium arising from pressure changes. This device was compared with membrane and needle hydrophones in terms of its pressure sensitivity, but no attempt was made to quantify the detected cavitation.

More recently, Koch and Jenderka [77] used a Fiber Optic Hydrophone (FOH) system based on a heterodyne interferometer to measure bubble activity in an ultrasonic cleaning bath filled with deionised, degassed water. The FOH was used to measure both the incident acoustic pressure and half harmonic and broadband bubble emission signals, simultaneously. Comparisons of the measured fundamental half harmonic and broadband "cavitation noise power" between 1-1.25 MHz were then made. These studies provided information regarding environments where cavitation is expected to occur, but have not addressed the lower limit of detection of cavitation signals at pressures close to the cavitation onset threshold, which is important for FUS applications.

A number of definitions of cavitation thresholds exist in the literature. Studies have used visual detection to determine a threshold pressure for either the appearance of cavitation bubbles coming out of solution [78] or the onset of oscillation and/or collapse of pre-existing microbubbles [79]. Typically, during biological studies, the amount of cavitation is quantified using a method considered appropriate for the application, and from these data a relevant pressure threshold can be defined if necessary. A number of studies have chosen to use a "cavitation dose" type measurement which measures the total amount of a "cavitation signal" received over a given time [80-82] but in these studies specific pressure thresholds have not been defined. Chen *et al.* [83] used summation of voltage signals over a frequency range below the FUS drive frequency as "cavitation dose".

Kyriakou *et al.* [84] measured broadband activity within adipose tissue exposed to HIFU at different frequencies. They used the variance of voltage signals detected using a 15 MHz centre frequency PCD, over a range of 5-20 MHz, after high-pass filtering at 5 MHz to exclude the HIFU drive frequency and the first 3 harmonics. Higher harmonic

frequencies were also excluded from the broadband range, but comb filtering the data in softwar. Variance values were used to quantify inertial cavitation. The threshold for detection of inertial cavitation was defined as the minimum negative pressure at which any signal greater than 6 standard deviations above noise occurred.

Inertial cavitation thresholds have been measured in a range of tissues and phantom materials by Maxwell *et al*. [85] for two-cycle HIFU pulses. To account for the many harmonics present in the drive signal, the presence of cavitation was determined by measuring the deviation of an integrated power spectrum from expected values, calculated from field measurements in the absence of cavitation. Thresholds were defined at the 50% probability level for which the measured integrated power was greater than 5 standard deviations above the expected value.

2.2.2. Methods of Cavitation Thresholds

For any FUS exposure the following are needed: a timer, a signal generator, an amplifier, a pick-off box for measuring drive voltage and current, a scope to read the voltage and current and a FUS transducer and an impedance matching box. As cavitation detection was required, a PCD, filters, pre-amplifiers and a data acquisition system were also used. The equipment used was as follows:

- Timer Box Ultrasound Timer 2.0 (built in house)
- Signal generator Agilent 33120A (Agilent Technologies, Singapore)
- Power Amplifier E&I A300 (Electronics & Innovation, Florida)
- Pick-off box built in house (to measure V/1000 and I*10)
- Oscilloscope LeCroy Waverunner 64Xi (LeCroy Corporation, New York)
- FUS transducer working at 1.66 MHz(Sonic Concepts, Washington)
- Matching Box (Sonic Concepts, Washington)
- Passive Cavitation Detector (PCD)
- Notch Filter (1.7 MHz) built in house
- Pre-amplifier (Model 7866, Advanced Receiver Research, Burlington, CT, USA)
- Desktop Computer as Data Acquisition System (Supermicro, United States)
- acoustic 15 well plates and well plate holder designed & built in house

- Gantry (Time and Precision, Hampshire, UK) and in house built Motion Controller
- Aluminium arm
- Control Computer Latitude E6510 (Dell Inc., United States)
- Perspex Water Tank
- Fibre-optic hydrophone PAFOH10 (Precision Acoustics, Dorchester, UK) and purpose built fibre-optic hydrophone holder

Exposures of Dulbecco's Modified Eagle Medium (DMEM) cell culture medium were made in acoustic well-plates developed *in-house* (see figure 2.9). These have a permanent, but replaceable, lower acoustically transparent window (19 micron thick Melinex) and are designed to be filled with the sample before an upper membrane is clamped into place (being careful to avoid trapping bubbles in any of the wells).

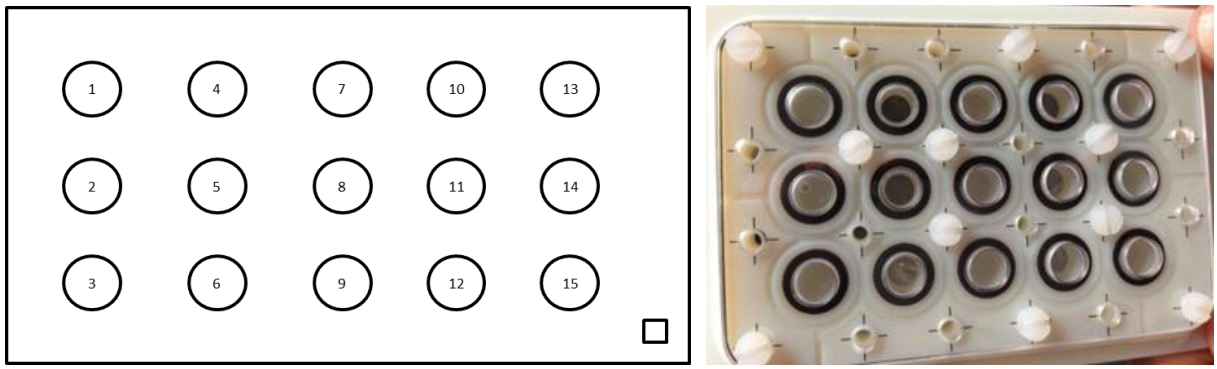

Figure 2.9. Schematic of well-plate built in house (left) and photograph (right). The volume of each well was approximately 0.5ml. The diameter is just under 7 mm wide which meant that if the 1.66 MHZ transducer was used the beam should just clear the sides of the well when the focal peak is placed in the middle of the well (in 3D).

In order to target each well on the well plate, a "small" radiotherapy platform (see Figure 2.10) and its motion controller (not shown) were used and controlled using Matlab code developed *in-house*. The radiotherapy platform allows precise control of positions in 3 orthogonal directions under remote computer control and *in-house* built software allow the movement between each well after localising on one of the corner wells.

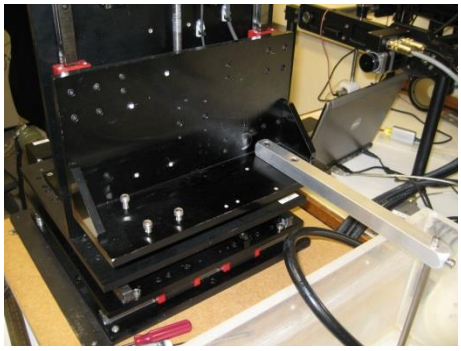

Figure 2.10. Radiotherapy Platform used to move the ultrasound transducer automatically and precisely from well to well.

The targeting process did not require imaging guidance, but did require good accuracy. This setup allows the placement of a 10 mm long by 1.0 mm diameter focal region in the centre of a 7 mm diameter, 7 mm long well using a specially built fibre-optic hydrophone holder designed to locate the centre of the well when filled with degassed water and have no upper acoustic window. It should be noted that with cells in medium or in medium only, it is very likely that acoustic cavitation will occur at much lower pressures than in tissue and that the radiation force associated with the ultrasonic pressure wave will vigorously stir the solution due to acoustic streaming. Both of these produce artefact effects. The setup for exposures *in vitro* is shown in Figure 2.11.

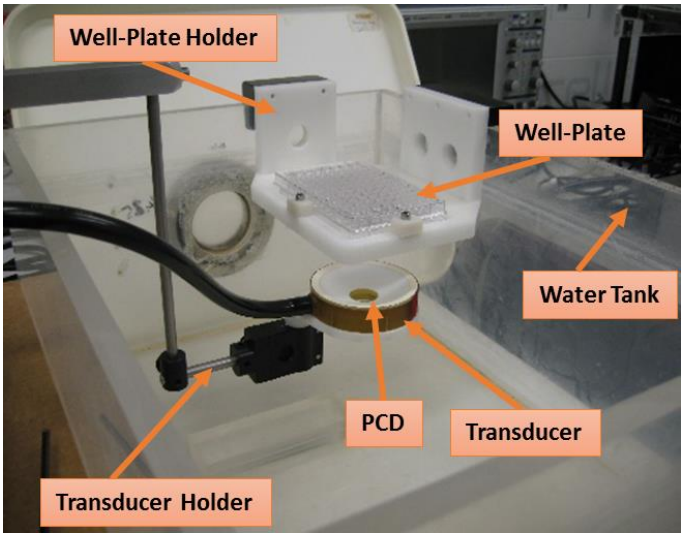

Figure 2.11. Example for setup to exposures in vitro (the tank is filled with degassed water prior to any exposure). The well-plate holder is holding a standard 96 well plate, which could not be used for US exposures because the thick perspex was not acoustically transparent and the plate could not be totally submerged. This means that there would be almost complete reflection of the ultrasound beam at the liquid air interface in each well and so, ultrasound exposure levels could not be accurately measured.

A PCD was used to detect any ultrasonic signals emitted by cavitating bubbles. In these experiments, the drive frequencies were 1.08, 1.34 and 1.66 MHz and broadband

signals in the range of 3-10 MHz were recorded. This range was chosen because apart from the primary resonance, a number of superharmonic resonances, usually of the fundamental and the half harmonic, can take place, for frequencies of excitation being below the natural frequency of the PCD which is 15 MHz. Adding to this, the highest contribution, when an effect is present in cavitation detection data, comes from lower frequencies. However, if lower frequencies are included in the analysis, there are potential complications from widening fundamental and second harmonics, which seem to be less problematic from the 3rd harmonic on – this is based on previous experiments on cavitation detection in the ICR's Therapeutic Ultrasound Team. The signal from the PCD is passed through a notch filter centred at 1.7 MHz (Allen Avionics Inc., NY, USA), which reduces the component of the signal at the fundamental frequency (f_0) of the HIFU drive field by ~80 dB. This is done in order to avoid saturating the digitising electronics and preventing detection of the lower amplitude broadband and harmonic signals. Then, the signal goes through a 20 dB preamplifier (Advanced Receiver Research, Burlington, CT, USA).

A data acquisition computer (DataQuest Solutions, Bedfordshire, UK), with two 500 GB SATA hard drive and 12 GB RAM, allows the storage and processing of large quantities of PCD data in real time. A built-in 12-bit high speed Peripheral Component Interconnect (PCI) data acquisition (DAQ) card (Spectrum Systementwicklung Microelectronic, Germany) with 256 MB on-board memory allows digitization and storage of data from up to 4 channels at a maximum of 50 MHz sampling rates, in First In First Out (FIFO) mode. This is important because, from the Nyquist limit this means that the highest frequency that can be reliably detected is 25 MHz. Which is much higher than the top of our broadband range of interest (10 MHz). A 2 step buffer strategy is used, whereby the on-board memory of the acquisition card is used as a hardware buffer, and a specific portion of the computer memory is set aside as an additional software data buffer. Data is transfered from the on-board memory of the acquisition card to the computer memory in small blocks via the dual buses of the PC. Both the block size and the software buffer size can be user defined.

The DAQ card is controlled by a 2-stage process. First, a code written *in-house* allows specification of the number of channels to be used, the desired sampling frequency, the input impedances from the devices connected to each channel, and the total amount of time for which data should be acquired. For the purpose of the studies presented in this thesis, continuous data acquisition was required for the duration of each exposure

(typically 0.5 s), with additional 'off-time' (0.2 s) data which is used to calculate the baseline noise level.

The second stage includes a Matlab code which was written to communicate with the acquisition card via Matlab drivers. This is based on a series of C and Matlab functions provided by the DAQ card manufacturer, but was runned entirely in Matlab. The code first asks the user to specify a unique file identifier for the data (*e.g.* an exposure number). The dynamic range of the digitising card must be selected to determine the voltage range over which the available digitisation levels are assigned. For the 12-bit card, the number of digitization levels was 212, or 4096. It was only possible to specify values of 200, 500, 1000, 2000 or 5000 mV. It is important to specify a suitable dynamic range for the expected signals. If the range specified is too high, the data would be contained within only a small number of digitisation levels, leading to quantisation effects. On the other hand, the use of a range which was too low for the detected signals would result in "clipping" of the peak voltages (positive and negative). This introduces discontinuities in the time domain, creating artefacts in the frequency domain which appear as data spikes. The decision to use a particular dynamic range was in the most part based on prior experience of the therapeutic ultrasound team, and both 1000 and 2000 mV were found suitable for the experiments described in this thesis.

Finally, the acquisition code sends the user-specified details to the acquisition card, and programs it to wait for an external voltage trigger. This is provided by connecting the synchronization port on a signal generator to a trigger channel on the data acquisition card. For the experiments described in this chapter, up to 2 channels were used, Ch0 was usually used to collect PCD data and Ch1 was used for the drive voltage. A sampling frequency of 33.2 MHz was used in all experiments throughout this thesis. Data were saved in the computer memory in segments, and stored in binary format. Upon subsequently reading of the files into Matlab, and with the knowledge of the dynamic range setting used for each exposure, the values were then converted from integers back into mV for processing.

This study of cavitation thresholds was done to i) study the difference in thresholds depending on the HIFU frequency used, ii) chose the levels of pressure to use in *in vitro* exposures, iii) decide on the best frequency to use when microbubbles were present (the best frequency being the one closest to the resonant frequency of the microbubbles). The SonoVue microbubbles used have resonant frequencies of 1.6, 2.1 and 3.1 MHz for bubbles of 4.0, 3.2 and 2.6 μm, respectively. According to the

manufacturer's sheet, the mean diameter of the microbubbles is 2.5µm, 90% are smaller than 6µm and 99% smaller than 11µm.

The results presented here are from cavitation detection at 1.08MHz, 1.34MHz and 1.66 MHz during exposure of DMEM only, and medium with 10 or 10% concentration of microbubbles. The Pulse Repetition Frequency was fixed at 100 Hz, the pulse length was 40 cycles and the exposure of 0.5 s. The pressures applied at 1.08 and 1.66 MHz varied from 0 to 1.8 MPa in increments of 0.3 MPa but at 1.34 MHz the pressures varied from 0.2 to 1.2 MPa, in increments of 0.2 MPa. At the three different frequencies tested, one exposure was made at each drive level. All the conditions tested are based on information gathered from the literature review.

In terms of threshold definition, the increments tested did not allow accurate determination of the exact level of pressure at which inertial cavitation onset, occuring within the 0.5s exposure, could be detected. It was therefore defined by the interval in which cavitation started to occur every time, such that in the time domain analysis, on a logarithmic scale, a "hump" one order of magnitude higher than the noise level (in terms of amplitude of the detected signal, in mV) was present (unique spikes above the threshold line are not considered as broadband). There is not enough data available for a quantitative definition of the inertial cavitation threshold in DMEM and therefore an initial study was done to get an estimate of what it might be.

A more rigorous study would require closer inspection of PCD broadband off-time noise data from several exposures. A baseline would then be defined, for example, from the calculation of the mean and standard deviation of the noise levels. The signal exceeding the defined signal baseline over a certain length of time could then be considered as inertial cavitation. Single data points exceeding the baseline noise level may occur during the FUS on-time, so it is important to consider an interval of time for the threshold which distinguished occasional spikes/interference from the surrounding environment , from real cavitation activity.

Signal Processing and Analysis

The signal has been integrated over the frequency range of 3-10 MHz. Summing data minimizes effects of inherent phase differences between voltage and current (caused by impedance mismatch) such that power fluctuations reflect impedance changes caused

by bubble formation in the acoustic propagation path. Then, data was Fourier transformed (FFT) using a Hanning window function.

The level of broadband emission was obtained using a two-step process. Following the FFT calculation, a ‘‘comb’’ software filter was used to remove any harmonics (produced by nonlinear propagation) and subharmonics of the drive signal from the data. This filter set the amplitude of each harmonic to zero, to prevent their contribution to the broadband signal. Summation of amplitudes in the resultant discontinuous frequency band gave the ‘‘integrated broadband’’ emission amplitude over the entire exposure time. Thus, half harmonic and integrated broadband amplitudes, could be plotted as a function of time.

Audible emission data were processed using Matlab to extract temporal information by using 2048 points per FFT calculation, yielding a temporal resolution of 9 ms.

2.2.3. Results and Discussion of Cavitation Thresholds Measurement

In the next section, some graphs are presented in the time domain, in which case the title of each plot contains information about the exposure number (Exp), the DAQ channel (e.g Ch0), ‘SC’ stands for Sonic Concepts and identifies the transducer, the Broadband (defined as BB) frequency range shown and the HIFU drive frequency (e.g. 1.08MHz) – see Figure 2.12. For graphs in the frequency domain, the title of each plot contains the exposure number (S) , the DAQ channel used (e.g. S1Ch0), time point at which the FFT was obtained (e.g. 0.0003323s), the drive frequency (e.g. 1.08MHz) and then what is being shown, e.g. the FFT (i.e. that over 0 to 11 MHz), the HH FFT (i.e. Half Harmonic FFT shown over 0 to 1 MHz) – see Figure 2.15. Comb filtered versions of these are denoted by an additional term “comb”, and a red dashed line present in some plots indicates the cavitation threshold – as in Figure 2.15.

Results at 1.08 MHz

i) DMEM alone

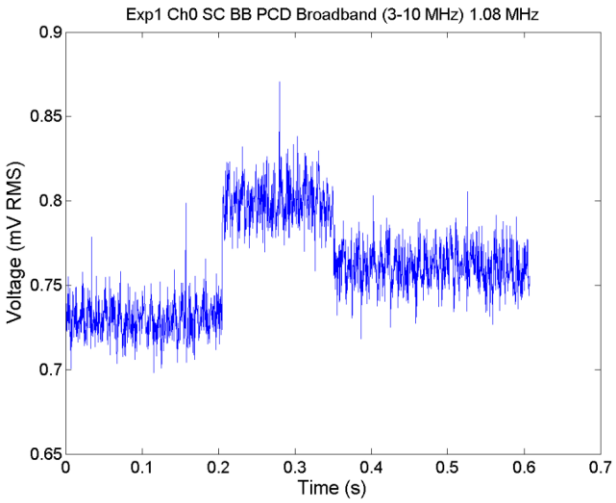

Figure 2.12. PCD broadband signal (frequency-integrated over 3-10 MHz) as a function of time for a single 1.08 MHz, 0.5 s exposure of DMEM with peak negative pressure 0 MPa. The exposure lasts 0.5 s of acquisition. No cavitation was detected, because no exposure was made. Therefore in this case the whole trace represents off-time noise of the entire PCD detection system. The graph title shows that this was exposure number one, with data acquired on Ch0 of the DAQ system.

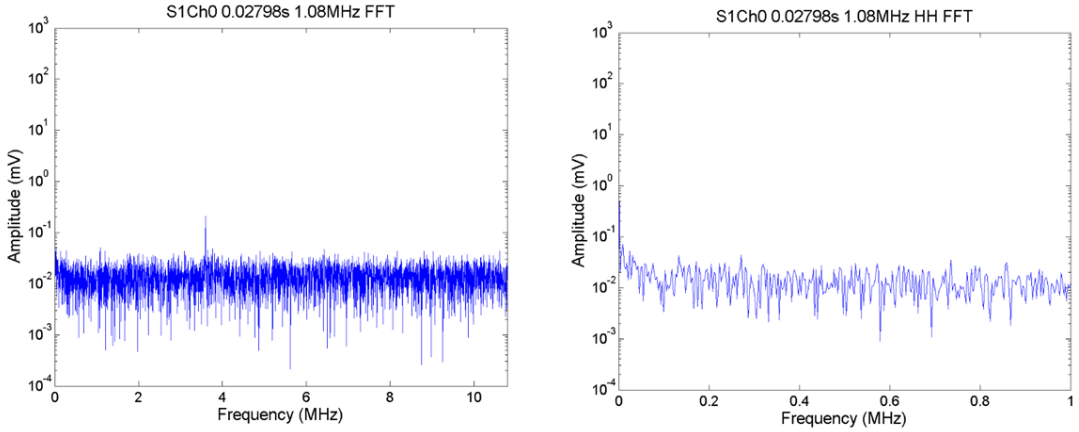

Figure 2.13. FFTs from a single segment of PCD data at 0.2798 s obtained during an 1.08 MHz, 0.5s exposure of DMEM. The FFTs show noise level broadband , only data between 3 to 10 MHz are summed, (left) and half harmonic at 0.504 MHz (right) of noise level. The peak value of this off-time noise is around 0.03 (3 x 10^-2). The title shows the exposure number (S1) and that data recorded channel 0 on the DAQ were processed

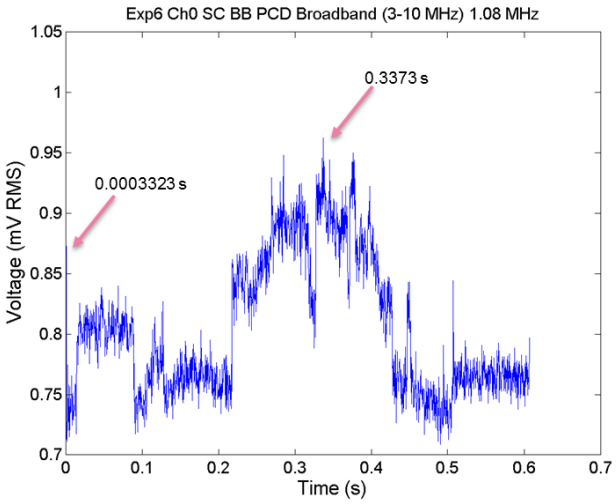

Figure 2.14. PCD broadband signal (3-10 MHz) as a function of time for a 1.08 MHz, 0.5s exposure of DMEM at a peak negative pressure of 1.5 MPa. The arrows show time points that were identified for analysis in the frequency domain because of their transiently increased amplitude above off-time noise.

In Figure 2.14, the arrows point towards data points that have significantly higher amplitude than the noise (Mean and SD of 0.785 ± 0.087 mV). The frequency domain results are shown in Figures 2.12 and 2.13. The results are inconclusive because there is not a big difference from the noise level and the previously defined threshold – there should be a bigger band of frequencies above the threshold to consider this as inertial cavitation. Figures 2.15 and 2.16 show there was 2nd harmonics (2.16 MHz) which the comb filter removed, but there are some other spikes around. This doesn't look like a wide frequency broadband effect.

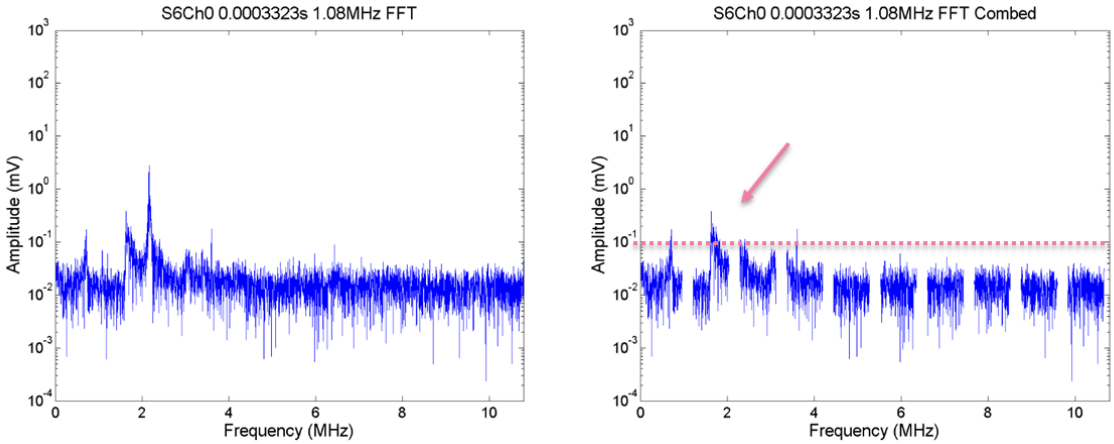

Figure 2.15. FFTs from a single segment of PCD data from a 1.08MHz, 0.5s exposure in DMEM. The whole FFT (left) and harmonic comb-filtered FFT are shown (right). To compute the broadband level the data between 3 and 10 MHz would be summed.

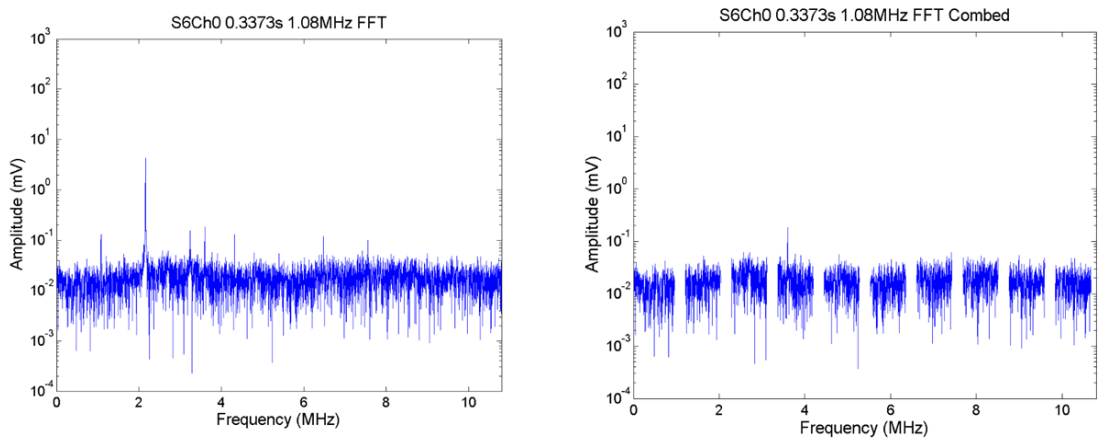

Figure 2.16. FFTs from a single segment of PCD data from a single exposure in DMEM. The FFTs show broadband component (left) and comb filtered broadband (right).

ii) DMEM plus 10% microbubbles

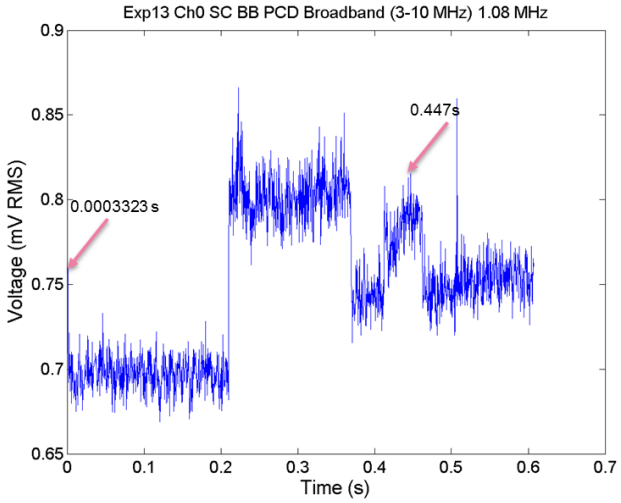

Figure 2.17. PCD broadband signal integrated over the band of 3-10 MHz as a function of time for a single exposure in DMEM with 10% concentration of microbubbles at a peak negative pressure of 0.3 MPa. The arrows show the time points analysed in the frequency domain.

Figure 2.17 shows that the broadband detected by the PCD at 0.3 MPa with microbubbles is similar amplitude to those at 1.5 MPa without added microbubbles (Figure 2.14). This suggests that microbubbles significantly lower the cavitation threshold as should be expected.

More in depth frequency domain analysis of some of the data in Figure 2.17 shows the presence of harmonics (in Figure 2.18), and ultra-harmonics (non-integer multiples of the insonation frequency) between 4 and 7 MHz (in Figure 2.19). Higher amplitude of harmonics and ultra-harmonics could represent non-linear propagation of the ultrasound

beam due to the oscillation of the MB . In Figure 2.18 the spike below 4 MHz is an artefact also seen in the off time.

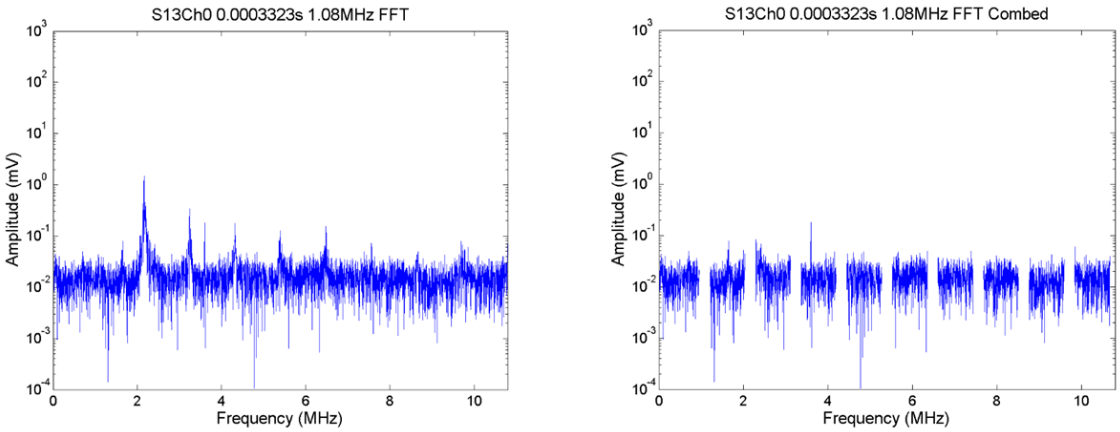

Figure 2.18. FFTs from a single segment of PCD data from a single exposure at 0.3 MPa in DMEM with 10% concentration of microbubbles. The FFTs show broadband component (left) and harmonic comb filtered broadband (right).

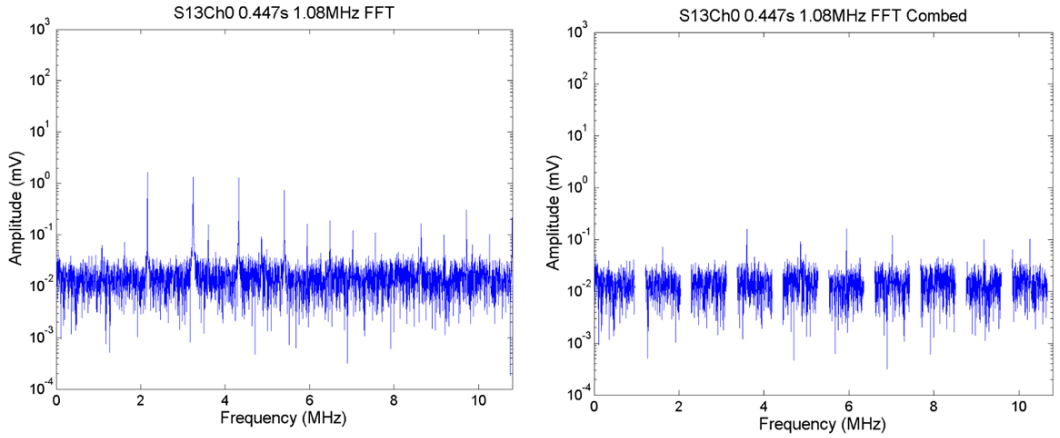

Figure 2.19. FFTs from a single segment of PCD data from a single exposure at 0.3 MPa in DMEM with 10% concentration of microbubbles. The FFTs show broadband component (left) and harmonic comb filtered broadband (right).

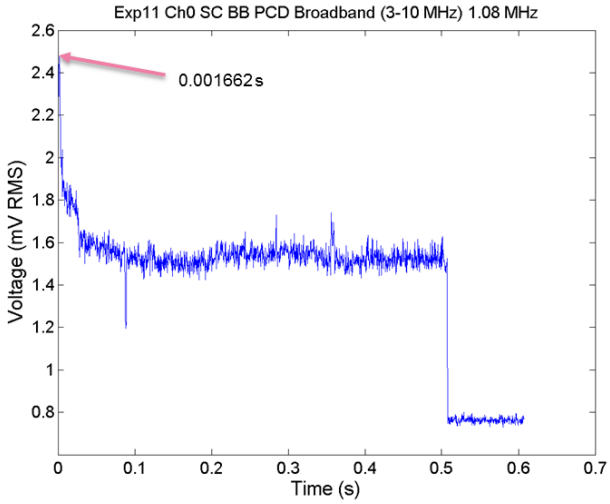

Figure 2.20. PCD broadband signal integrated over the band of 3-10 MHz as a function of time for a single exposure in DMEM with 10% concentration of microbubbles at a peak negative pressure of 0.9 MPa. The arrows show the time points analysed in the frequency domain.

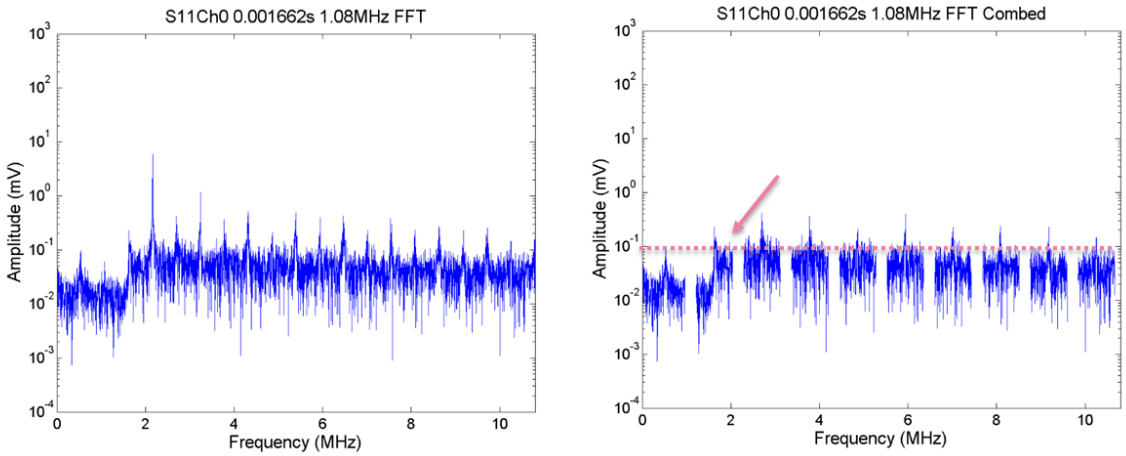

Figure 2.21. FFTs from a single segment of PCD data from a single exposure in DMEM with 10% concentration of microbubbles at 0.9 MPa. The FFTs show broadband component (left) and harmonic comb filtered broadband (right). Comparing this to the off-time noise (over 3-10 MHz), there is a clear elevation and broadband, suggesting this could well be cavitation.

Figure 2.21 shows harmonics, which are succesfully comb filtered and ultra-harmonics which are not, but more importantly, compared to the off-time noise reference level obtained from Figure 2.12, there is an increased amplitude above ~0.03mV across the 3-10 MHz broadband integration frequency range.

Regarding the definiton of cavitation threshold, it is suggested that the threshold is around 0.9MPa. This happens at an amplitude of 2.47 mV in terms of broadband amplitude at the time point 0.00166s. This early activity suggests that as the ultrasound beam reaches the target, microbubbles vibrate non-linearly and collapse. The continued

activity in terms of harmonics and ultra-harmonics could be due to smaller bubbles perhaps originating from those destroyed (daughters) that continue oscillating .

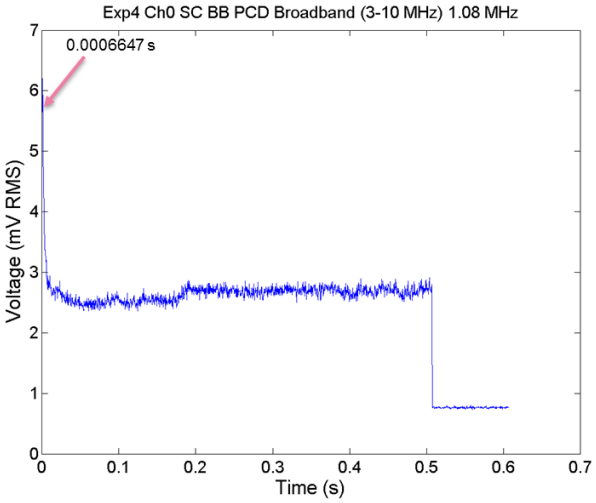

Figure 2.22. PCD broadband signal integrated over the band of 3-10 MHz as a function of time for a single exposure in DMEM with 10% concentration of microbubbles at a peak negative pressure of 1.2 MPa. The arrow shows a time point analysed in the frequency domain.

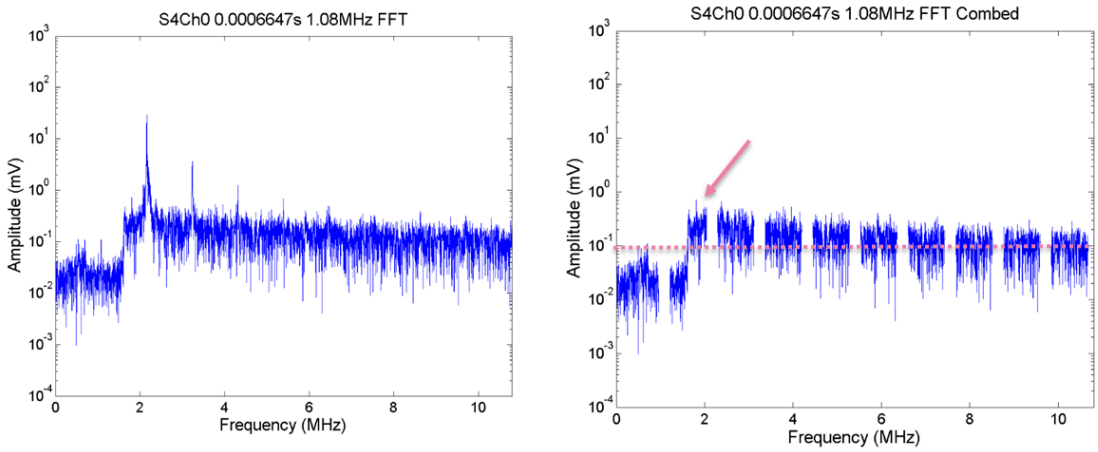

Figure 2.23. FFTs from a single segment of PCD data from a single exposure in DMEM with 10% concentration of microbubbles. The FFTs show broadband component (left) and harmonic comb filtered broadband (right).

Figure 2.22, shows results from cavitation detection at 1.2 MPa, above the reference cavitation threshold (as in Figure 2.23). In Figure 2.22 it is possible to see a higher amplitude broadband signal in the time domain. Following the logic used before, the "massive" destruction of microbubbles happens at the time point of 0.000665s – earlier than at 0.9 MPa and with an amplitude approximately 2.5 times higher (6.21 compared to 2.47 mV).

iii) DMEM plus 20% microbubbles

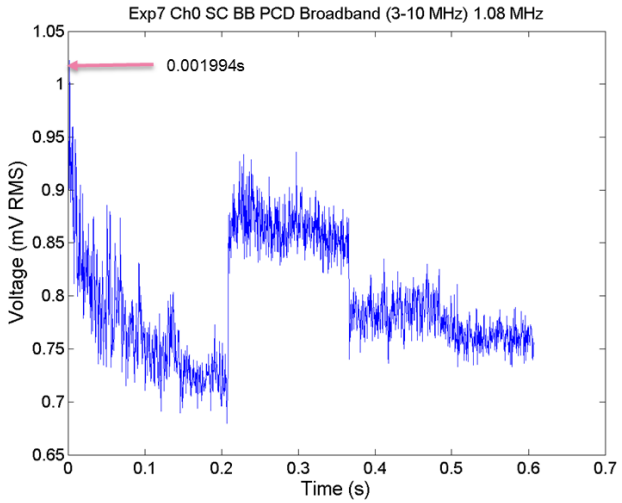

Figure 2.24. PCD broadband signal integrated over the band of 3-10 MHz as a function of time for a single exposure in DMEM with 20% concentration of microbubbles at a peak negative pressure of 0.6 MPa. The arrows points towards a time points chosen to analyse in the frequency domain.

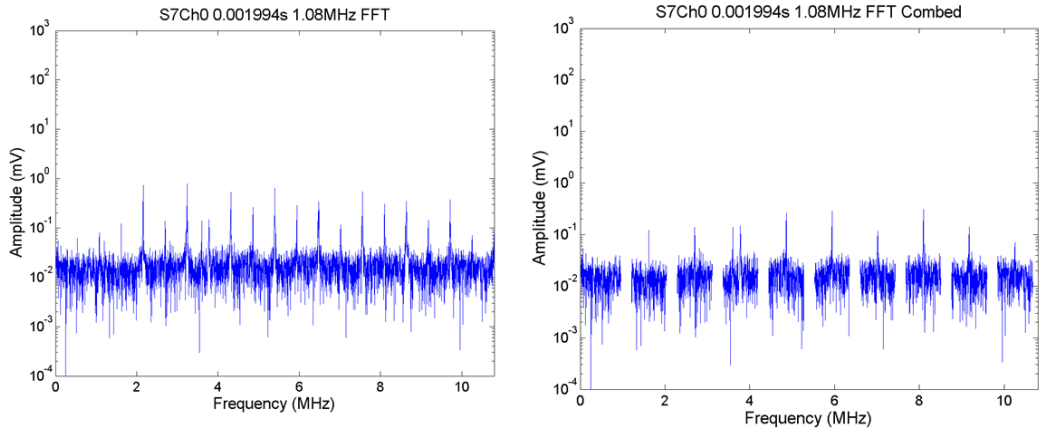

Figure 2.25. FFTs from a single segment of PCD data from a single exposure in DMEM with 20% concentration of microbubbles. The FFTs show broadband component (left) and harmonic comb filtered broadband (right).

The higher broadband amplitude detected in the beginning of the exposure of DMEM with 20% concentration of microbubbles at 0.6 MPa (Figure 2.24), could be due to a decreased cavitation threshold in the presence of more dissolved microbubbles in the sample. Figure 2.25 disproves this hypothesis because this shows the presence of only harmonics and ultra-harmonics. There is no broadband seen at 0.6 MPa.

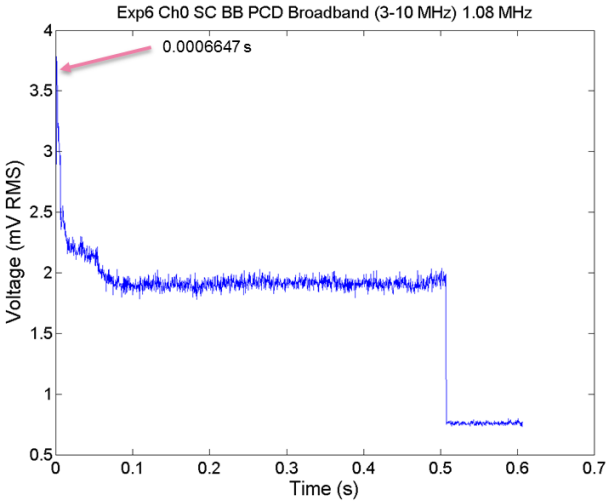

Figure 2.26. PCD broadband signal integrated over the band of 3-10 MHz as a function of time for a single exposure in DMEM with 20% concentration of microbubbles at a peak negative pressure of 0.9 MPa. The arrow show a time point chosen to analyse in the frequency domain.

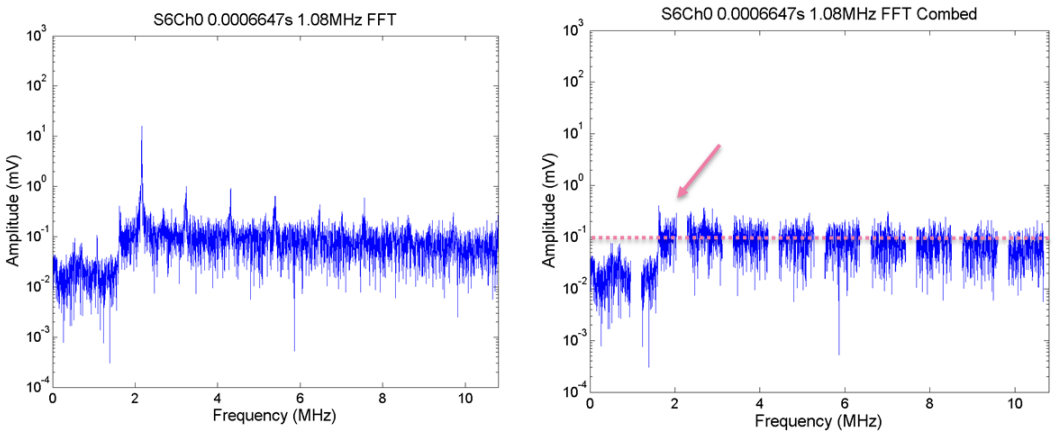

Figure 2.27. FFTs from a single segment of PCD data from a single exposure in DMEM with 20% concentration of microbubbles. The FFTs show broadband component (left) and harmonic comb filtered broadband (right). Comparing this to the off-time noise (over 3-10 MHz), there is a clear elevation and broadband, suggesting this could well be cavitation.

At 0.9 MPa, harmonics and broadband activity can be seen in Figure 2.27. Detection is above the cavitation threshold previously defined at an amplitude of 3.74 mV in terms of broadband at the early time point of 0.000665s. The detected amplitude in the frequency domain suggests that the cavitation threshold is not at 0.9 MPa but lies between 0.6 and 0.9 MPa – the pressures tested. To find the threshold more precisely, measurements at pressures lower than 0.9 MPa would need to be carried.

Results at 1.34 MHz

i) DMEM alone

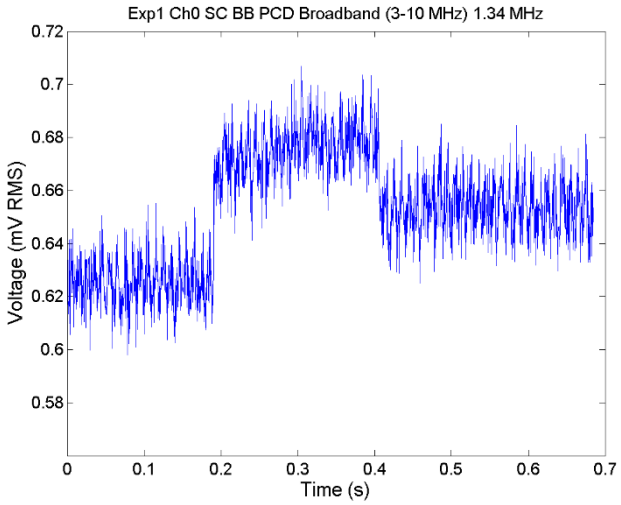

Figure 2.28. PCD broadband signal (frequency-integrated over 3-10 MHz) as a function of time for a single 1.34 MHz, 0.5 s exposure of DMEM with peak negative pressure 0 MPa. The last 0.1 s of acquisition is the off-time noise. No cavitation was detected, because no exposure was made. Therefore in this case the whole trace represents off-time noise of the entire PCD detection system. The graph title shows that this was exposure number one, with data acquired on Ch0 of the DAQ system. Average noise is 0.655 ± 0.051 mV, and highest noise is ~0.7 mV.

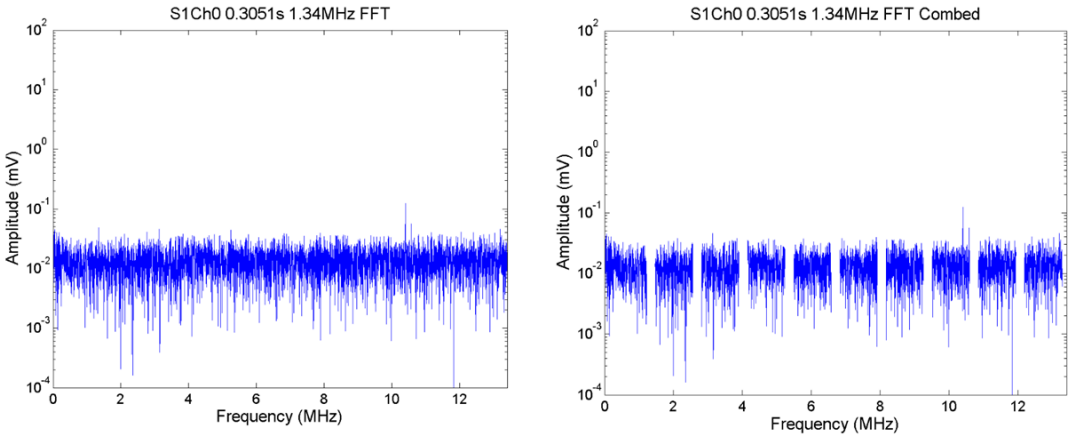

Figure 2.29. FFTs from a single segment of PCD data from a single exposure in DMEM. The FFTs show broadband component (left) and harmonic comb filtered broadband (right). FFTs from a single segment of PCD data at 0.3051 s obtained during an 1.34 MHz, 0.5s exposure of DMEM. The FFTs show noise level broadband , only data between 3 to 10 MHz are summed, (left) and comb filtered broadband (right) of noise level. The peak value of this off-time noise is around 0.03 (3 x 10^-2). The title shows the exposure number (S1) and that data recorded channel 0 on the DAQ were processed

The noise level at 1.34 MHz was of mean and SD 0.655 ± 0.051 mV in the PCD broadband signal. The cavitation threshold in DMEM was found to lie between 0.85 and 1.06 MPa, since measurement at focal peak negative pressures of 0.85 MPa did not show any broadband but at 1.06 MPa, values above the cavitation threshold were found (Figure

2.31). Broadband was detected at 0.000665 s with an amplitude of approximately 3.55 mV.

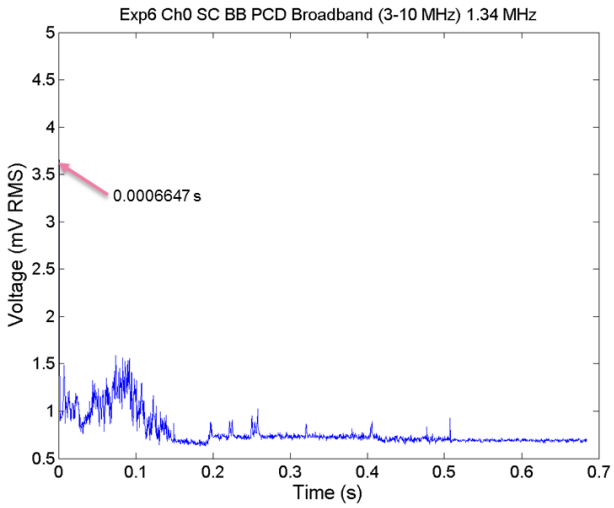

Figure 2.30. PCD broadband signal integrated over the band of 3-10 MHz as a function of time for a single exposure in DMEM at a peak negative pressure of 1.06 MPa. The arrows show the time points chosen to analyse in the frequency domain.

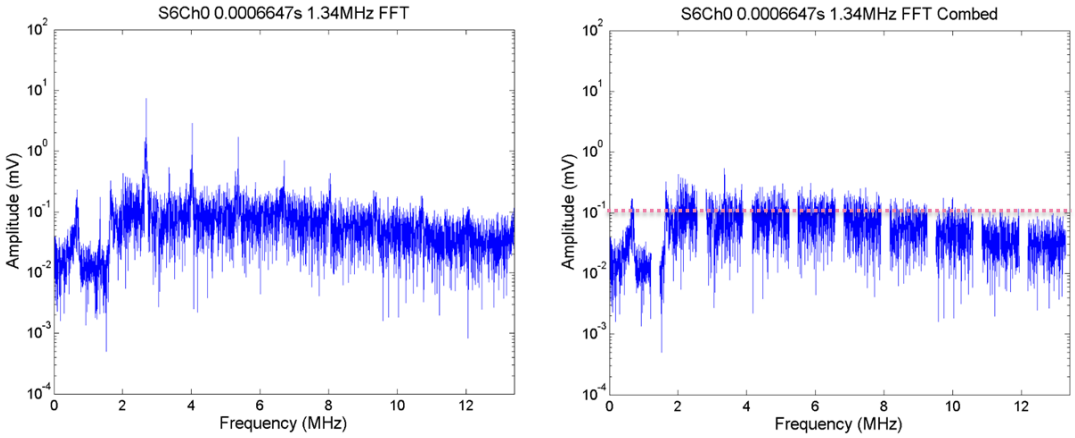

Figure 2.31. FFTs from a single segment of PCD data from a single exposure in DMEM. The FFTs show broadband component (left) and harmonic comb filtered broadband (right).

It is important to remember that, at 1.08 MHz, it was not possible to detect a cavitation threshold in the range of pressures tested (from 0.3 to 1.8 MPa). There is a difference between these measurements – the medium (DMEM) was of the same, but was tested under different conditions. For the first measurements at 1.08 MHz, the medium used had been transfered from the main bottle (stored in a cold room at approximately 5ºC) to a falcon tube one day before the experiment, and for the experiments at 1.34 MHz

the sample was transfered to a falcon tube on the day of the experiment. This probably made a difference in the quantity of dissolved gases in the sample. In all the experiments at 1.34 and 1.66 MHz, the samples of DMEM were maintained at room temperature (~23º) for approximately 1h prior to experiments.

The other difference in between experiments at 1.08 MHz and at 1.34 MHz is that the beam width at 1.08 MHz is wider, so the energy is spread into a wider region. In terms of experimental variation it would have been important to repeat at least measurements at one frequency to see how reproducible the results were. It is not possible to state if the reason for the difference in results is the state of the medium or the use of a different frequency. There are also uncertainties in the pressures - each pressure quoted is +/- 10%. This is not a big value but the pressure levels tested were quite far apart so the uncertainty in the cavitation threshold is bigger than this. Finally, by definition, it is harder to detect smaller amounts of broadband, so the sensitivity of the hydrophone decreases with the amount of cavitation.

ii) DMEM plus 10% of microbubbles

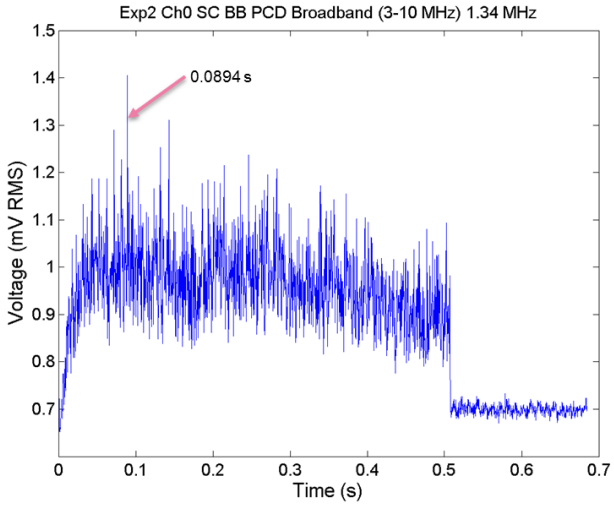

Figure 2.32. PCD broadband signal integrated over the band of 3-10 MHz as a function of time for a single exposure in DMEM with 10% concentration of microbubbles at a peak negative pressure of 0.21 MPa. The arrow shows a time point analysed in the frequency domain.

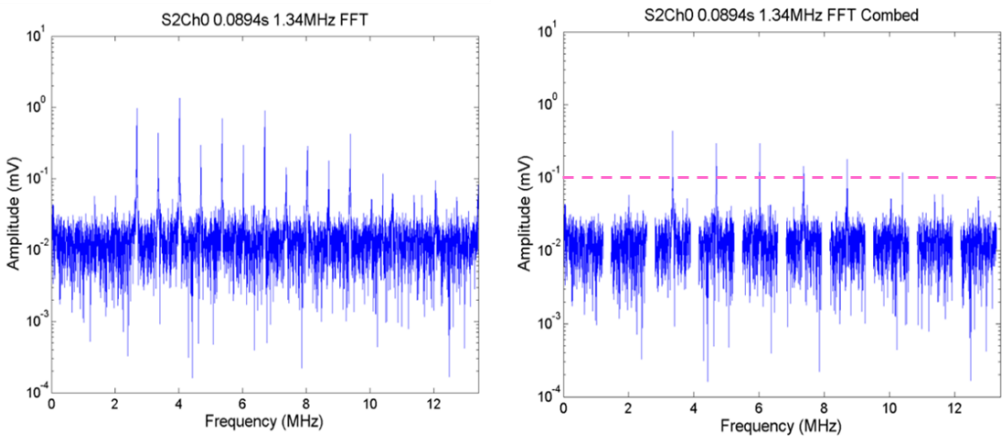

Figure 2.33. FFTs from a single segment of PCD data from a single exposure in DMEM with 10% concentration of microbubbles. The FFTs show broadband component (left) and harmonic comb filtered broadband (right).

Figures 2.32 and 2.33 show the influence of microbubbles in DMEM with 10% microbubble concentration at 0.21 MPa. The presence of harmonics (1st harmonic with lower amplitude and then, 2nd to the 7th harmonic with higher amplitude) suggest nonlinear HIFU propagation and ultraharmonics in the absence of broadband signal suggest stable (non-destructive) bubble oscillation. This happened at 1.08 MHz but the amplitude of harmonics and ultraharmonics was lower than at 1.34 MHz – see Figures 2.19 and 2.21. This difference may be due to driving at a value closer to the resonant frequency of the SonoVue Microbubbles.

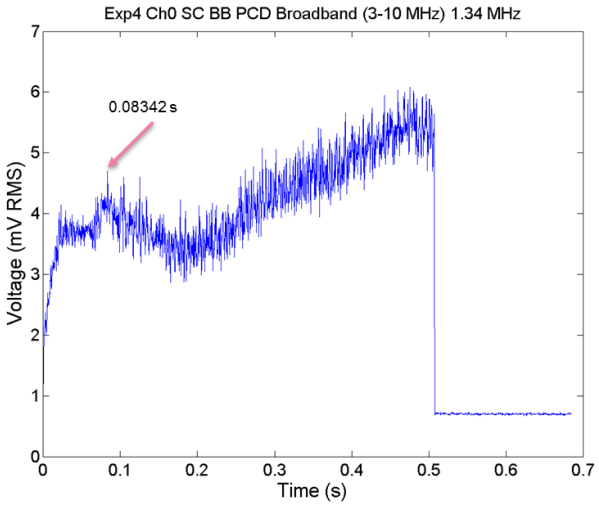

Figure 2.34. PCD broadband signal integrated over the band of 3-10 MHz as a function of time for a single exposure in DMEM medium with 10% concentration of microbubbles at a peak negative pressure of 0.64 MPa. The arrows show a time point chosen to analyse in the frequency domain through FFT.

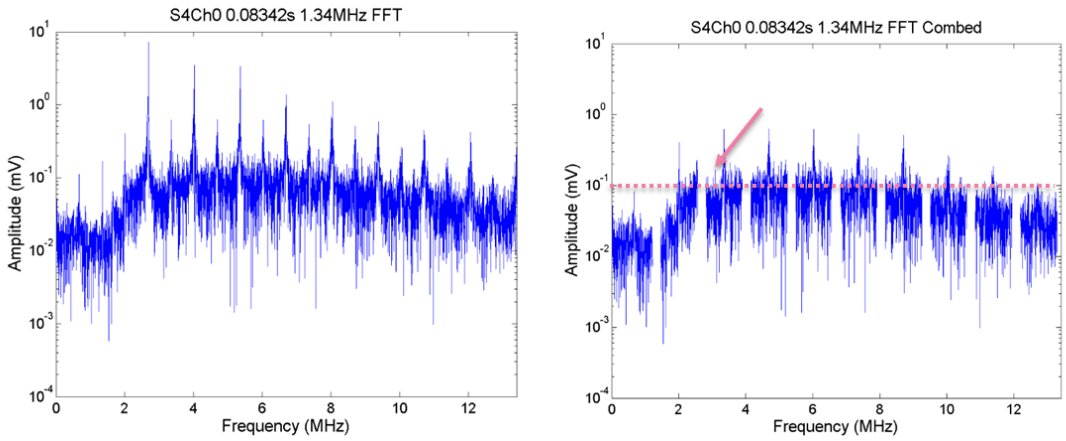

Figure 2.35. FFTs from a single segment of PCD data from a single exposure in DMEM with 10% concentration of microbubbles. The FFTs show broadband component (left) and harmonic comb filtered broadband (right). Comparing this to the off-time noise (over 3-10 MHz), there is a clear elevation and broadband, suggesting this could well be cavitation.

At 1.34 MHz, the inertial cavitation threshold in DMEM lies between 0.42 and 0.64 MPa. To compare broadband activity at 1.08 and 1.34 MHz, in DMEM medium with 10% microbubbles see figures 2.22 and 2.34. This shows that at 1.08 MHz, the greatest destruction of microbubbles is at the beginning of the exposure, but at 1.34 MHz, broadband activity is sustained (and on average increasing) throughout a large band of frequencies. Again, this could be due to the fact that at this higher frequency, we are closer to the resonant frequency of the microbubbles and so, sustained cavitation events are possible.

These microbubbles are excellent ultrasound scatterers due to their high compressibility. In an ultrasound field they act as resonant systems, resulting in energy at the subharmonic, ultraharmonic and higher harmonic frequencies in the backscattered ultrasound signal. Any medium with a real pressure wave in it is likely to be non-linear - propagation of FUS creates harmonics (in the absence of bubbles). Only when there are bubbles it is possible to get half harmonic (and potentially other subharmonics), and, at finite pressures, harmonics of these. So half and ultra harmonics only occur when there are bubbles, but there are strong harmonics due to non-linear propagation. Although the bubbles will also contribute to the harmonics of the FUS, this will be a very small fraction of the total harmonic energy.

iii) DMEM plus 20% microbubbles

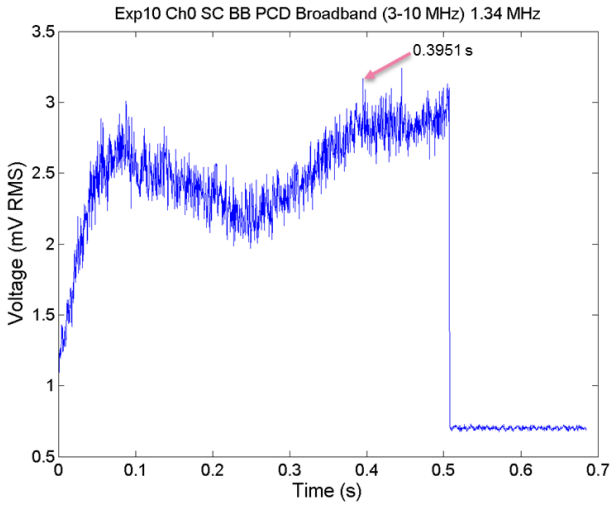

Figure 2.36. PCD broadband signal integrated over the band of 3-10 MHz as a function of time for a single exposure in DMEM with 20% concentration of microbubbles at a peak negative pressure of 0.64 MPa. The arrow points towards a time point chosen to analyse in the frequency domain.

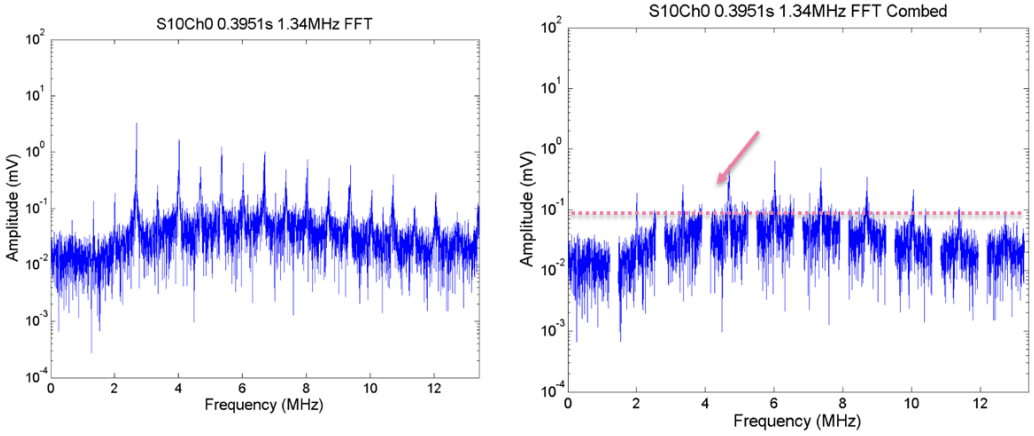

Figure 2.37. FFTs from a single segment of PCD data from a single exposure in DMEM with 20% concentration of microbubbles. The FFTs show broadband component (left) and harmonic comb filtered broadband (right). Comparing this to the off-time noise (over 3-10 MHz), there is a clear elevation and broadband, suggesting this could well be cavitation.

The detection lies again in the range of 0.42 MPa and 0.64 MPa (see Figures 2.36 and 2.37) and, in contrast to what happens at 1.08 MHz (Figure 2.26), there is no big difference in terms of amplitude of broadband in the time domain. A concentration of 20% of microbubbles appears to make no difference in terms of cavitation threshold. This could be due to a systematic error before the measurement, or while plating the sample but no other measurement was made to compare the results in terms of broadband amplitude.

Results at 1.66 MHz

i) DMEM alone

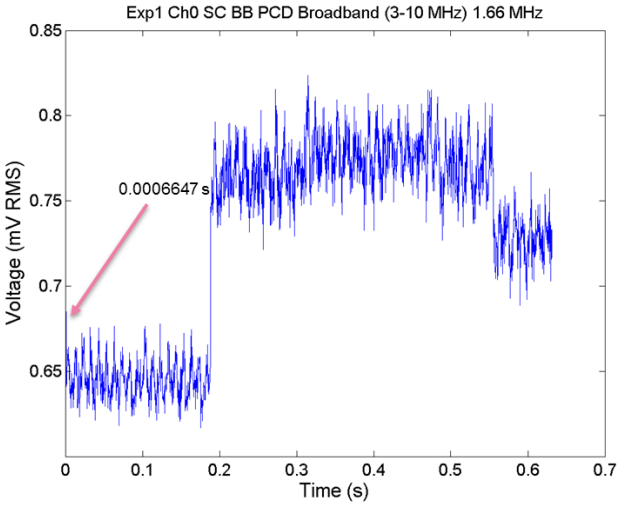

Figure 2.38. PCD broadband signal (frequency-integrated over 3-10 MHz) as a function of time for a single 1.66 MHz, 0.5 s exposure of DMEM with peak negative pressure 0 MPa. No cavitation was detected, because no exposure was made. Therefore in this case the whole trace represents off-time noise of the entire PCD detection system. The graph title shows that this was exposure number one, with data acquired on Ch0 of the DAQ system. Average noise is 0.730 ± 0.0941 mV, and highest noise is ~0.8 mV.

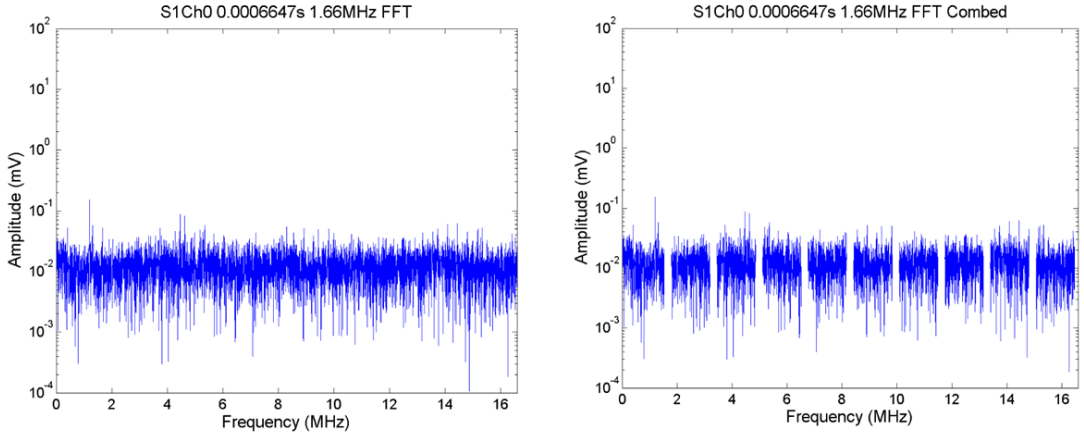

Figure 2.39. FFTs from a single segment of PCD data from a single exposure in DMEM. The FFTs show broadband component (left) and harmonic comb filtered broadband (right) of noise level.

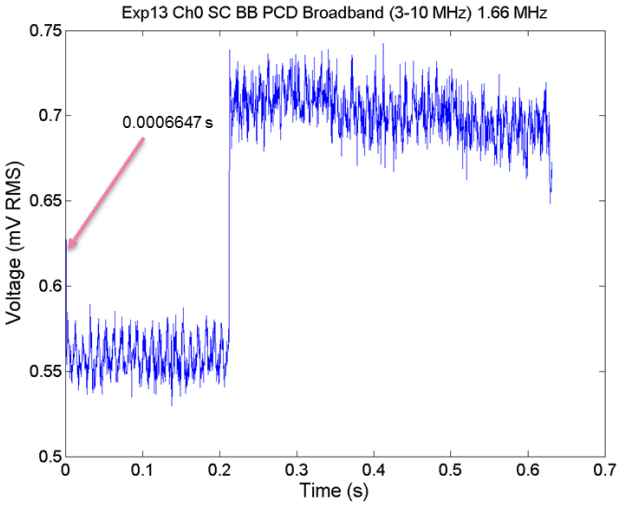

Figure 2.40. PCD broadband signal integrated over the band of 3-10 MHz as a function of time for a single exposure in DMEM at a peak negative pressure of 1.8 MPa. The arrow points towards a time point chosen to analyse in the frequency domain.

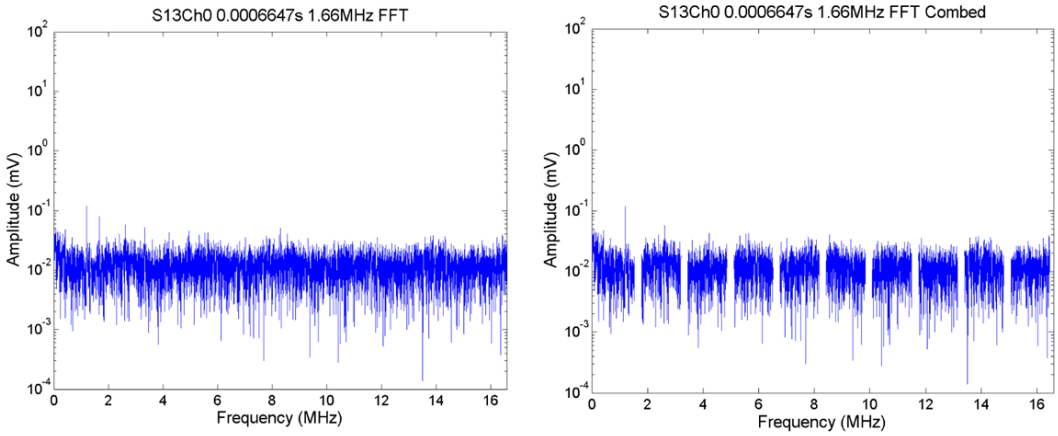

Figure 2.41. FFTs from a single segment of PCD data from a single exposure in DMEM. The FFTs show broadband component (left) and harmonic comb filtered broadband (right).

Figures 2.38 – 2.41 are data acquired during exposure of DMEM to a range of pressures from 0 to 1.8 MPa,. Figures 2.38 and 2.39 show the noise level, with an average value of 0.730 ± 0.0941 mV. Figures 2.40 and 2.41 contain the data from the highest exposure level tested at 1.66 MHz which show that no cavitation was detected by the PCD.

ii) DMEM plus 10% microbubbles

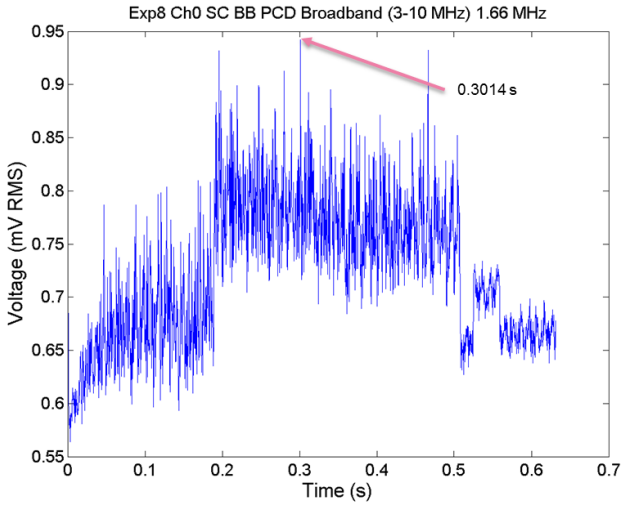

Figure 2.42. PCD broadband signal integrated over the band of 3-10 MHz as a function of time for a single exposure in DMEM with 20% concentration of microbubbles at a peak negative pressure of 0.3 MPa. The arrow points towards a time point chosen to analyse in the frequency domain.

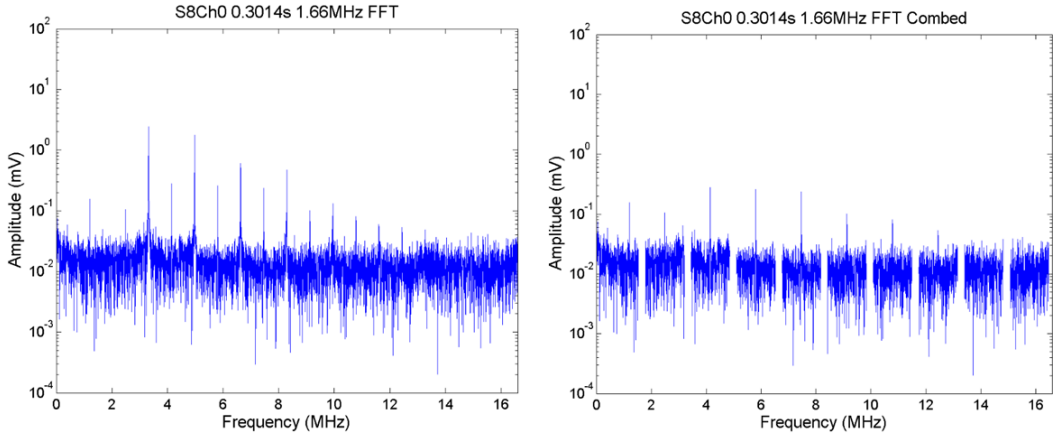

Figure 2.43. FFTs from a single segment of PCD data from a single exposure in DMEM with 10% concentration of microbubbles. The FFTs show broadband component (left) and harmonic comb filtered broadband (right).

Figures 2.42 and 2.43 result from an exposure at a PNP of 0.3 MPa in DMEM in the presence of 10% microbubble concentration. In Figure 2.43, 2nd to 6th harmonics and some ultraharmonics are detected. This happens at a low amplitude, in terms of broadband in the time domain (a maximum of ~0.943 mV) as can be seen in figure 2.42. This is similar to what happens at 1.08 and 1.34 MHz, at amplitudes of 0.871 and 1.41 mV maximum, respectively.

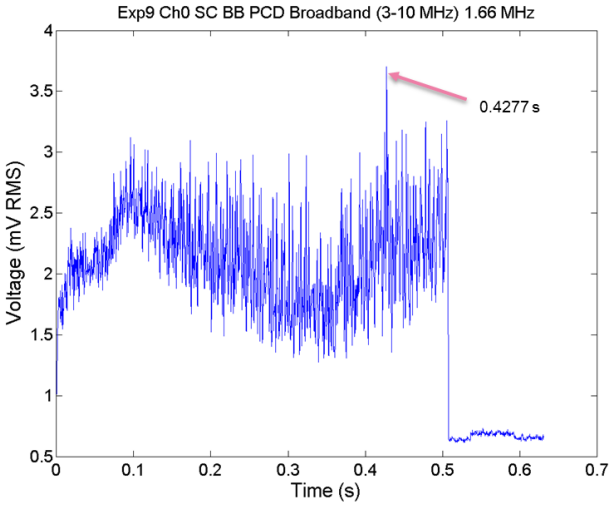

Figure 2.44. PCD broadband signal integrated over the band of 3-10 MHz as a function of time for a single exposure in DMEM with 10% concentration of microbubbles at a peak negative pressure of 0.6 MPa. The arrow points towards a time point chosen to analyse in the frequency domain.

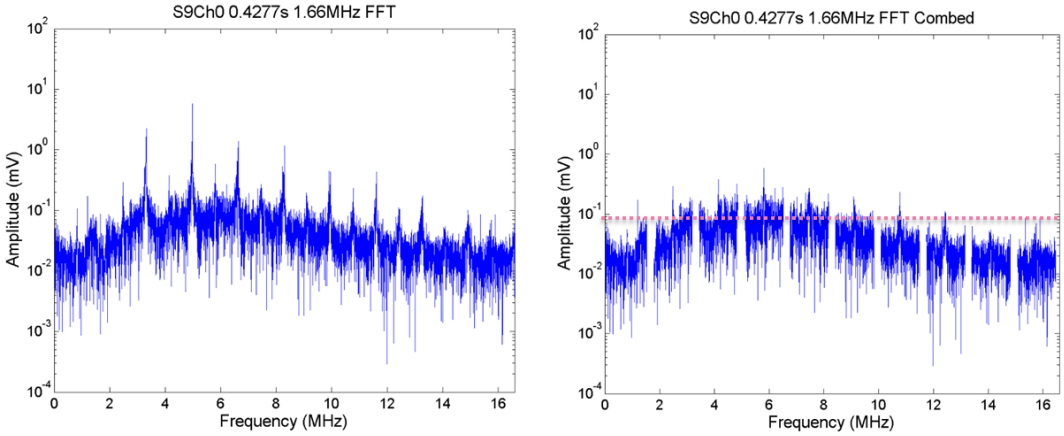

Figure 2.45. FFTs from a single segment of PCD data from a single exposure in DMEM with 10% concentration of microbubbles. The FFTs show broadband component (left) and harmonic comb filtered broadband (right). Comparing this to the off-time noise (over 3-10 MHz), there is a clear elevation and broadband, suggesting this could well be cavitation.

Data from exposures in DMEM with 10% microbubble concentration suggests that the inertial cavitation threshold lies between 0.3 and 0.6 MPa. Figures 2.44 and 2.45 are data from measurements at 0.6 MPa. At this pressure 2nd to 6th harmonic are detectable and there is a low prevalence of ultraharmonics – small spikes can be seen in Figure 47 (right), between the filtered harmonics.

iii) DMEM plus 20% microbubble concentration

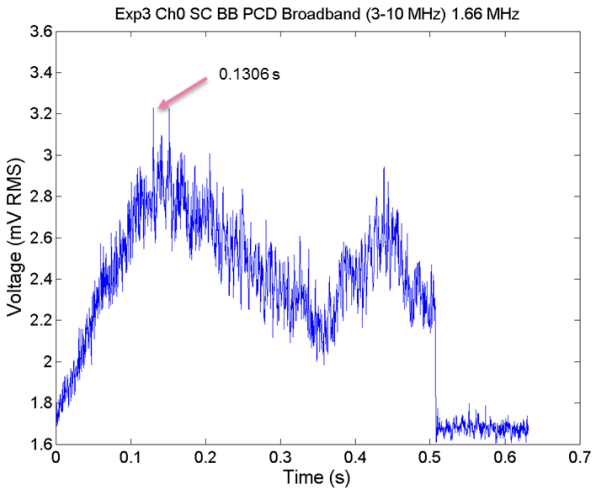

Figure 2.46. PCD broadband signal integrated over the band of 3-10 MHz as a function of time for a single exposure in DMEM with 20% concentration of microbubbles at a peak negative pressure of 0.6 MPa. The arrow points towards a time point chosen to analyse in the frequency domain.

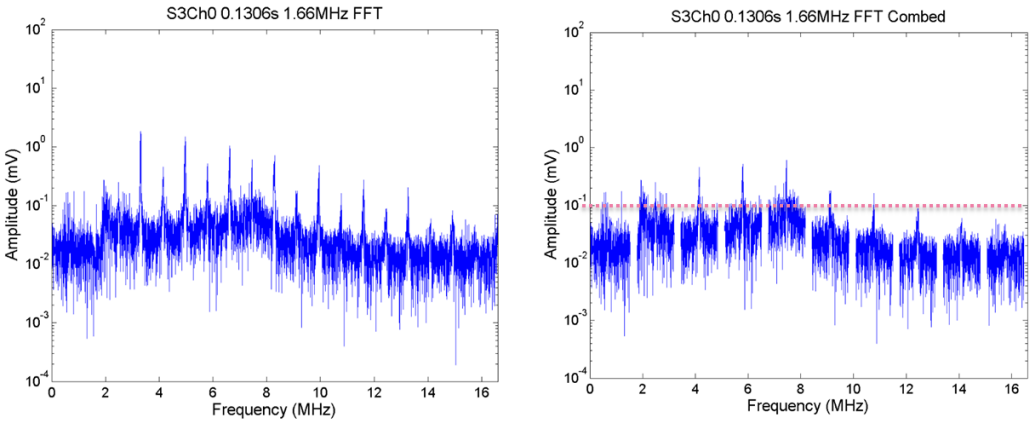

Figure 2.47. FFTs from a single segment of PCD data from a single exposure in DMEM with 20% concentration of microbubbles. The FFTs show broadband component (left) and harmonic comb filtered broadband (right). Comparing this to the off-time noise (over 3-10 MHz), there is a clear elevation and broadband, suggesting this could well be cavitation.

Finally, the measurements at 1.66 MHz in DMEM with a 20% concentration of microbubbles suggests an inertial cavitation threshold between 0.3 and 0.6 MPa (Figure 2.47). At 0.6 MPa, a maximum broadband level around 3.2 mV was detected (Figure 2.46).

As a summary, at 1.08 MHz in the absence of microbubbles, there is no detection of broadband in the range of pressures tested, in the presence of 10% and 20% microbubbles, inertial cavitation seems to be present at a pressure of 1.2 MPa and in the

the interval of 0.6-0.9 MPa, respectively. At 1.34 MHz, the inertial cavitation threshold lies in the intervals of 0.85-1.06 MHz, 0.42-0.64 MHz and 0.6-0.9 MHz in the absence and in the presence of 10 and 20% microbubbles, respectively. At 1.66 MHz, there was no cavitation threshold detected from 0 to 1.8 MPa in the absence of microbubbles and in the presence of 10 and 20% microbubbles it was between 0.3-0.6 MPa and 0.6-0.9 MPa, respectively. *In vivo* a 1.5 MHz transducer will be used, this analyses discards the use of the transducer at 1.08 MHz which has been tested just to have a better compreension of how frequency can influence the inertial cavitation threshols. The difference in frequency from 1.34 MHz and 1.66 MHz to 1.5 MHz is the same (±0.16 MHz). As the higher broadband amplitude seen happens at 1.34 MHz and as *in vivo* there is attenuating medium and inertial cavitation is not likely to happen, the 1.66 MHz transducer will be used to perform *in vitro* experiments.

The limitation of this study is that it is only possible to make a qualitative analyses rather than a quantitative one and if it was done presently, only the two frequencies of more interest would be tested as these experiments are very time consuming and there was not enough time to make repeats on the experiments made to test the reproducibility of the study.

3. *In Vitro* Study on the Effects of Focused Ultrasound on BN175 Sarcoma Cell Line

3.1. Introduction to the *In Vitro* Study

Research into the potential of ultrasound and microbubbles to enhance drug delivery has been undertaken over the last decades, and concepts such as sonoporation, i.e. the formation of temporary pores in the cell membrane, and enhanced endocytosis have been suggested as the main biological mechanisms involved [88, 89]. In general, the uptake of drugs or small molecules is attributed to ultrasound mediated transient permeabilization of the cell membrane. This transient permeabilization can be the result of stable and/or inertial cavitation events in the presence or absence of artificial microbubbles.

At very low acoustic pressures, microbubbles oscillate in a symmetrical, linear way, but at higher ultrasound intensities, microbubbles behave non-linearly as the microbubbles become more resistant to compression than to expansion [86]. During stable microbubble cavitation there is gas influx (during expansion) and gas efflux (during compression). In the case of symmetrical oscillations, the net gas influx over one expansion/compression cycle is zero. However, when the expansion phase extends, there is net gas influx.The microbubble grows until it reaches its resonant size, whereupon it undergoes stable, low amplitude oscillation. Such stable oscillations create a liquid flow around the microbubbles - microstreaming [87]. Oscillating microbubbles in the vicinity of cells, exert shear stresses. At these lower ultrasound intensities, two mechanisms which contribute to the uptake of cell impermeable molecules, namely (i) the formation of small pores [88] and (ii) endocytosis [89] have been postulated.

At higher ultrasound intensities, the oscillation amplitude of a microbubble can grow rapidly during the low pressure phase, until the microbubble collapses. What happens is that the bubbles grow “too” big and then when they start collapsing the forces that makes them grow again is not big enough to stop the collapse so the bubbles implode. This type of cavitation is described as inertial cavitation. During collapse, shock waves

can be generated in the fluid and jet formation can occur - an asymmetrical collapse which results in the formation of a liquid jet towards a nearby surface. It has been shown that shock waves and microjets create very high forces that can create pores in the cell membrane [90]. While stably cavitating microbubbles need to have direct contact with the cell to affect the membrane, the effects of inertial cavitating microbubbles extend over a larger distance [91].

The main objectives of the project are to study tumor virus distribution and then to quantify viral particle uptake using appropriate assays (e.g. qPCR, Plaque Assay, Immunofluorescence). As an initial approach, *in vitro* experiments were performed with the BN175 rat sarcoma line in the presence or absence of (i) focused ultrasound (ii) microbubbles and (iii) focused ultrasound and microbubbles. The physical parameters to be optimised in terms of maintained cell viability are peak negative pressure, Duty Cycle (the percentage of time it takes for a signal to complete an on-and-off cycle in which a signal is active), pulse repetition frequency, exposure duration and microbubble concentration. Once a range of optimal parameters was found, they were used *in vivo* in Brown Norwegian rats in order to determine optimal *in vivo* conditions. Optimal conditions mean that cell viability is not compromised and while experimenting *in vivo*, the virus can get into the tumor cells and replicate.

3.2. Methods for the *In Vitro* Study using BN175 Cell Line

3.2.1. Cell Culture

In order to initiate *in vitro* experiments, it was necessary to learn how to work in a cell culture facility, and in a biochemical laboratory, and to start culturing cells and to practise the assays used. These were the MTT assay for cell viability, and FACs analysis used to study the integrity of a cell membrane after an ultrasound exposure.

Equipment used for Cell Culture and Plating

Laboratory consumables e.g. pipettes, plates, flasks, tips

Light Microscope
Microbiological Safety Cabinet (Hood)
Haemocytometer
0.25% Trypsin/0.05% EDTA solution
Dulbeccos Phosphate Buffered Saline (PBS) without calcium and magnesium
5% Trigene
2mM L-Glutamine
Fetal Bovine Serum (FCS) in a working concentrations of 10% in DMEM
50U/ml Penicillin/ 50mg/ml Streptomycin (Pen/Strep)
High glucose (4500mg/L) Dulbeccos Modified Eagles Medium (DMEM)

Preparation of DMEM:

BN175 murine sarcoma cells were maintained in a sub-confluent monolayer at 37 ^{o}C in a humidified atmosphere containing 5 % CO_2. They were propagated using high glucose DMEM supplemented with 10 % FBS, 2 mM L-glutamine, 50 U / ml penicillin, 50 mg / ml streptomycin B, and sub-cultured using 0.25% Trypsin/EDTA. Screening for mycoplasma contamination was carried out on a monthly basis.

Procedure:

Cell Passaging:

1. Aspirate medium
2. Rinse flask with PBS to remove excess media (as this reduces efficacy of trypsin)
3. Add trypsin and leave at 37ºC until cells are dislodged
4. Transfer cells in trypsin to falcon tube containing an equal volume of medium to trypsin added (inactivates enzyme)
5. Centrifuge at 1200 rpm for 4 minutes at room temperature
6. Resuspend in DMEM
7. Passage cells to a flask using a split ratio of 1 in 4 to provide optimal cell growth between passages
8. Add medium to cells enough to cover the surface of the flask.

9. Transfer the flask into 5% CO_2 humidified atmosphere at 37 ºC.
10. Decontaminate spare cells using 5% Trigene for 24 hours.

Cell Plating:

1. Harvest cells with trypsine and resuspend in media
2. Make 1:10 dilution (100µl cells + 900µl media)
3. Pipette 20µl onto both sides of a haemocytometer, under cover slip, and count cells located in 25 square areas from each side.
4. Average the two counts if the difference is less than 10% between the two sides. If the difference is higher than 10 % then repeat the cell count. The concentration of cells/ml is then defined as $n \times 10^5\ cells/ml$
5. Add medium to get the desired concentration of cells in a master solution
6. Plate cells in the wells of the acoustic well plate.

3.2.2. For FUS exposures *in vitro*

For *in vitro* experiments, all the FUS exposure and cavitation monitoring equipment and methods described in Chapter 2 were used. The cell culture is ready for use in experiments two weeks after seedin in flasks. During this time, the cells must to be passaged, approximately twice a week – this is necessary when cells are at 90% confluence in the culture flask. When the cells were ready, the *in vitro* exposures were carried out as follows:

Controls:

1. DMEM + Ultrasound exposure
2. DMEM + Ultrasound exposure + Microbubbles
3. BN175 rat sarcoma cell line in DMEM + Ultrasound exposure
4. BN175 rat sarcoma cell line in DMEM + Ultrasound exposure + Microbubbles

Effects studied:

i. Cell viability and Proliferation profile in medium only, compared to cells with or without microbubbles, no ultrasound exposure
ii. Replication of cells in exposed medium compared to those in unexposed medium

iii. Response of microbubbles to ultrasound in medium, compared to their response in the presence of cells

Range of parameters to test:

- Peak Negative Pressure of 0, 0.6, 0.9 and 1.8 MPa
- DC of 2, 5 and 20%
- PRF of 10, 100 and 1 kHz
- Δt of 1, 5 and 10 seconds

Procedure:

1. Prepare a master solution to give 15×10^3 cells/well (well volume 0.5 ml) in a hood (semi-sterile environment)
2. Pipette 0.47 ml of solution into each well in the well-plate (see figure 50)
3. Expose wells to one of the ultrasound parameters under test (procedure described in section 2.2.2.)
4. Transfer the well plate into the hood. Aliquot x μl of cell suspension in the wells of a 96-well plate. Perform MTT assay immediately, 1 and 3 days after an ultrasoun exposure.

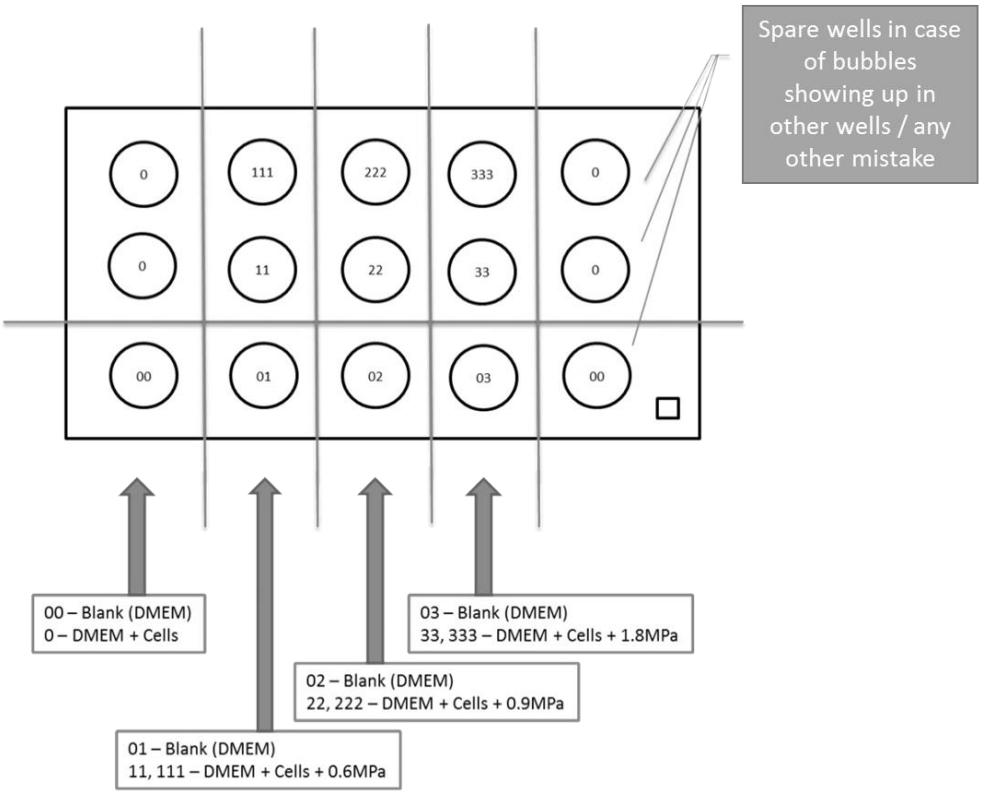

Figure 3.1. Schematic of the design of exposures. The arrows show examples of different conditions used to study the effect of pressure on BN175 cell culture. In each well-plate only 3 conditions were tested in order to guarantee the quality of the results. Other designs were tested but the error bars associated with each result were too big to allow a valid conclusion.

3.3. Results and Discussion of the *In Vitro* Study

3.3.1. Results from MTT Assays

MTT Assays

The MTT assay is a colorimetric assay that measures the reduction of yellow 3-(4,5-dimethythiazol- 2-yl)-2,5-diphenyl tetrazolium bromide (MTT) by mitochondrial succinate dehydrogenase. The MTT enters the cells and passes into the mitochondria where it is reduced to an insoluble, coloured (dark purple) formazan product. The cells are then solubilised with an organic solvent (eg. isopropanol) and the released, solubilised formazan reagent is measured spectrophotometrically. Since reduction of MTT can only occur in metabolically active cells the level of activity, and thus the colour intensity, is a

measure of the viability of the cells. This assay was used to verify the number of living cells imediately, one and three days after an ultrasound exposure.

The results shown here are allways relative to the unexposed control population of each day. The Optical Density (OD) is normalised to 100% so that the effect on different days can be compared. A more accurate way of applying this assay would be to standardize a Viability Curve of the number of cells as function of the OD read in the spectrophotometer. For the duration of this project, this was not possible because the cell line was really unstable and the cell culture did not allways grow at the same rate between experiments. Although, the results are presented in a relative manner which is still good enough for the purpose of this pilot study.

The *in vitro* study was performed using the 1.66 MHz transducer . This was chosen because the transducer of the VIFU system (used for *in vivo* experiments) only works at 1.5 MHz, and the transducers available for *in vitro* measurements could only be driven at 1.08, 1.34 and 1.66 MHz. The transducer which operated at 1.08 and 1.34 was most effective at 1.08 MHz, and so this frequency was tested, although this much lower than that that would be used *in vivo*. While 1.34 MHz, is as closer to the frequency of the VIFU transducer to be used, the broadband detection at 1.66 MHz is of lower amplitude in the time domain and in *in vivo* experiments cavitation is not as likely to occur as it happens in a non-attenuating medium – as previously discussed Chapter 2, in section 2.2.3.

Fixed conditions have been used for each parameter under investigation on the day of exposure, 1 and 3 days after at 1.66 MHz. For the study on the effect of pressure on cell viability (compared to control) the fixed parameters were PRF of 100 Hz, DE of 0.5 seconds and 40 cycles. For the study on the effect of pulse repetition frequency the fixed parameters were PNP of 0.6MPa, DE of 0.5 seconds and 40 cycles. To investigate the effect of duration of exposure the fixed parameters used were PNP of 0.6MPa, 100Hz PRF and 40 cycles. Finally, to study the effect of duty cycle the fixed parameters used were PNP of 0.6MPa, 100Hz PRF and 40 cycles.

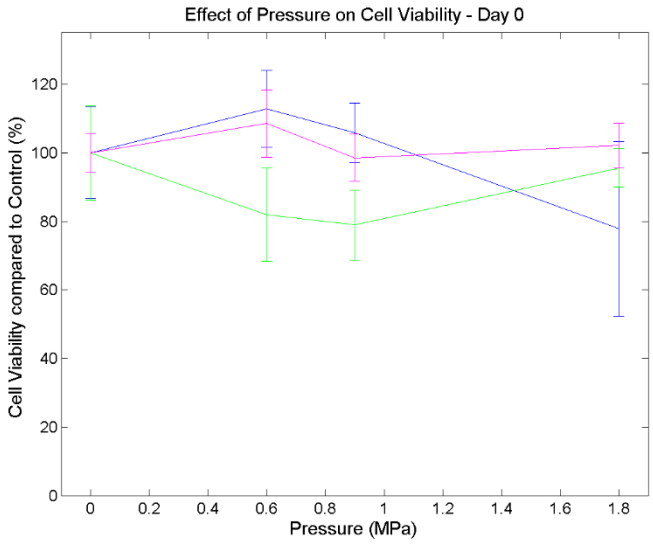

Figure 3.2. Results from 3 independent experiments on viability of cells only, exposed to different levels of pressure. Error bars shown are the standard deviation for each sample (n=8) at the different drive levels used.

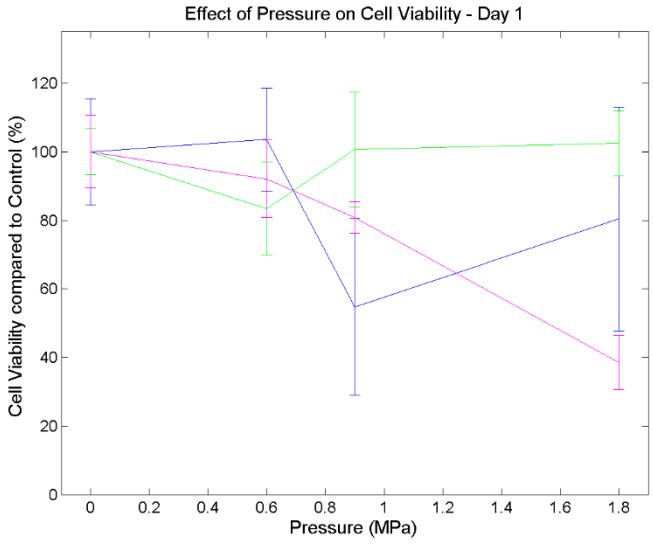

Figure 3.3. Results from 3 independent experiments on viability of cells only exposed to different levels of pressure 1 day after exposure. Error bars shown are the percentage of standard deviation of each sample (n=8) for the different drive levels used.

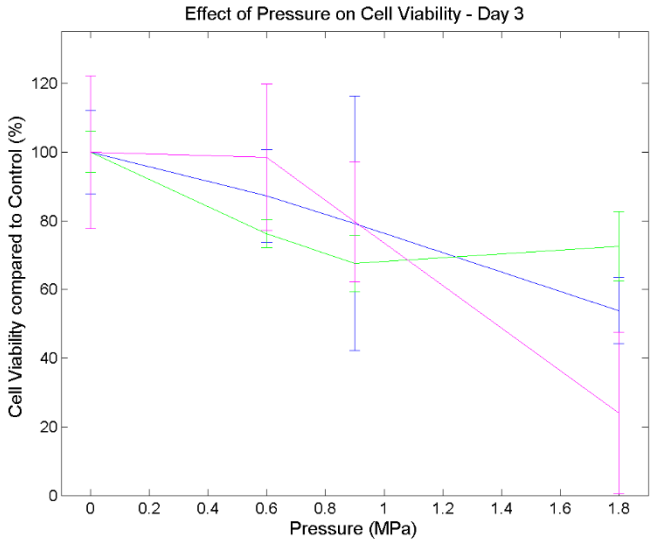

Figure 3.4. Results from 3 independent experiments on viability of cells only exposed to different levels of pressure 3 days after exposure. Error bars shown are the percentage of standard deviation of each sample (n=8) for the different drive levels used.

Figures 3.2 – 3.4, represent the data from 3 independent experiments with a fixed number of cells (approximately 15000 cells per well) in DMEM, from day 0 to day 3, respectively. These cells were exposed to three different levels of pressure at 1.66 MHz. The pressure levels were no ultrasound exposure (0 MPa), at the level to just get inertial cavitation (0.6 MPa), during inertial cavitation (0.9 MPa) and at a high level of inertial cavitation (1.8 MPa) – from information collected during the analysis of cavitation thresholds in Section 2.2.3.

In day 0, the exposure seems to have a minimal effect on the viability of cells as the viability is within a standard deviation of 100% (Figure 3.2). One day after the exposure (Figure 3.3), there is high variability in the results and their associated standard deviation. A difference in viability of ~ ±20% at 0.6 MPa suggests that there is no effect of ultrasound up until, and including at, day 3 – see Figure 3.4. At 0.9 MPa no effect is seen at day 0, but the results from days 1 and 3 suggest that approximately 80% of the cells were killed. At 1.8 MPa, it is clear that the effect of ultrasound exposure is greater – in day 0, approximately 85% of the cells survive; in day 1, despite a large standard deviation, an average viability of 75% is found, and in day 3, only ~ 45% of the cells are alive. These experiments require a lot of practice to perfect and improve experimental technique. Poor pippeting, errors in counting cells or making dilutions, loss while transferring cells from one flask to another, loss of cells while transferring them to the well plate and/or while taking them out. The systematic errors mentioned above, can also

be seen at 0 MPa, in which no exposure is applied, and a spread in survival is seen. The differences in the cell cycle kinetics contribute to the error as biological variability. There are four phases in the cell cycle, taking from 10 – 20 hours depending on cell type and developmental state. The Interphase stage comprises G1, S, and G2 phases - when macromolecules are synthesized, the cell roughly doubles its cellular mass and is prepared for the mitotic (M) phase. Nondividing cells exit the G1 phase, entering a quiescent G0 state. The results here are the average values from 3 independent experiments. The standard deviation between measurements is, for most of the results in this section, different, but the error bars match in almost all cases. This means that there is reproducibility between independent experiments but more experiments are necessary to increase the reproducibility of this study.

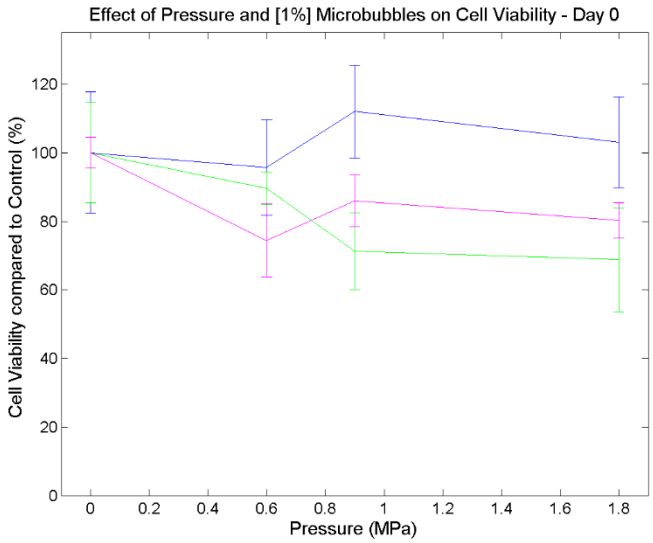

Figure 3.5. Results from 3 independent experiments on viability of cells only exposed to different levels of pressure with 1% concentration of microbubbles in the sample, on the day of exposure. Error bars shown are the percentage of standard deviation of each sample (n=8) for the different drive levels used.

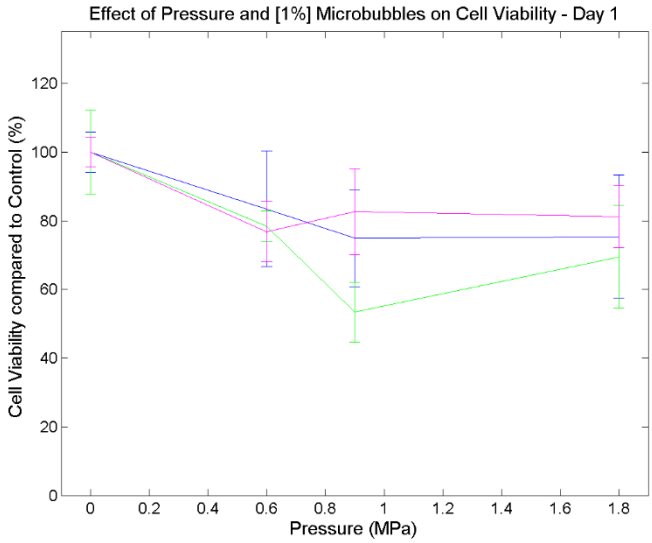

Figure 3.6. Results from 3 independent experiments on viability of cells only exposed to different levels of pressure with 1% concentration of microbubbles in the sample, 1 day after exposure. Error bars shown are the percentage of standard deviation of each sample (n=8) for the different drive levels used

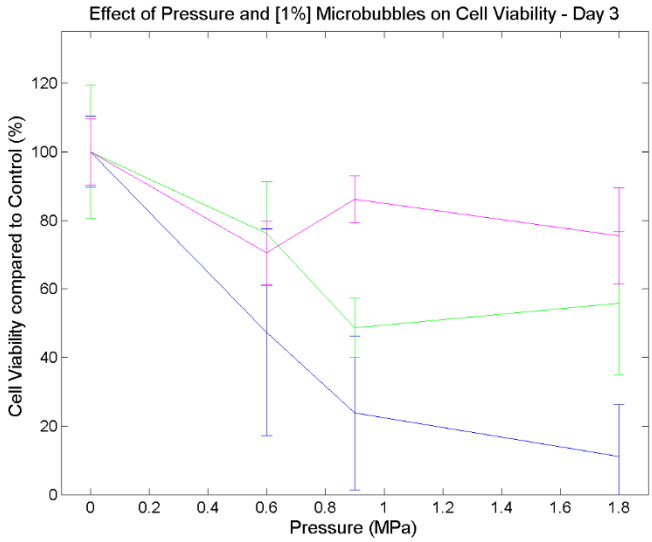

Figure 3.7. Results from 3 independent experiments on viability of cells only exposed to different levels of pressure with 1% concentration of microbubbles in the sample, 3 day after exposure. Error bars shown are the percentage of standard deviation of each sample (n=8) for the different drive levels used

Figures 3.5-3.7, represent the data from 3 independent experiments with a fixed number of cells (approximately 15000 cells per well) in DMEM with a 1% concentration of microbubbles in solution, from day 0 to day 3, respectively. The trend of this group of results is similar to that without microbubbles. A pressure of 0.6 MPa gives a viability close to 100% in day 0, ~ 85% in day 1 and a viability of approximately 55% in day 3 (these are averages from 3 independent measurements).

At 0.9 MPa, in day 0, one of the three experiments is not comparable to the other two the error bars do not overlap. This lack of overlap is also seen at Day 3. Despite this, it can be seen that a concentration of 1% microbubbles has little added effect on the number of cells surviving, compared with the results seen in their absence, at all ultrasound exposure levels.

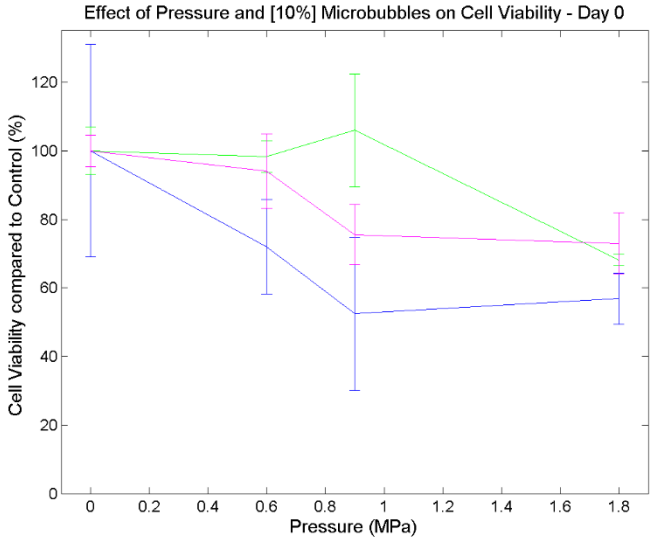

Figure 3.8. Results from 3 independent experiments on viability of cells only exposed to different levels of pressure with 10% concentration of microbubbles in the sample, on the day of exposure. Error bars shown are the percentage of standard deviation of each sample (n=8) for the different drive levels used.

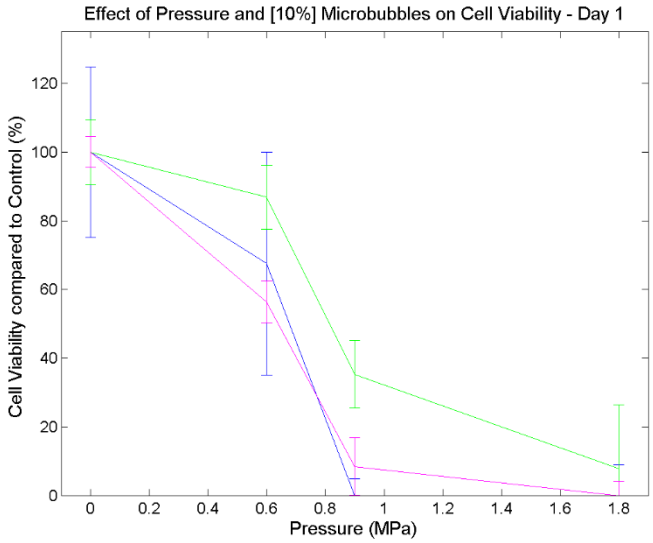

Figure 3.9. Results from 3 independent experiments on viability of cells only exposed to different levels of pressure with 10% concentration of microbubbles in the sample, 1 day after exposure.. Error bars shown are the percentage of standard deviation of each sample (n=8) for the different drive levels used.

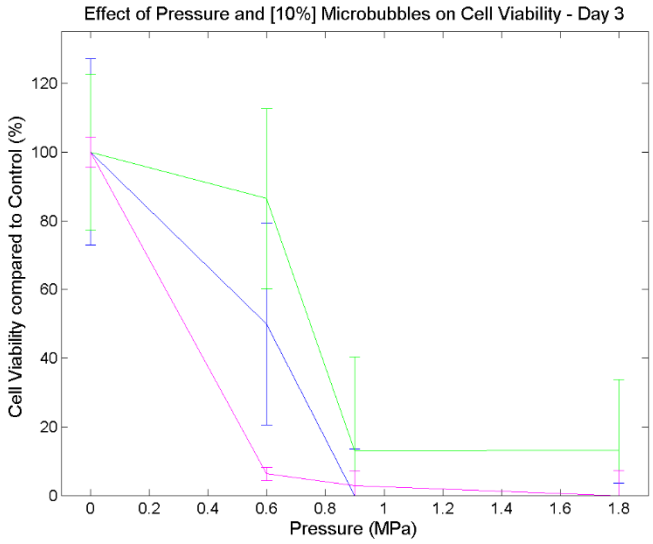

Figure 3.10. Results from 3 independent experiments on viability of cells only exposed to different levels of pressure with 10% concentration of microbubbles in the sample, 3 day after exposure. Error bars shown are the percentage of standard deviation of each sample (n=8) for the different drive levels used.

Figures 3.8-3.10, represent the data from 3 independent experiments with ~ 15000 cells/ well with a 10% concentration of microbubbles, from days 0 to 3, respectively. In day 0, at 0.6 MPa only 20% of the cells seem to be unaffected by the exposure to ultrasound in the presence of microbubbles. This value increases to 40% in day 1 and in day 3, the large spread in survival found makes it difficult to draw a firm conclusion – see Figure 3.10. This spread could be due to poor experimental technique, as discussed earlier or to a problem with the cells themselves. At 0.9 MPa, only two independent experiments seem to be reproducible for day 0 because one (the green one in Figure 3.8) is really diferent in terms of result and associated error. However, it is not possible to determine if the results represented by the green trace are bad results when compared to the other two sets of results (presented in blue and red traces in Figure 3.8) – more experiments would be needed to guarantee the reproducibility of this study. Considering this, all the results are under analysis and so, it can be considered that in day 0 approximately 75% of the cells are alive after the exposure to ultrasound in the presence of 10% concentration of microbubbles; approximately 25% in day and around 20% are alive of day 3. The higher level of pressure gives a viability close to 70% in day 0, 20% in days 1 and 3.

The results presented so far suggest that increasing the concentration of microbubbles decreases the cell viability which can be attributed to the increased level of inertial cavitation. This might compromise the membranes in such a way that they

can not survive or reproduce. The influence of inertial cavitation is also suggested by the fact that even whithout microbubbles, an increased pressure amplitude for reduces the viability of the cells. Figures 3.11 – 3.13 summarise the results for each condition tested, on the day of exposure, 1 and 3 days after the exposure.

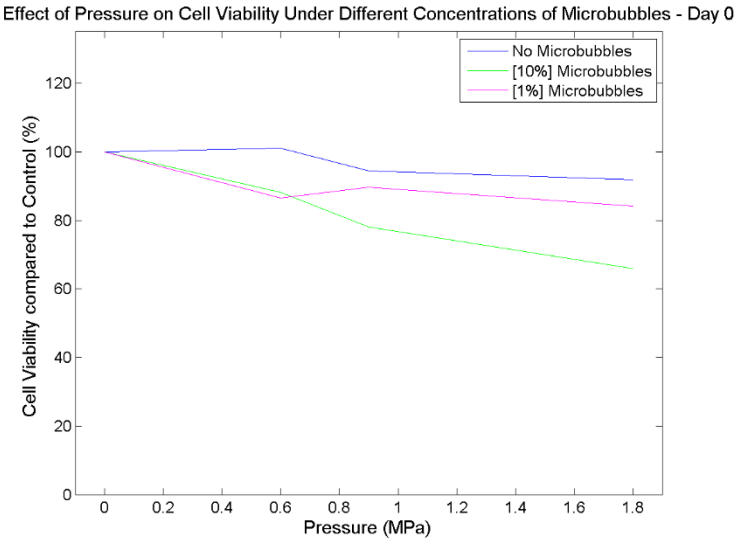

Figure 3.11. Results from 3 independent experiments on viability of cells in the absence and presence of microbubbles and exposed to different levels of pressure - on the day of treatment. Each line plotted corresponds to the mean of the results of the 3 independent experiments done under different concentrations of microbubbles. Error bars have been left off for clarity of the results.

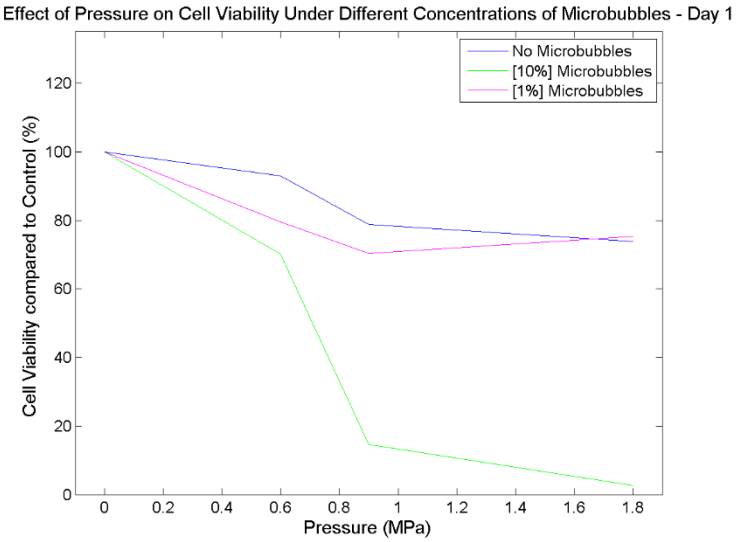

Figure 3.12. Results from 3 independent experiments on viability of cells in the absence and presence of microbubbles and exposed to different levels of pressure – 1 day after the treatment. Each line plotted corresponds to the mean of the results of the 3 independent experiments done under different concentrations of microbubbles. Error bars have been left off for clarity of the results.

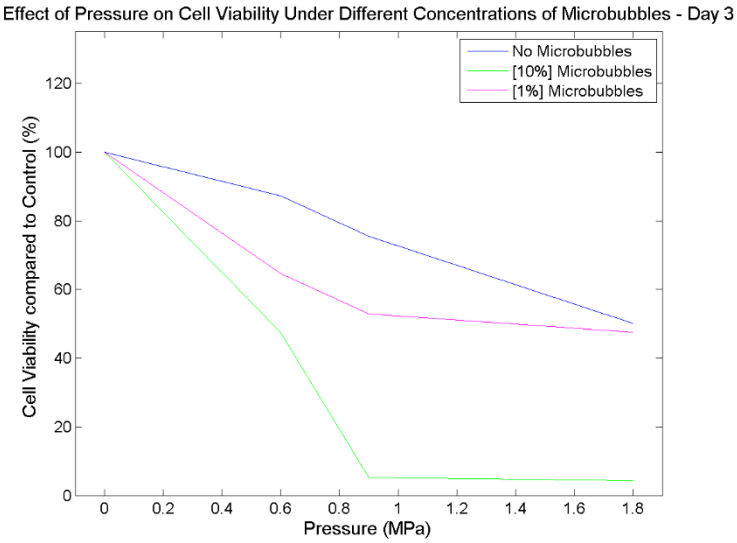

Figure 3.13. Results from 3 independent experiments on viability of cells in the absence and presence of microbubbles and exposed to different levels of pressure – 3 days after the treatment. Each line plotted corresponds to the mean of the results of the 3 independent experiments done under different concentrations of microbubbles. Error bars have been left off for clarity of the results.

2 . Study of the effect of Pulse Repetition Frequency (PRF)

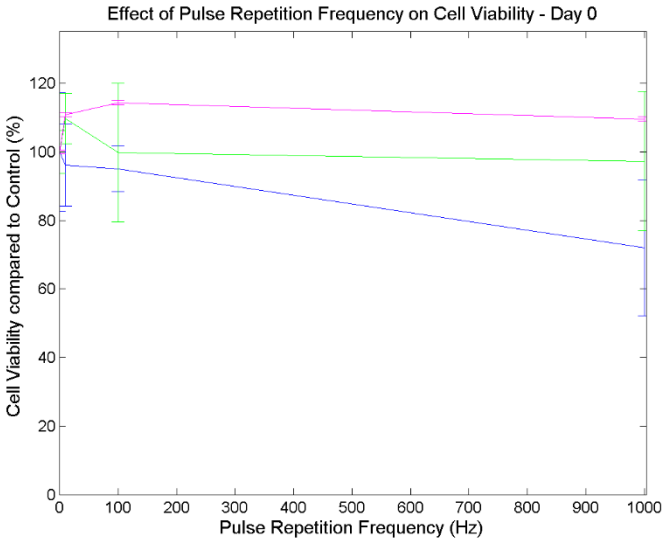

Figure 3.14. Results from 3 independent experiments on viability of cells only exposed with different Pulse Repetition Frequencies on the day of exposure. The levels of PRF used are 10, 100 and 1000 Hz Error bars shown are the percentage of standard deviation of each sample (n=8) for the different drive levels used

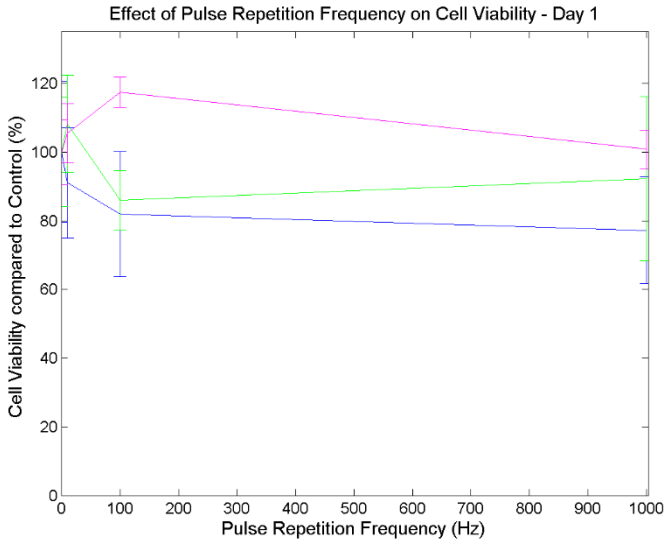

Figure 3.15. Results from 3 independent experiments on viability of cells only exposed to different levels of Pulse Repetition Frequency 1 day after exposure. The levels of PRF used are 10 100 and 1000 Hz. Error bars shown are the percentage of standard deviation of each sample (n=8) for the different drive levels used

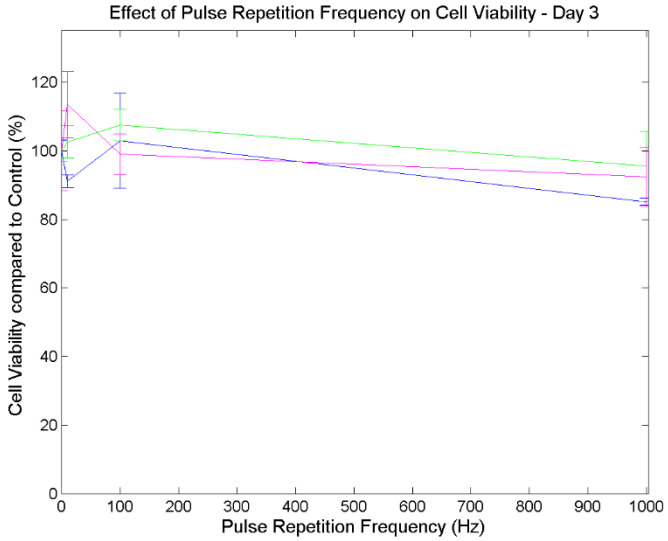

Figure 3.16. Results from 3 independent experiments on viability of cells only exposed to different levels of Pulse Repetition Frequency 3 days after exposure. The levels of PRF used are 10 100 and 1000 Hz. Error bars shown are the percentage of standard deviation of each sample (n=8) for the different drive levels used

The effect of Pulse Repetition Frequency was studied at a pressure that has minimal effect on the viability, (0.6 MPa). The other (fixed) parameters were 40 cycles, 0.5 s of continuous exposure . The values of PRF tested were 10, 100 and 1000 Hz.

Figures 3.14 – 3.16 show the data from 3 independent experiments with ~ 15000 cells per well) in DMEM, from day 0 to day 3, respectively. These figures show the minor effect of this parameter on the cell survival. On the three time points selected for analysis,

the greatest effect is at a PRF of 1000Hz in day 0 but this result also has the highest standard deviation, and so may be statistically insignificant. As the results already analysed show a minimal impact of PRF on cell viability, only one (extreme) condition, with 10% microbubble concentration, was tested . The results are shown in Figures 3.17-3.19.

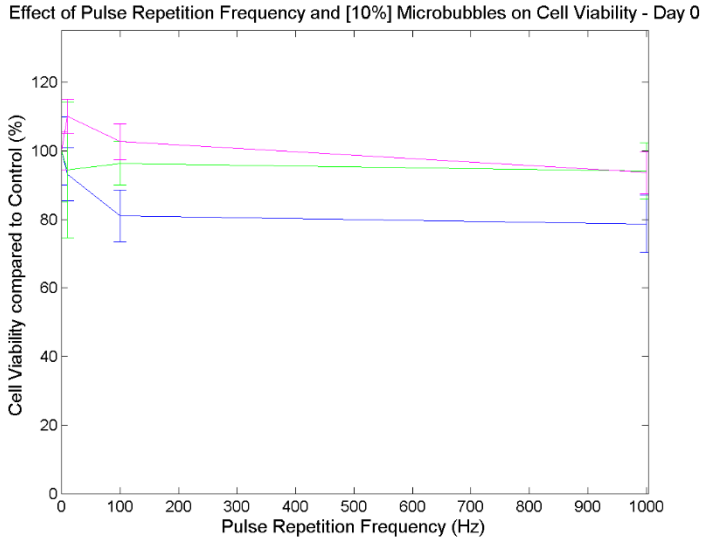

Figure 3.17. Results from 3 independent experiments on viability of cells only exposed to different levels of Pulse Repetition Frequency on the day of exposure with 10% concentration of microbubbles in solution. The levels of PRF used are 10 100 and 1000 Hz. Error bars shown are the percentage of standard deviation of each sample (n=8) for the different drive levels used

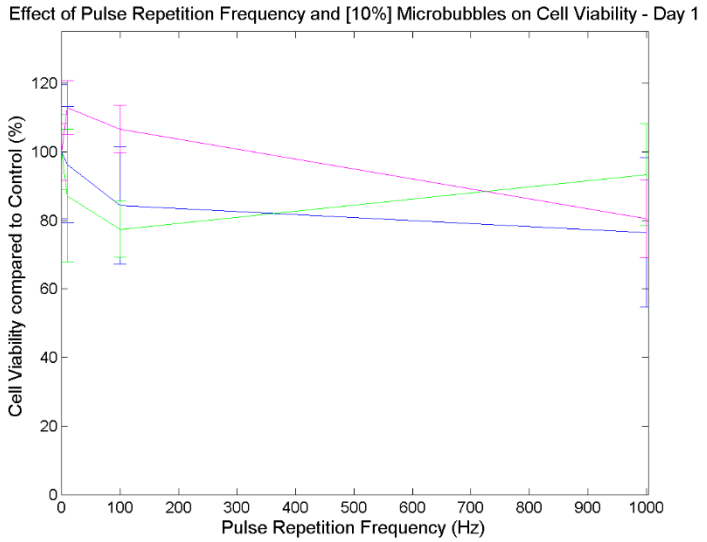

Figure 3.18. Results from 3 independent experiments on viability of cells only exposed to different levels of Pulse Repetition Frequency 1 day after exposure with 10% concentration of microbubbles in solution. The levels of PRF used are 10 100 and 1000 Hz. Error bars shown are the percentage of standard deviation of each sample (n=8) for the different drive levels used

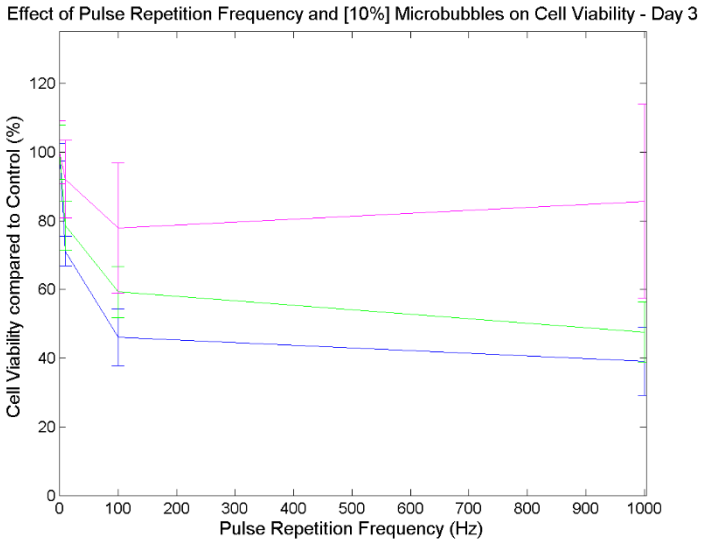

Figure 3.19. Results from 3 independent experiments on viability of cells only exposed to different levels of Pulse Repetition Frequency 3 days after exposure with 10% concentration of microbubbles in solution. The levels of PRF used are 10 100 and 1000 Hz. Error bars shown are the percentage of standard deviation of each sample (n=8) for the different drive levels used

Figures 3.17 – 3.19 confirm the small difference in the results using different values of PRF in the presence of 10% concentration of microbubbles. In days 0 and 1, the survival is ~ 100%. The data points at a PRF of 100 Hz are a repeat of those shown in Figures 3.2-3.4, and the viability measured is the same, within experimental error.

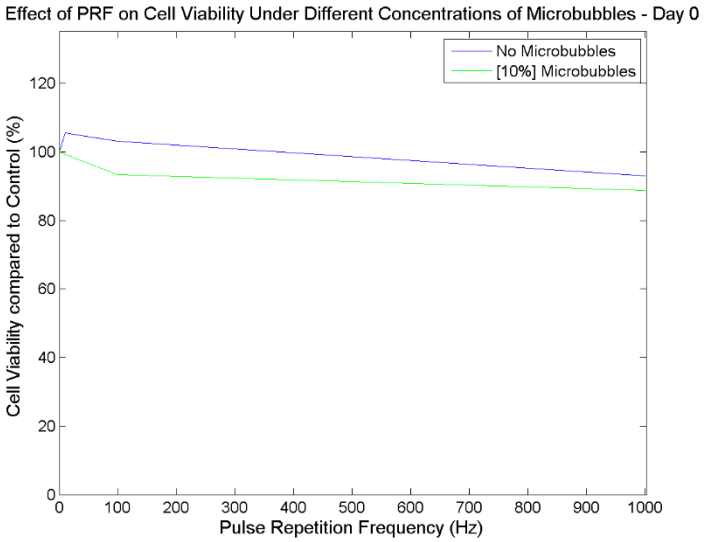

Figure 3.20. Results from 3 independent experiments on viability of cells in the absence and presence of microbubbles and exposed under different levels of pulse repetition frequency – day of the treatment. Each line plotted corresponds to the mean of the results of the 3 independent experiments done under different concentrations of microbubbles. Error bars are omitted for effects of clarity of results.

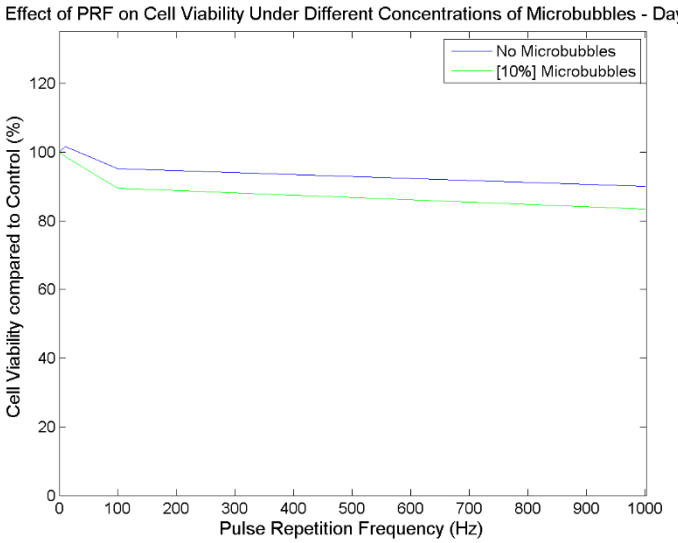

Figure 3.21. Results from 3 independent experiments on viability of cells in the absence and presence of microbubbles and exposed under different levels of pulse repetition frequency – 1 day after the treatment. Each line plotted corresponds to the mean of the results of the 3 independent experiments done under different concentrations of microbubbles. Error bars are omitted for effects of clarity of results.

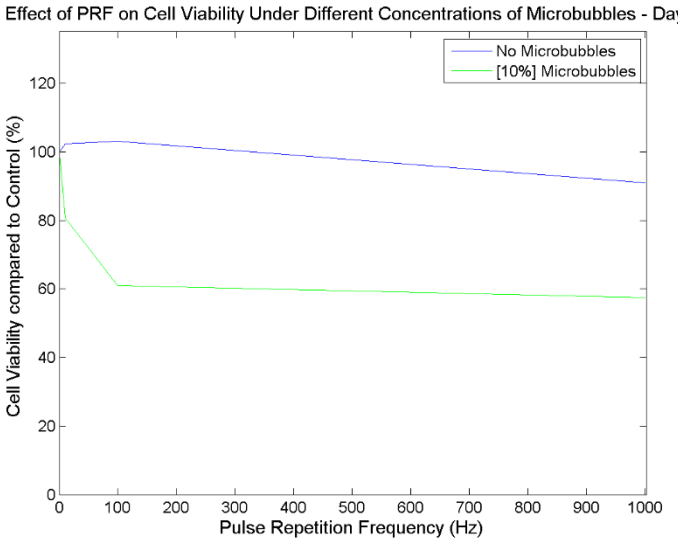

Figure 3.22. Results from 3 independent experiments on viability of cells in the absence and presence of microbubbles and exposed under different levels of pulse repetition frequency – 3 days after the treatment. Each line plotted corresponds to the mean of the results of the 3 independent experiments done under different concentrations of microbubbles. Error bars are omitted for effects of clarity of results.

Figures 3.20 – 3.22 summarise the trend for each condition tested in the day of exposure, 1 and 3 days after the exposure. The presence of 10% microbubbles on the sample is responsible for more cell death 3 days after the exposure – see Figure 3.22.

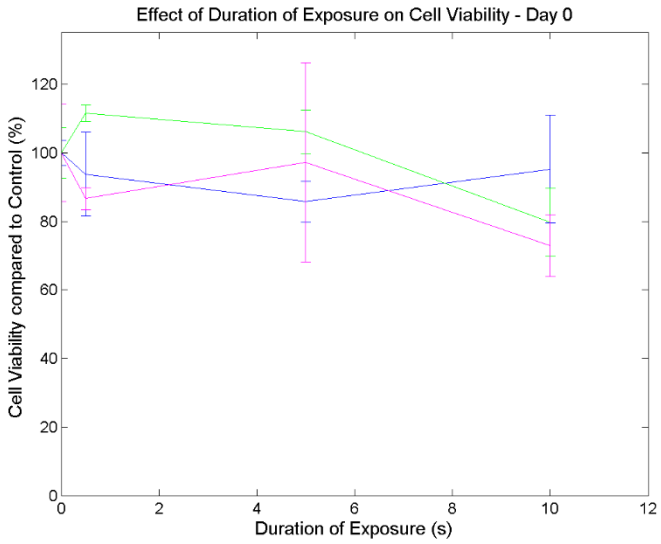

Figure 3.23. Results from 3 independent experiments on viability of cells only exposed to ultrasound during 0.5, 5 and 10 seconds on the day of exposure. Error bars shown are the percentage of standard deviation of each sample (n=8) for the different drive levels used.

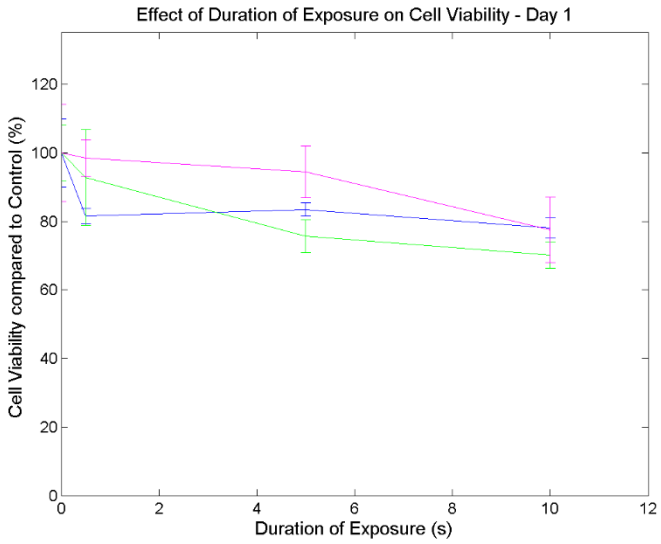

Figure 3.24. Results from 3 independent experiments on viability of cells only exposed to ultrasound during 0.5, 5 and 10 seconds, 1 day after exposure. Error bars shown are the percentage of standard deviation of each sample (n=8) for the different drive levels used.

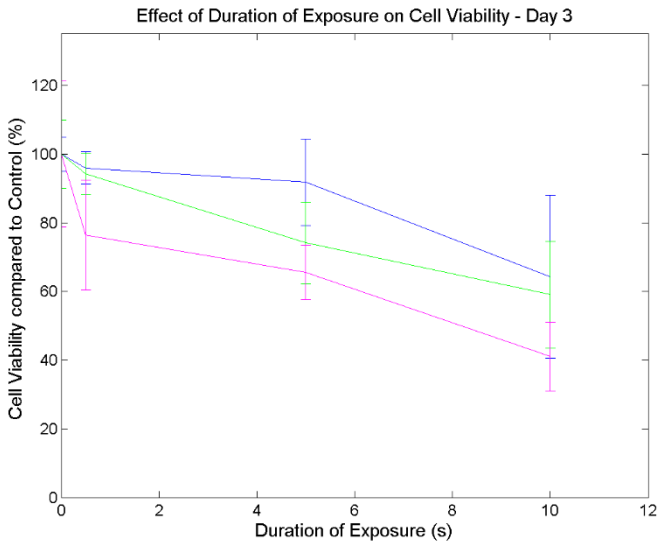

Figure 3.25. Results from 3 independent experiments on viability of cells only exposed to ultrasound during 0.5, 5 and 10 seconds, 3 days after exposure. Error bars shown are the percentage of standard deviation of each sample (n=8) for the different drive levels used.

The effect of exposure time was also studied at a pressure of 0.6 MPa. The times chosen for study were 1, 5 and 10 seconds. This times were chosen because *in vivo*, an exposure grid needs to be defined and each point of the grid must be exposed for only a few seconds to allow the exposure of a large volume of the tumor during the conduct of theisolated limb perfusion.

Figures 3.23 – 3.25 represent the data from 3 independent experiments with ~ 15000 cells/ well) in DMEM, from day 0 to day 3, respectively, to test the effect of exposure duration on the viability of cells. These figures show the minor effect of this parameter on their survival. This is thought to be due mainly to the fact that the medium is not acoustically absorbing enough to raise the temperature to a cytotoxic level. An interesting issue to analyse is whether the effect on the membranes is greater for a longer exposure.

On the day of exposure, the survival is ~ 100% for all exposure times. One day after the exposure, exposures of 1 and 5 seconds give survival around 100%, but an exposure of 10 seconds yields a decrease of around 15% in cell viability. Three days after the exposure, the cells exposed to ultrasound for one or five seconds have their viability decreased to approximately 80% and the group of cells exposed to ultrasound during 10 seconds show a percentage of viability around 50% relative to unexposed controls.

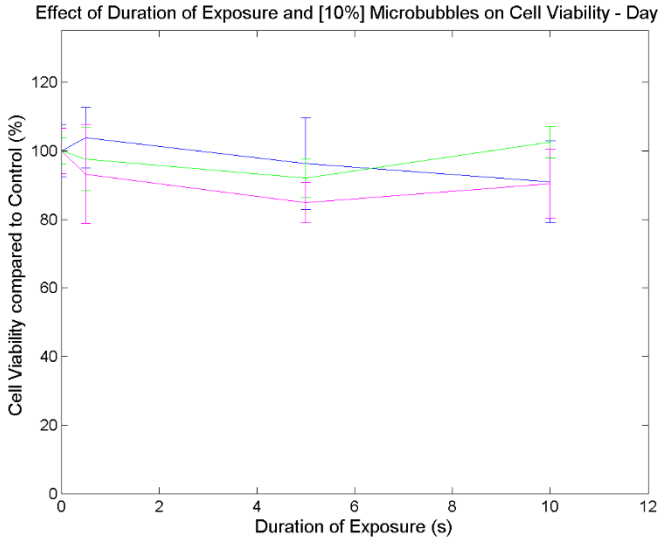

Figure 3.26. Results from 3 independent experiments on viability of cells only exposed to ultrasound during 0.5, 5 and 10 seconds with 10% concentration of microbubbles in solution, on the day of exposure. Error bars shown are the percentage of standard deviation of each sample (n=8) for the different drive levels used.

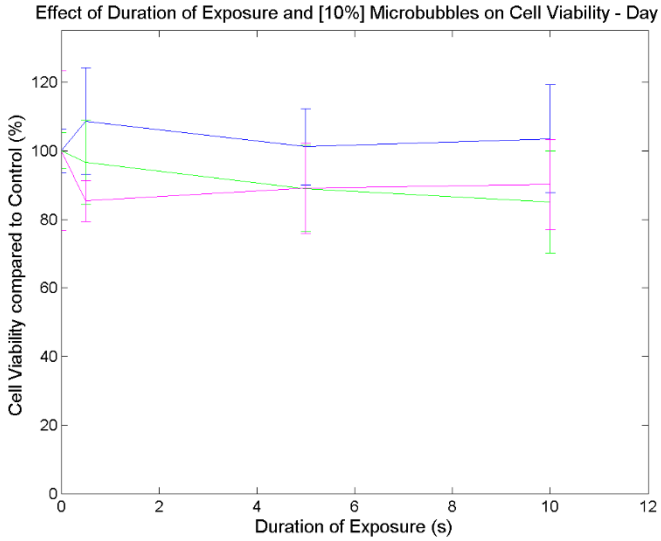

Figure 3.27. Results from 3 independent experiments on viability of cells only exposed to ultrasound during 0.5, 5 and 10 seconds with 10% concentration of microbubbles in solution, 1 day after exposure. Error bars shown are the percentage of standard deviation of each sample (n=8) for the different drive levels used.

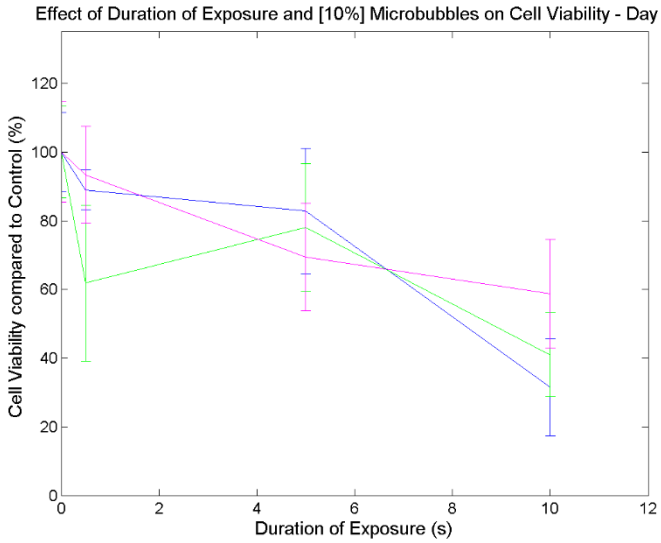

Figure 3.28. Results from 3 independent experiments on viability of cells only exposed to ultrasound during 0.5, 5 and 10 seconds with 10% concentration of microbubbles in solution, 3 days after exposure. Error bars shown are the percentage of standard deviation of each sample (n=8) for the different drive levels used.

Once again, since the variation in exposure time had little effect on cell survival, the most extreme condition, in terms of inertial cavitation, was also tested - cells in DMEM with a concentration of microbubbles of 10% -. The results are shown in Figures 3.26 – 3.27, for the day of the experiment, 1 and 3 days after, respectively.

Even in the presence of a 10% concentration of microbubbles, changing the exposure time has little effect on cell viability in days 0 and 1, where the survival is ~ 100%. In day 3, 70%, 80% and 60% survival is associated with exposures of 1, 5 and 10 seconds respectively. The cells used are a sarcoma line, and it may not be a disadvantage if the cells die a few days after the exposure. The main goal is to help the virus to get through the membranes of the cell to allowit to start replicating and spreading throughout the tumor. In the presence or absence of virus, a delayed cell killing may be advantageous..

As a summary, Figures 3.29 – 3.31 try to show a trend for each condition tested in the day of exposure, 1 day and 3 days after the exposure. The presence of 10% microbubbles on the sample has a similiar effect to that seen in the absence of microbubbles in terms of viability, considering the mean of the three independent experiments – see Figure 3.31.

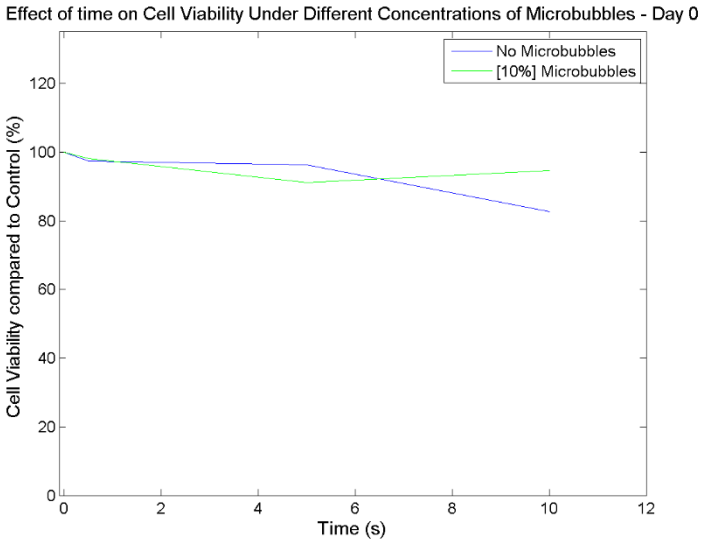

Figure 3.29. Results from 3 independent experiments on viability of cells in the absence and presence of microbubbles and exposed to different exposure duration – day of the treatment. Each line plotted corresponds to the mean of the results of the 3 independent experiments done under different concentrations of microbubbles. Error bars are omitted for clear reading of the results.

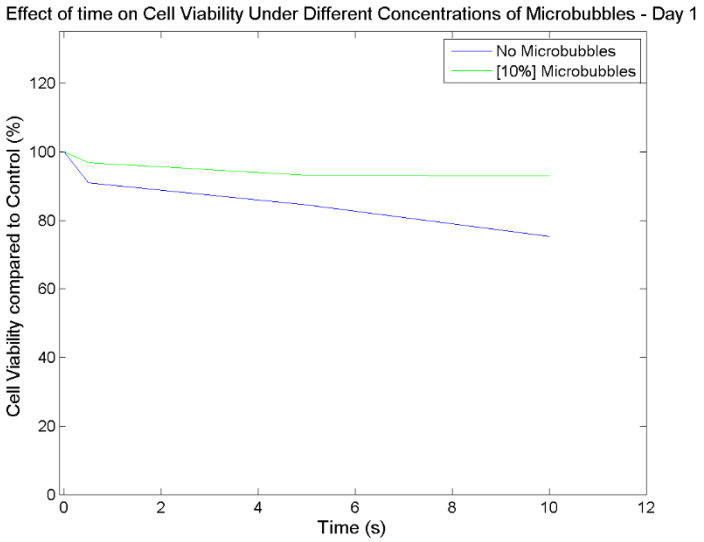

Figure 3.30. Results from 3 independent experiments on viability of cells in the absence and presence of microbubbles and exposed to different exposure duration – 1 day after the treatment. Each line plotted corresponds to the mean of the results of the 3 independent experiments done under different concentrations of microbubbles. Error bars are omitted for clear reading of the results.

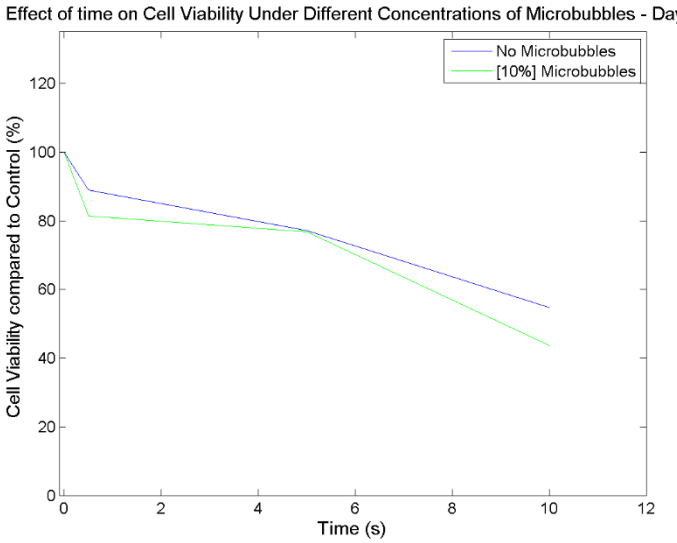

Figure 3.31. Results from 3 independent experiments on viability of cells in the absence and presence of microbubbles and exposed to different exposure duration – 3 days after the treatment. Each line plotted corresponds to the mean of the results of the 3 independent experiments done under different concentrations of microbubbles. Error bars are omitted for clear reading of the results.

4. Study of the effect of Duty Cycle

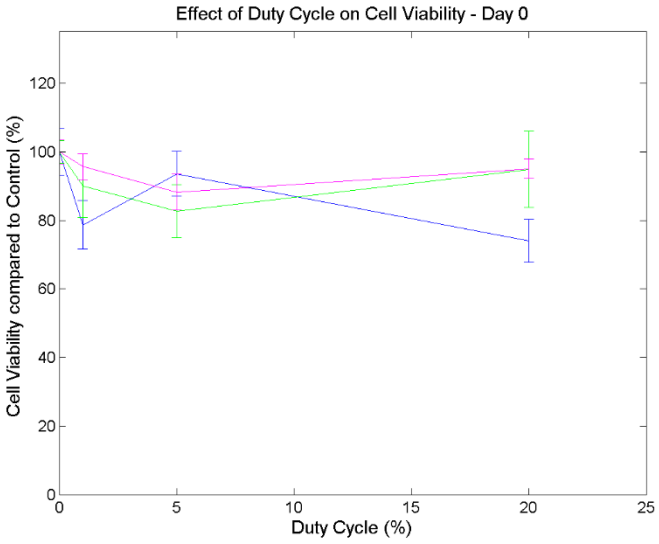

Figure 3.32. Results from 3 independent experiments on viability of cells only exposed to different levels of Duty Cycle on the day of exposure. Error bars shown are the percentage of standard deviation of each sample (n=8) for the different drive levels used.

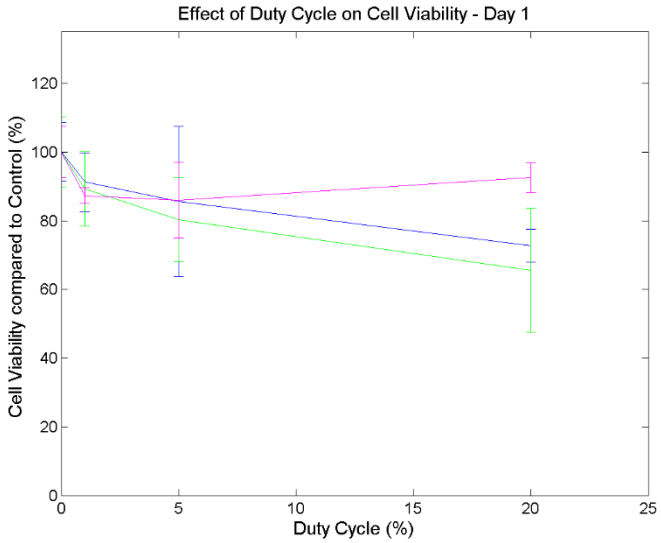

Figure 3.33. Results from 3 independent experiments on viability of cells only exposed to different levels of Duration of Exposure 1 day after exposure. Error bars shown are the percentage of standard deviation of each sample (n=8) for the different drive levels used.

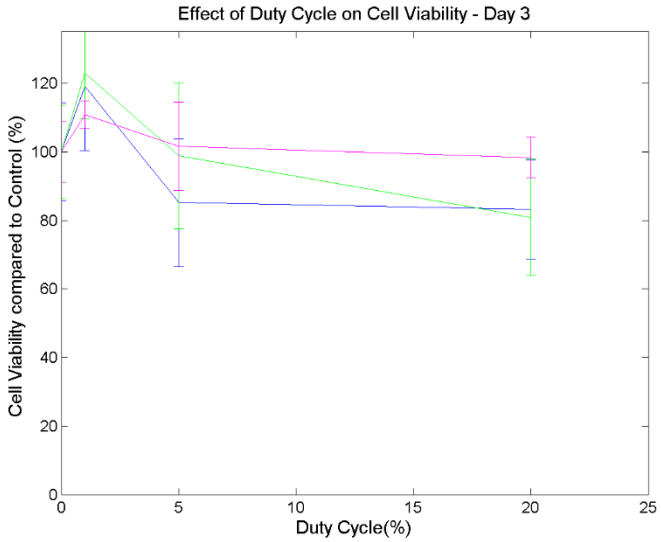

Figure 3.34. Results from 3 independent experiments on viability of cells only exposed to different levels of Duration of Exposure 3 days after exposure. Error bars shown are the percentage of standard deviation of each sample (n=8) for the different drive levels used.

The effect of Duty Cycle was also studied at a pressure that has minimal effect on the viability, 0.6 MPa. The values chosen to test were 2, 5 and 20%. These were chosen because *in vivo*, a continuous exposure would give an unwanted rise in temperature, so it is important to reduce the amount of time the ultrasound in ON during the total time of exposure.

Figures 3.32 – 3.34 show the data from 3 independent experiments ~ 15000 cells /wellfrom days 0 to 3 showing the effect of the Duty Cycle in the viability of cells. Only a minor effect is seen immediately after exposure when this parameter is varied.of In days 1 and 2, exposure with a 5% duty cycle gives a viability of ~ 100%, but with a duty cycle of 20%, a reduction of approximately 25% in viability is seen. In day 3 there is an ~ 20% increase in viability with a duty cycle of 2%, as is seen in Figure 3.34. For a duty cycle of 5%, the viability is around 95% and for a duty cycle of 20%, it is around 85% - greater than 1 day after the exposure. This shows the ability of the viable cells to proliferate after the exposure.

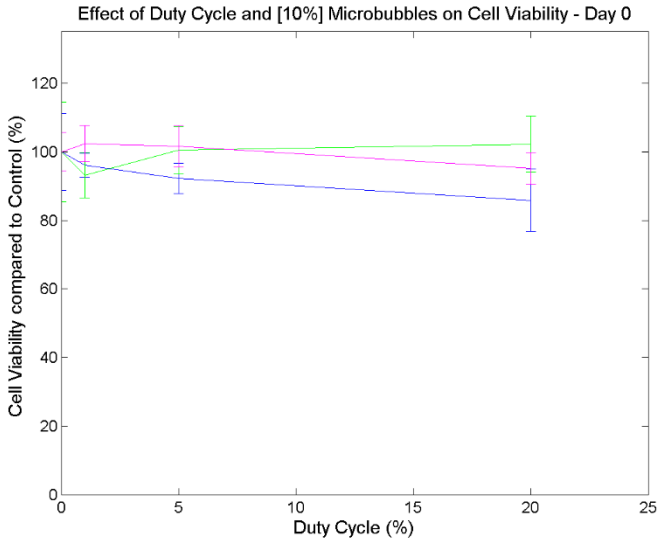

Figure 3.35. Results from 3 independent experiments on viability of cells only exposed to different levels of Duty Cycle with 10% concentration of microbubbles in solution, on the day of exposure. Error bars shown are the percentage of standard deviation of each sample (n=8) for the different drive levels used.

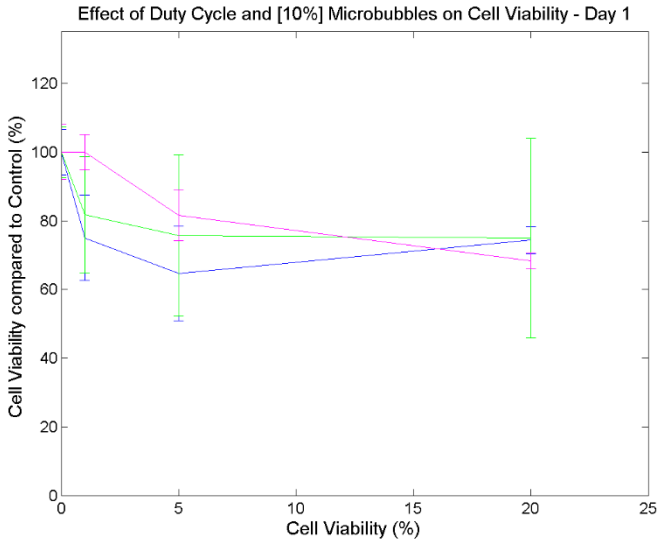

Figure 3.36. Results from 3 independent experiments on viability of cells only exposed to different levels of Duration of Exposure with 10% concentration of microbubbles in solution, 1 day after exposure. Error bars shown are the percentage of standard deviation of each sample (n=8) for the different drive levels used.

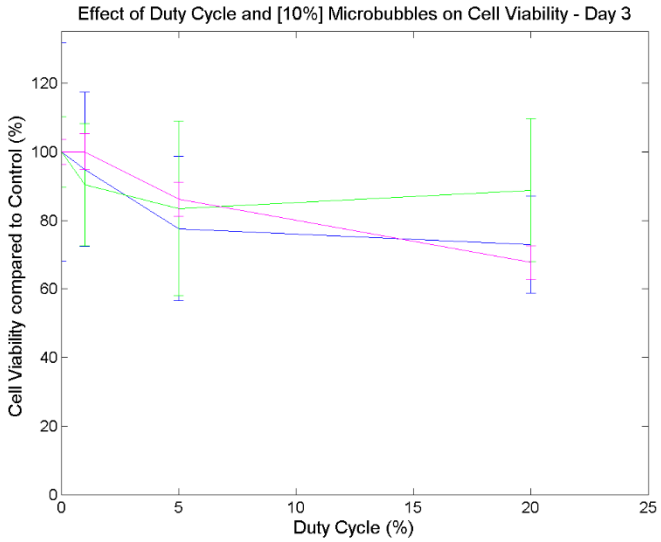

Figure 3.37. Results from 3 independent experiments on viability of cells only exposed to different levels of Duration of Exposure with 10% concentration of microbubbles in solution, 3 days after exposure. Error bars shown are the percentage of standard deviation of each sample (n=8) for the different drive levels used.

Cells were exposed in DMEM with a 10% concentration of microbubbles to see the effect of duty cycle on cell viability, in the presence of cavitation nuclei. The results are shown in Figures 3.35 – 3.37.

On the day of exposure, the presence of microbubbles has no visible effect on the cell viability. One day after the experiment, there is a decrease in viability. However, the viability is the same for all duty cycles. The average survival at 2, 5 and 10% duty cycle

is 87.5, 80 and 75% respectively (Figure 3.36). The average survival rates in day 3 are ~ 92.5, 82 and 85% at a duty cycle of 2, 5 and 10%, respectively, but given the large standard deviations, these may not be statistically significantly different from those in day 1.

Figures 3.38 – 3.40 summarise the trend for each condition tested on the day of exposure, 1 and 3 days after the exposure. The presence of 10% microbubbles on the sample has a similiar effect to that in the absence of microbubbles in terms of viability, considering the mean of the three independent experiments, for all the days under test.

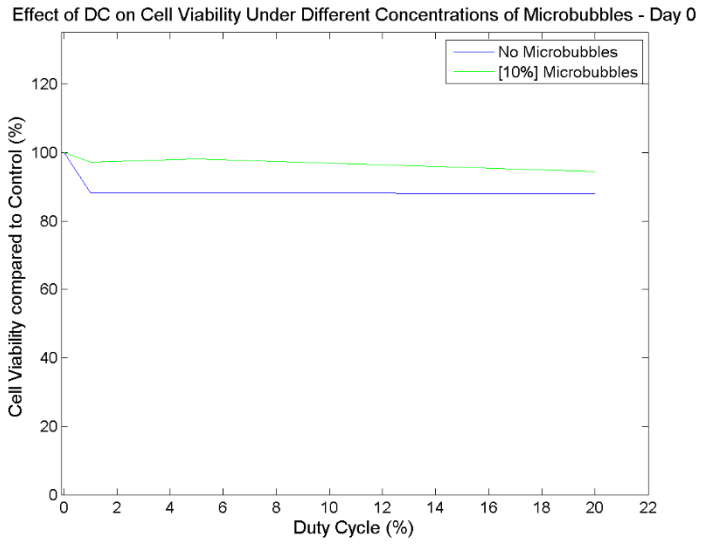

Figure 3.38. Results from 3 independent experiments on viability of cells in the absence and presence of microbubbles and exposed under different duty cycle – day of the treatment. Each line plotted corresponds to the mean of the results of the 3 independent experiments done under different concentrations of microbubbles. Error bars are omitted for clear reading of the results.

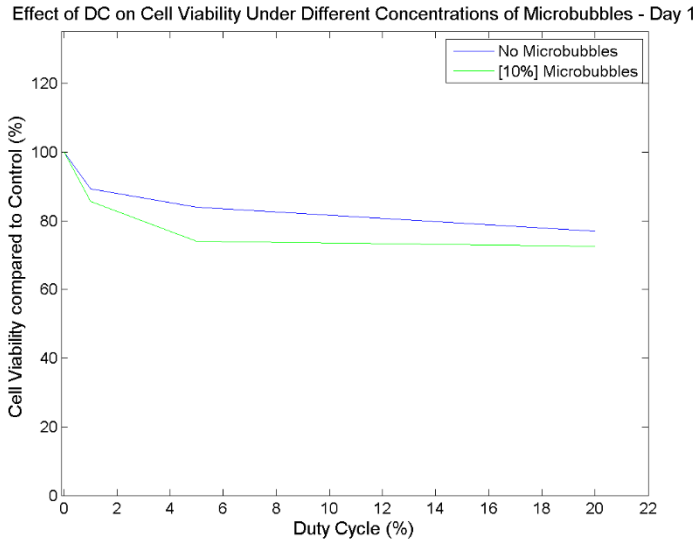

Figure 3.39. Results from 3 independent experiments on viability of cells in the absence and presence of microbubbles and exposed under different duty cycle – 1 day after the treatment. Each line plotted corresponds to the mean of the results of the 3 independent experiments done under different concentrations of microbubbles. Error bars are omitted for clear reading of the results.

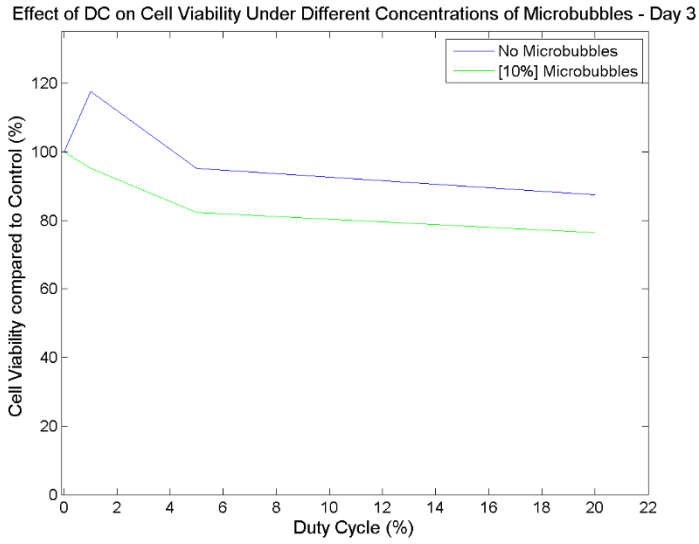

Figure 3.40. Results from 3 independent experiments on viability of cells in the absence and presence of microbubbles and exposed under different duty cycle – 3 days after the treatment. Each line plotted corresponds to the mean of the results of the 3 independent experiments done under different concentrations of microbubbles. Error bars are omitted for clear reading of the results.

→ Effect of Ultrasound exposure at different acoustic Pressures of DMEM on cell survival

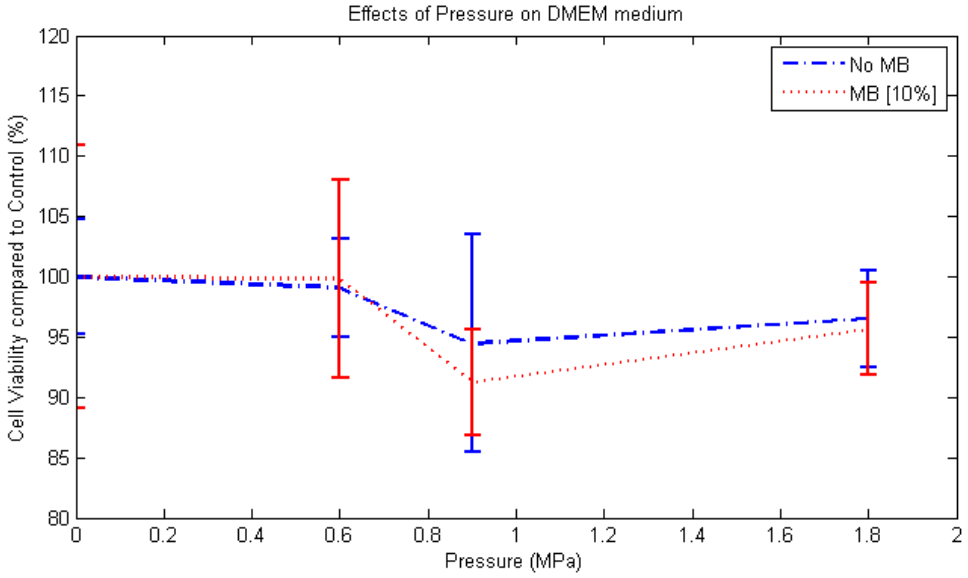

Figure 3.41. Study on the effects of pressure on DMEM. Medium was exposed to ultrasound under different drive levels of pressure and then cells were added to the exposed medium to verify if they would attach and grow compared to control (same number of cells added to unexposed medium). Error bars shown are the percentage of standard deviation of each sample (n=8) for the different drive levels.

The effect of ultrasound in DMEM was tested to investigate the changes seen in the experiments with cells had to do with effects on the cells themselves, or if there was some change in the medium, for example in the pH, that could end up killing the cells. Figure 3.41 shows the results of this experiment and it is possible to see that both in the absence and in the presence of SonoVue microbubbles, the cell viability are allways close to 100%, within errors. There may be some toxicity associated with the presence of microbubbles but this was statistically insignificant. Any ultrasound induced change in the mediumwas sufficiently small (approximately ±10% in terms of percentage of viability compared to control) that it would not be an important factor in *in vitro* experiments. FACS analysis was used to investigate whether there was any change in cell membranes.

3.3.3. Results of FACs Analysis

"FACS" stands for Fluorescence-Activated Cell Sorting. This is a type of flow cytometry – an analytical cell-biology technique that utilizes light to rapidly and accurately count and profile cells in a heterogenous fluid mixture. When additional information is required, antibodies tagged with fluorescent dyes, and raised against highly specific cell surface antigens can be used to better identify and segregate specific sub-populations within a larger group. In a flow cytometer a source of light is used to illuminate sample cells, travelling through a channel with photomultipliers, to detect refracted or emitted light from the cells. Data acquired by the sensors is then processed giving a detailed "picture" of the sample and emissions from fluorescent dyes. A flow cytometer is made up of three main systems: fluidics, optics, and electronics. The fluidics system transports particles in a stream to the laser beam for interrogation; The optical system consists of lasers to illuminate the particles in the sample stream and optical filters to direct the resulting light signals to the appropriate detectors; The electronics convert the detected light signals into signals that can be processed by a computer with the appropriate software.

For the purpose of this thesis, this assay was used to detect the presence of a dye named Propidium Iodide (PI) dye inside a living cell. Propidium iodide is a membrane impermeable dye that is generally excluded from viable cells. It binds to double stranded DNA by intercalating between base pairs. PI is excited at 488 nm and emits at a maximum wavelength of 617 nm. Pi detection is an indicationthat there is a change in the cell membrane after an ultrasound exposure.

The amount of scattered light detected by the photomultipliers is related to the size and shape of the cells. The light intensity in the forward direction (along the axis that the light is traveling) defines the size of the cell, and the amount of light scattered to the side (perpendicular to the axis that the light is traveling) is related to their shape and homogeneity (granularity/complexity). Specialized software (FACSDiva, Version 6.1.3) allows the choice of a gate in which cells of interest (in terms of size and shape) are included. The difference from controls is determined from the statistical information on the populations under analysis.

The controls under study were unexposed cells, those exposed at 0.6 MPa (low exposure) and those exposed at 1.8MPa (high exposure), with or without PI. All the

controls include microbubbles (20% concentration to guarantee an extreme condition) to be sure that cavitation was present. Figures 3.42-3.44 show the data for controls without PI, which were used to help interpret the results on exposed cells. Population 1 (P1), defines the group of cells under study. The low level of Side-Scattered Light relates to dead cells and the high Forward-Scattered signal shows cell doublets, i.e. the double detection of the signal from a cell, giving the impression that a cell is bigger than the others. The P1 gate includes two subpopulations. The one on the left (P3) and the one on the right. The one on the left is the dying population the one on the right is the living one (P2).

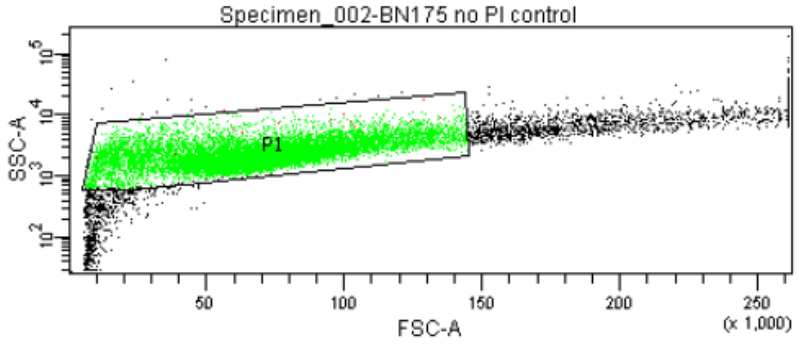

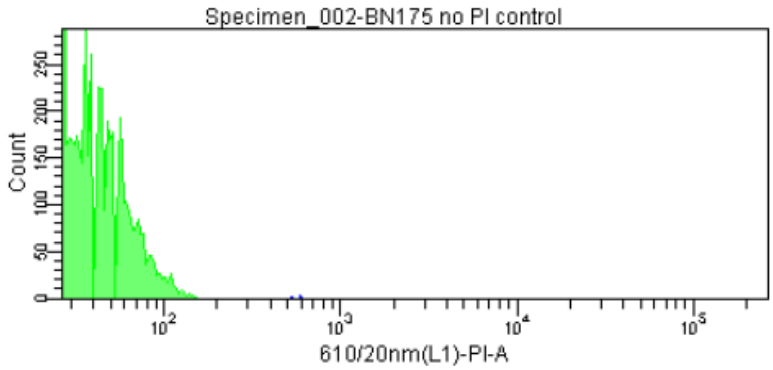

Tube: BN175 no PI control

Population	#Events	%Parent	%Total
All Events	13,540	####	100.0
P1	11,156	82.4	82.4
P2	11,133	99.8	82.2
P3	3	0.0	0.0

Figure 3.42. Flow cytometric analysis of control BN175 cells (not exposed to ultrasound) in DMEM with 20% SonoVue Microbubbles. From top to bottom, first a dot plot shows the counts of the cells in terms of size (x axis) and shape (y axis). The gate (placed around the green dots) defines the population of interest – live cells; then, an histogram shows the counts of emissions detected by the filter 610/20nm(L1)-PI, which is the filter used to distinguish populations with/without PI; finally, a table of statistics gives useful information on the populations – from all the events detected, the population of interest was identified and then inside this population P2 and P3 distinguish the populations without and with PI, respectively. The definition of P2 and P3 was made with data from controls with PI (Figures 3.45-3.47). The gates are fixed for all the analysis.

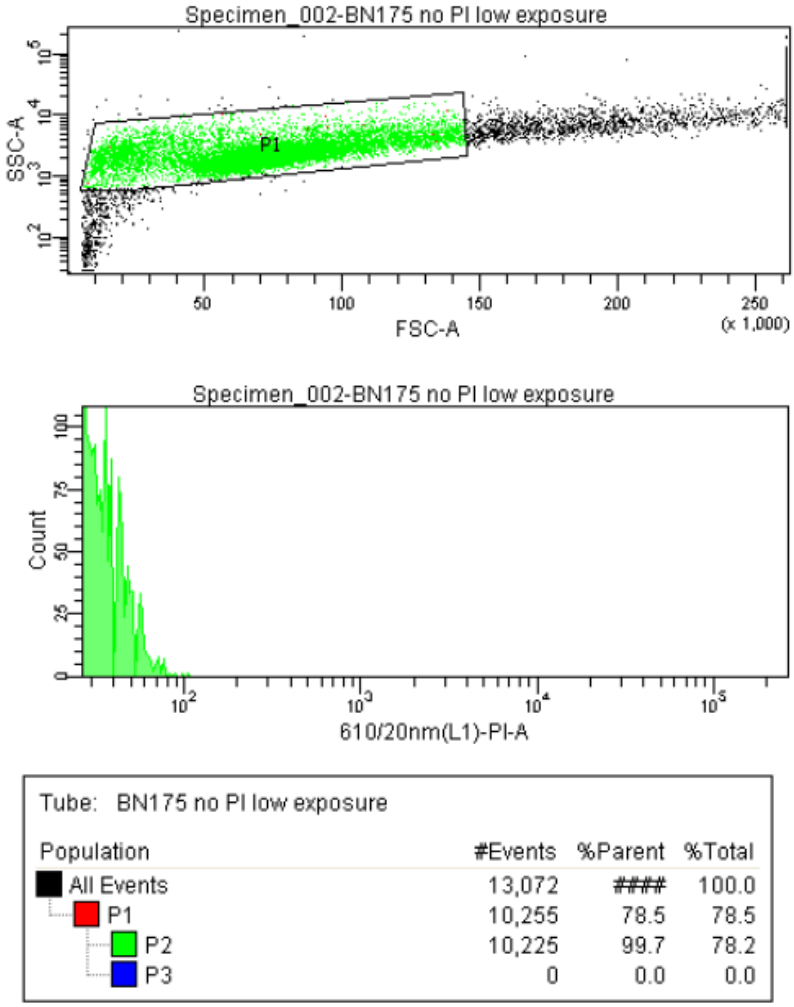

Tube: BN175 no PI low exposure

Population	#Events	%Parent	%Total
All Events	13,072	####	100.0
P1	10,255	78.5	78.5
P2	10,225	99.7	78.2
P3	0	0.0	0.0

Figure 3.43. Flow cytometric analysis of BN175 cells exposed to ultrasound at peak negative pressure of 0.6 MPa in DMEM with 20% concentration of SonoVue microbubbles. From top to bottom, first a dot plot shows the counts of the cells in terms of size (x axis) and shape (y axis). The gate (placed around the green dots) defines the population of interest – live cells; then, an histogram shows the counts of emissions detected by the filter 610/20nm(L1)-PI, which is the filter used to distinguish populations with/without PI; finally, a table of statistics gives useful information on the populations – from all the events detected, the population of interest was identified and then inside this population P2 and P3 distinguish the populations without and with PI, respectively. The definition of P2 and P3 was made with data from controls with PI (Figures 3.45-3.47). The gates are fixed for all the analysis.

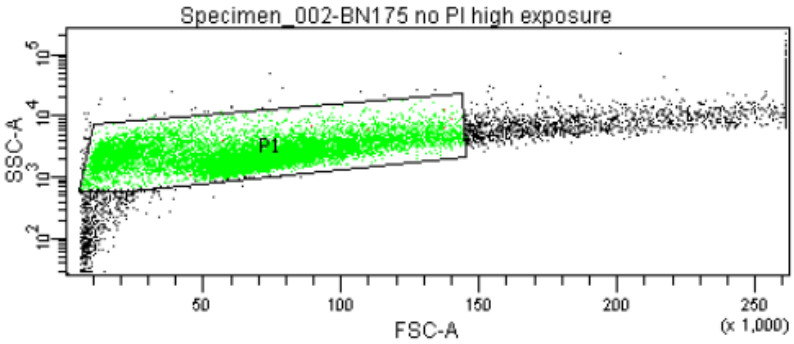

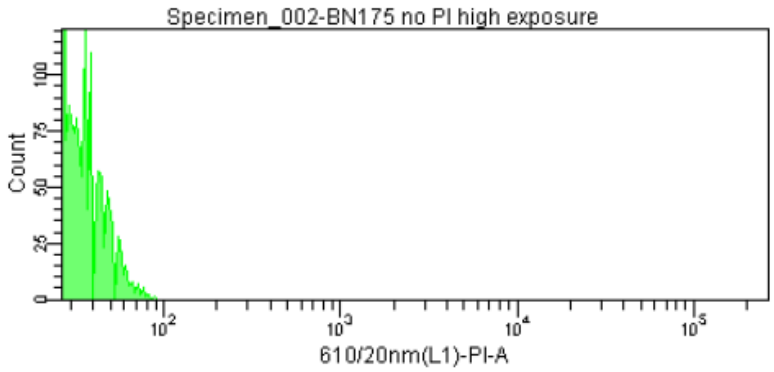

Tube: BN175 no PI high exposure

Population	#Events	%Parent	%Total
All Events	12,838	####	100.0
P1	10,223	79.6	79.6
P2	10,190	99.7	79.4
P3	0	0.0	0.0

Figure 3.44. Flow cytometric analysis of BN175 cells exposed to ultrasound at peak negative pressure of 1.8MPa in DMEM with 20% concentration of SonoVue microbubbles. From top to bottom, first a dot plot shows the counts of the cells in terms of size (x axis) and shape (y axis). The gate (placed around the green dots) defines the population of interest – live cells; then, an histogram shows the counts of emissions detected by the filter 610/20nm(L1)-PI, which is the filter used to distinguish populations with/without PI; finally, a table of statistics gives useful information on the populations – from all the events detected, the population of interest was identified and then inside this population P2 and P3 distinguish the populations without and with PI, respectively. The definition of P2 and P3 was made with data from controls with PI (Figures 3.45-3.47). The gates are fixed for all the analysis.

Figures 3.45-3.47 are interesting not only because of the clear distinction between populations with, and without, PI but also because in terms of statistics, there is a difference between unexposed, low and high exposure controls. Statistics show that in the unexposed control, 11% of the population has PI inside its membranes compared to 15.3 and 20.8% at low and high exposure, respectively. This suggests that there is increased permeabilization of the membranes that allows the PI to get inside the cells. Also, there is a reduction in the number of living cells detected in the same gate as we go from unexposed to low and then high exposure – 67.2, 63.6 and 59.3%, respectively. For the

controls without PI, these values are, from unexposed to low and then high exposure, 82.2, 78.2 and 79.4%, respectively.

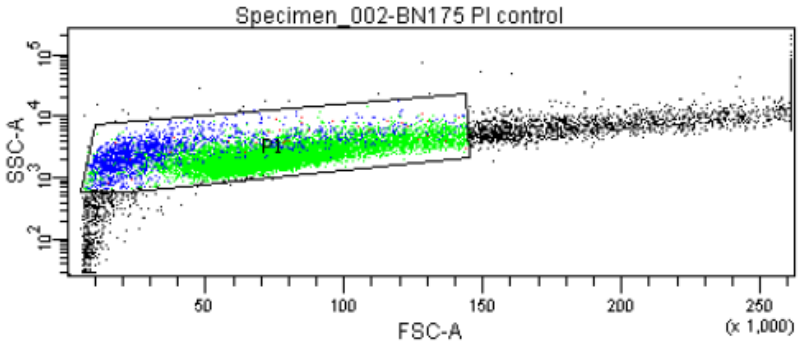

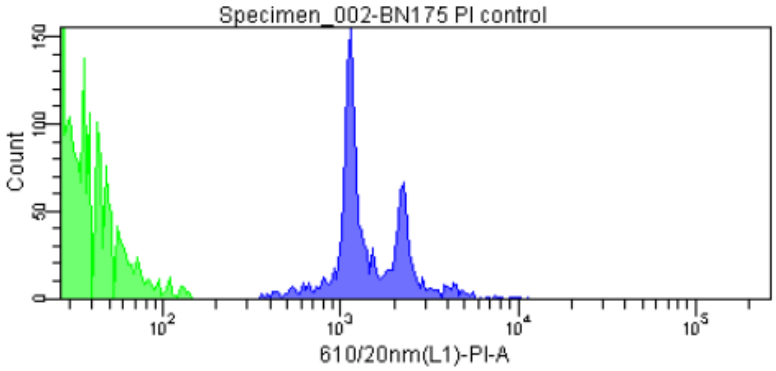

Tube: BN175 PI control

Population	#Events	%Parent	%Total
All Events	13,935	####	100.0
P1	11,018	79.1	79.1
P2	9,363	85.0	67.2
P3	1,527	13.9	11.0

Figure 3.45. Flow cytometric analysis of unexposed BN175 cellsin DMEM with 20% concentration of SonoVue microbubbles. From top to bottom, first a dot plot shows the counts of the cells in terms of size (x axis) and shape (y axis). The gate (placed around the green dots) defines the population of interest – live cells; then, an histogram shows the counts of emissions detected by the filter 610/20nm(L1)-PI, which is the filter used to distinguish populations with/without PI; finally, a table of statistics gives useful information on the populations – from all the events detected, the population of interest was identified and then inside this population P2 and P3 distinguish the populations without and with PI, respectively. The gates are fixed for all the analysis. Clear distinction of two populations help in the definition of P2 (green) and P3 (blue). The gates are fixed in all the analysis.

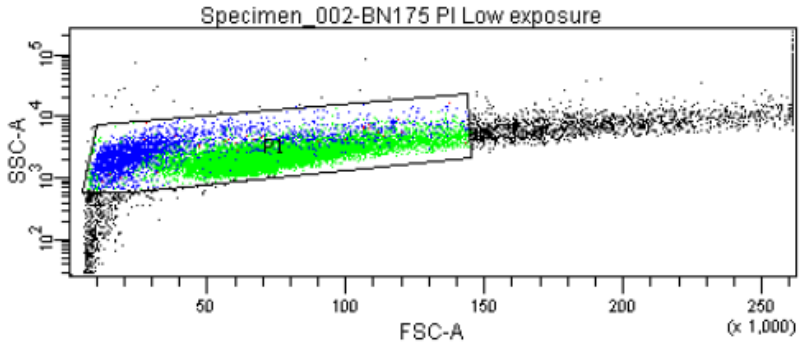

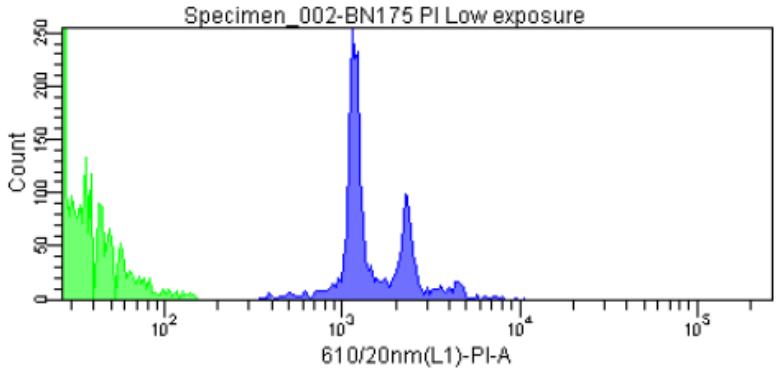

Tube: BN175 PI Low exposure

Population	#Events	%Parent	%Total
All Events	14,373	####	100.0
P1	11,469	79.8	79.8
P2	9,146	79.7	63.6
P3	2,195	19.1	15.3

Figure 3.46. Flow cytometric analysis of BN175 cells exposed to ultrasound at a peak negative pressure of 0.6MPa in DMEM with 20% concentration of SonoVue microbubbles. From top to bottom, first a dot plot shows the counts of the cells in terms of size (x axis) and shape (y axis). The gate (placed around the green dots) defines the population of interest – live cells; then, an histogram shows the counts of emissions detected by the filter 610/20nm(L1)-PI, which is the filter used to distinguish populations with/without PI; finally, a table of statistics gives useful information on the populations – from all the events detected, the population of interest was identified and then inside this population P2 and P3 distinguish the populations without and with PI, respectively. The gates are fixed for all the analysis.

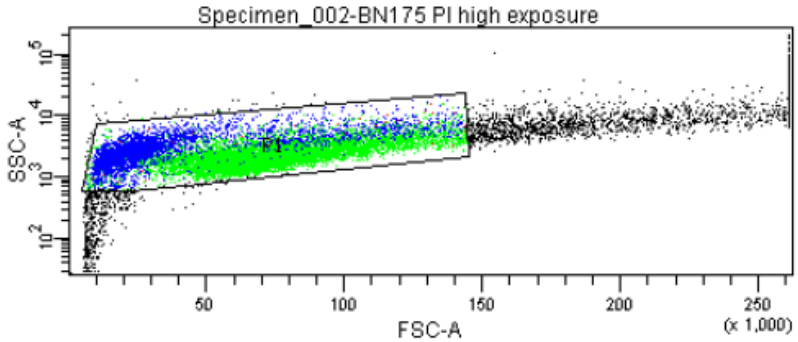

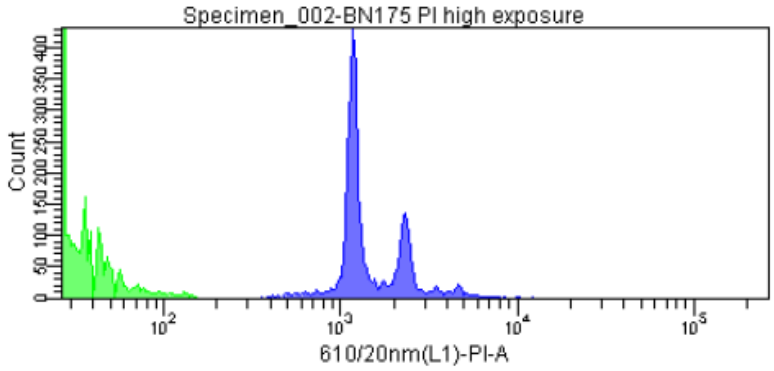

Tube: BN175 PI high exposure

Population	#Events	%Parent	%Total
All Events	15,341	####	100.0
P1	12,430	81.0	81.0
P2	9,099	73.2	59.3
P3	3,191	25.7	20.8

Figure 3.47. Flow cytometric analysis of BN175 cells exposed to ultrasound at a peak negative pressure of 0.6MPa in DMEM with 20% concentration of SonoVue microbubbles. From top to bottom, first a dot plot shows the counts of the cells in terms of size (x axis) and shape (y axis). The gate (placed around the green dots) defines the population of interest – live cells; then, an histogram shows the counts of emissions detected by the filter 610/20nm(L1)-PI, which is the filter used to distinguish populations with/without PI; finally, a table of statistics gives useful information on the populations – from all the events detected, the population of interest was identified and then inside this population P2 and P3 distinguish the populations without and with PI, respectively. The gates are fixed for all the analysis.

4. *In Vivo* Study on the Development of a Combined Treatment for Cancer using Virus and Focused Ultrasound

4.1. Introduction to the *In Vivo* Study

Sonoporation describes the ultrasound technique in which the permeability of a cell membrane is changed. This alteration in the membrane generates a passage through which small molecules can enter. During the last decades, research on Focused Ultrasound and microbubble mediated Virotherapy has been carried out and proved to be a promising approach to cancer treatment. The treatments under study include strategies such as viral transduction of tumour cells with 'suicide genes', using viral infection to trigger immune-mediated tumour cell death, and the use of oncolytic viruses for their anti-tumour action.

Pre-clinical studies have identified isolated organ perfusion as a successful modality for the extravasation of particles within perfused tissue. For oncolytic viruses, sonoporation seems to be an important method of increasing viral uptake in cells, but the safety and efficiency of the overall process must be optimised for clinical use. Although the combination of focused ultrasound and the biological effects of virus has already been suggested as a useful technique to cancer treatment, the addition of a novel technique such as happens with Isolated Limb Perfusion to avoid uncontrolled infection of other organs may provide a more efficient way of killing malignant cells.

The toxicity of viral therapy is a concern and to minimize it, ILP was developed. This is a chemotherapeutic technique using melphalan, tumour necrosis factor-alpha and oncolytic vaccinia virus and involving the cannulation of the blood vessels which feed the tumour-bearing region and isolation of the limb from the systemic circulation by tourniquet. This is necessary because of the severe toxicity of TNF-α. In this project, the combination of ILP and FUS in the presence of microbubbles to increase viral penetration of tumour bulk in Brown Norwegian rats transfected with BN175 fibrosarcoma cells is

studied. The perfused leg forms a collateral blood supply, which supplies the limb while the femoral artery and vein are isolated from the systemic circulation.

For the purpose of this dissertation the aims of this *in vivo* studie are:

1. Characterisation of the effects of FUS and MB on standard ILP with melphalan/TNF-alpha in rat distal limb sarcoma.
2. Evaluation of FUS + MB over low (~7MPa) and high (~11MPa) ultrasound pressures as a means of enhancing intratumoural delivery of oncolytic virotherapy during ILP.

These studies included the evaluation of viral biodistribution using viral plaque assays, quantitative PCR, analysis of gene expression and non-invasive imaging (bioluminescent and GFP/RFP imaging) for characterisation of the effects of therapeutic FUS + MB with ILP-delivered oncolytic virotherapy.

4.2. Methods used for the *In Vivo* Study

This part of the project was carried out, as part of a joint study, with the help of Henry Smith – a Clinical Research Fellow at the Institute of Cancer Research. Henry has implanted the tumors in the rats, operated on them and then, after the treatment with ultrasound, extracted organs and analysed the tumors.

Cell line, Cytotoxic Agents and Perfusion System

- The BN175 rat sarcoma cell line is tumorigenic in Brown Norwegian rats. Cells were passaged and cultured in DMEM.

- Melphalan (SigmaAldrich, St Louis) was reconstituted using the manufacturer's instructions. GLV-1h68 was produced and provided by Genelux Corporation (San Diego).

- GLV-1h68 was constructed by inserting three expression cassettes into the F14.5L, J2R and A56R loci of the viral genome.

- Recombinant rat TNF-α (First Link Ltd, Birmingham, UK) was dissolved in PBS to a concentration of 100 mg/mL.

-Therapeutic agents were added to the perfusate reservoir at the following doses: melphalan - 40 μg, TNF-α - 50 μg, GLV-1h68 - 1×10^7 plaque forming units (pfu).

The ILP technique is shown schematically in figure 4.1.

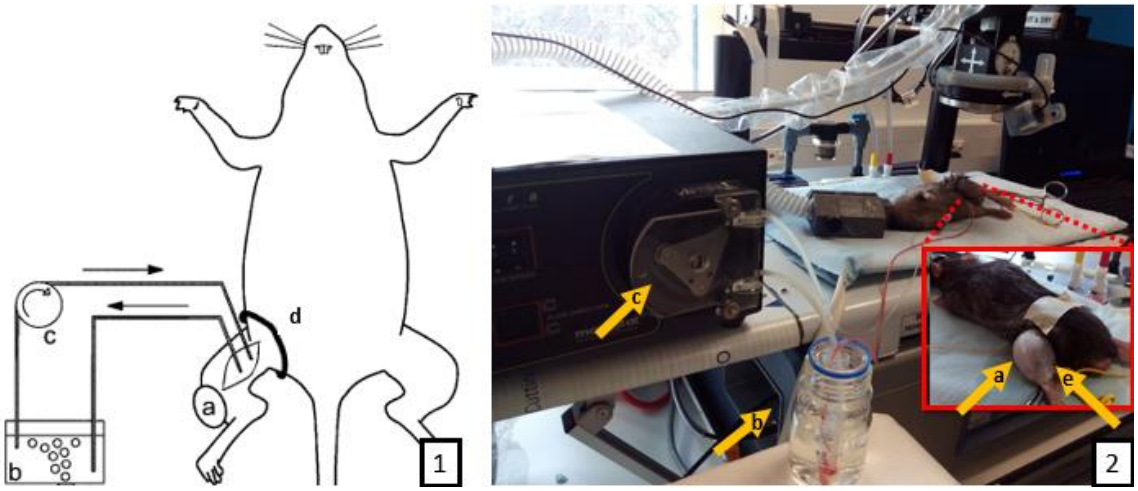

Figure 4.1. On the left (1) - Schematic of Isolated Limb Perfusion Technique in a rat: a – Soft Tissue Sarcoma; b- perfusion reservoir; c- roller pump; d-tourniquet. Adapted from: Wilfred K. de Roos et al, "Isolated Limb Perfusion for Local Gene Delivery - Efficient and Targeted Adenovirus-Mediated Gene Transfer Into Soft Tissue Sarcomas", Annal of Surgery, 2000, 232(6), p. 814-821; On the right (2) – Superposition of photos from the ILP system used. The yellow arrows point to the components labelled in figure 4.1.1.

Animals

- Specific pathogen-free, male Brown Norwegian rats (200–250 g) aged 8-10 weeks, were housed in compliance with all relevant regulatory requirements and fed standard chow and water ad libitum.

- BN175 cells were harvested from tissue culture flasks and washed in PBS three times prior to injection of 1×10^7cells in 500µl of PBS on the outside of the left leg. Tumour growth was assessed every 48 hr by direct calliper measurement in two orthogonal dimensions. Tumour volume was calculated using the formula: $Volume = \frac{1}{2}(width^2 \times breadth)$. ILP was performed when tumours had a maximum diameter between 0.8 and 1.2 cm in all directions. Perfusion was performed for 13 min and washout for 2 min. Transient limb dysfunction (in the form of decreased limb movement) usually occurred immediately after the procedure,
but full function in the perfused limb was seen within 2 hr of recovery. The therapeutic groups consisted of six animals.

- The ILP technique involved the cannulation of blood vessels. An incision was made in the groin as shown in figure 4.2.a, the vessels were dissected and cannulated as shown in figure 4.2.b. The cannula were about 20cm long and were connected to the perfusion circuit.

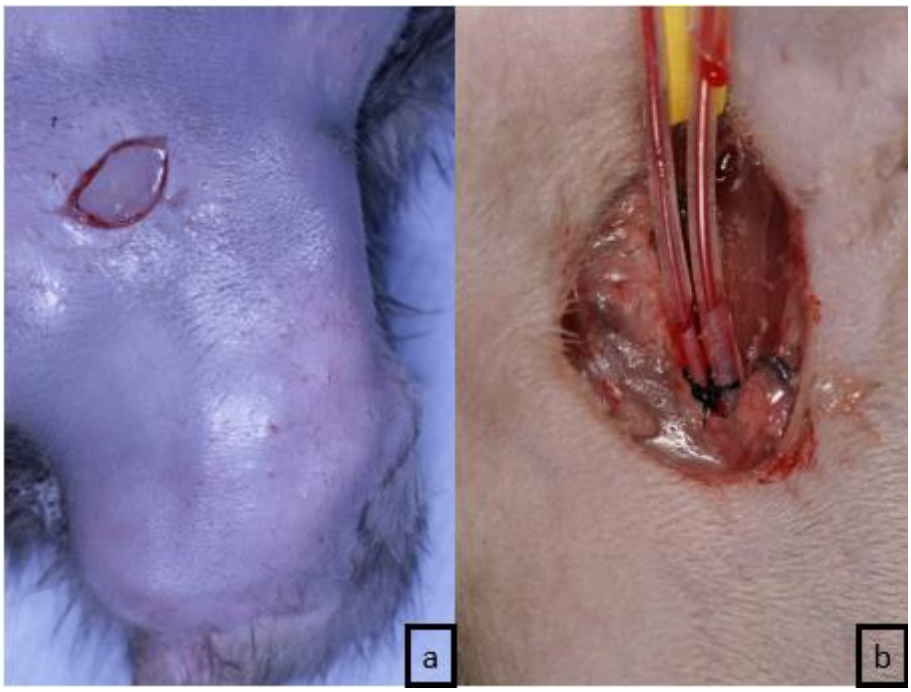

Figure 4.2. Cannulation of Blood Vessels: a- incision in the groin; b- dissected vessels cannulated. The yellow band is a rubber band used to retract the inguinal ligament (not present in the figure).

Equipment, Treatment and Experiments using VIFU 2000

1. Equipment Design: Cavitation Detection in conjunction with the VIFU system

The VIFU 2000 is a pre-clinical HIFU (High Intensity Focused Ultrasound) system (Alpinion, Korea) uniquely designed for investigating a wide range of HIFU applications in small animals. This system enables users to undertake real time image guided research in projects such as ultrasound meditated drug delivery studies, ablation of solid tumors, and mechanical and cavitation effects in ex-vivo/in-vivo systems.

No cavitation detection was possible with the system available, so it was necessary to design a holder for a PCD (that used for *in vitro* experiments, with the same detection system – see section 2.2.2). This was done with the help of the ICR Mechanical Workshop. A picture of the holder is shown in Figure 4.3.

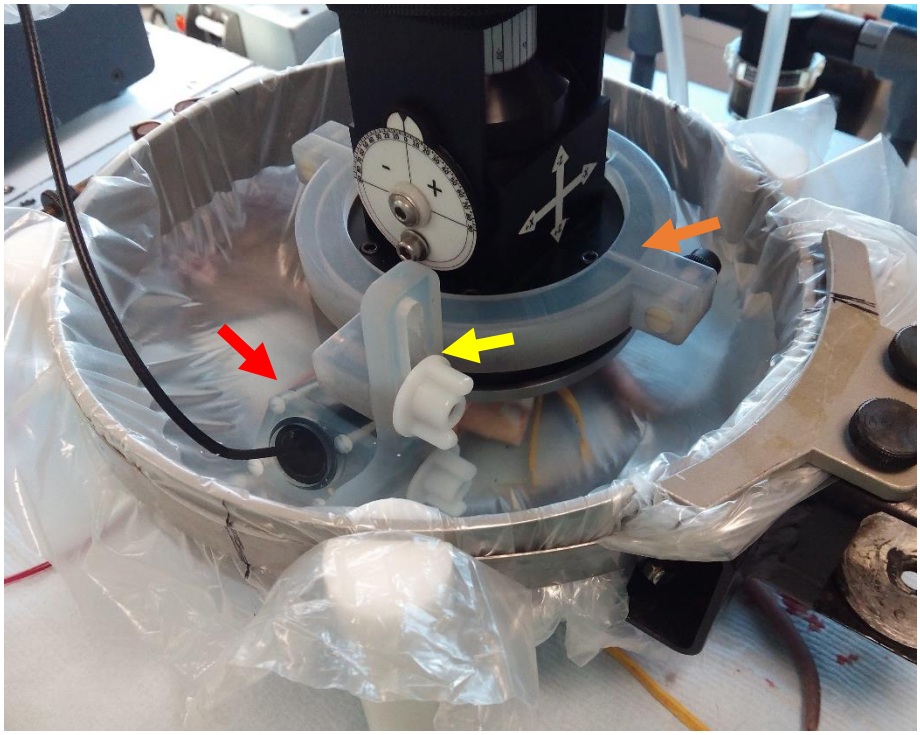

Figure 4.3. Picture of the PCD holder, built in-house, and placed around the VIFU 2000 dry transducer, inside a water bag full of degassed water, to provide coupling . The orange arrow points to the ring that fixes the holder to the transducer. the yellow arrow indicates the piece of the holder that allows movement of the PCD in two directions for positioning and the red arrow points tothe piece of the design that holds the PCD in place.

2. Calibration of the VIFU system

An attempt to calibrate the VIFU system was made using a micrometric gantry to move a hydrophone in the ultrasound field. This was needed because the VIFU system's gantry did not allow sufficiently accurate measurements. It was necessary to localise the peak of the ultrasound beam (as described in section 2.1.2) and once the peak had been found, pressure data was acquired at 0.5mm intervals along one direction orthogonal to the beam axis. It was found that the VIFU gantry did not reproducibly return to zero after a scan, and so accurate beam plotting was not possible. However, the measurement using the micrometric gantry was not perfect because a water tank was needed for coupling and so the gantry was positioned at a small angle to the transducer, and this led to less accurate calibration of the system – this can be seen in figure 4.4. The focus was found and it can be seen in figure 4.4 that a pressure peak is present. From figure 4.4 to figure 4.5, in terms of calibration, the transducer was rotated through 90º and the measurement was repeated – a flat top can be seen. This is because the beam was slightly displaced in this axis, with respect to the hydrophone.

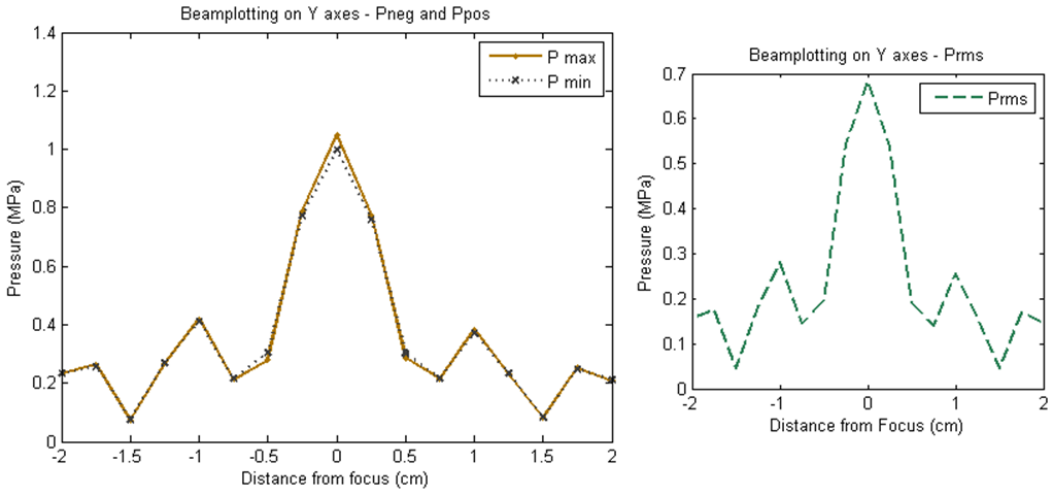

Figure 4.4. Beamplotting of Y axes of VIFU 2000 dry system transducer at a power level of 4.8 W

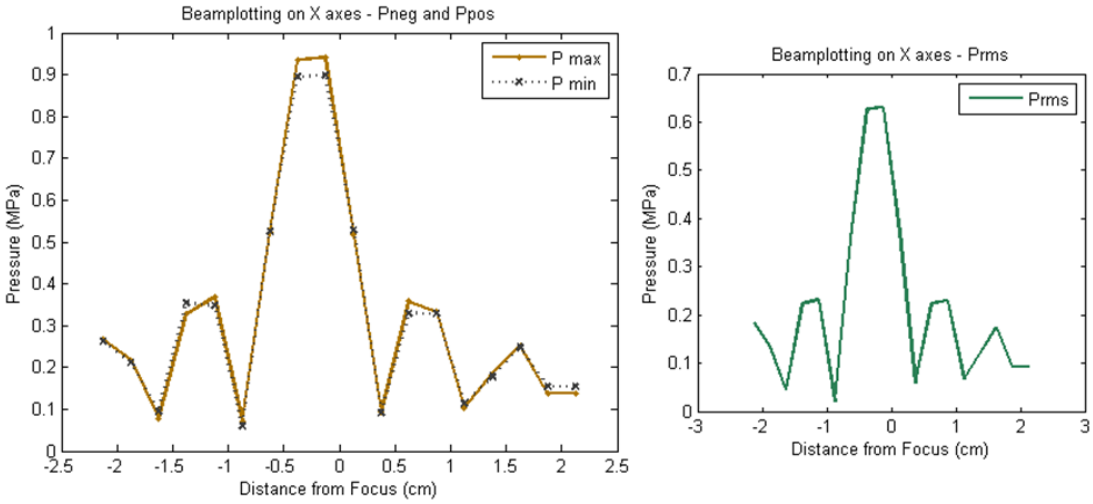

Figure 4.5. Beamplotting of X axes of VIFU 2000 dry system transducer at a power level of 4.8 W

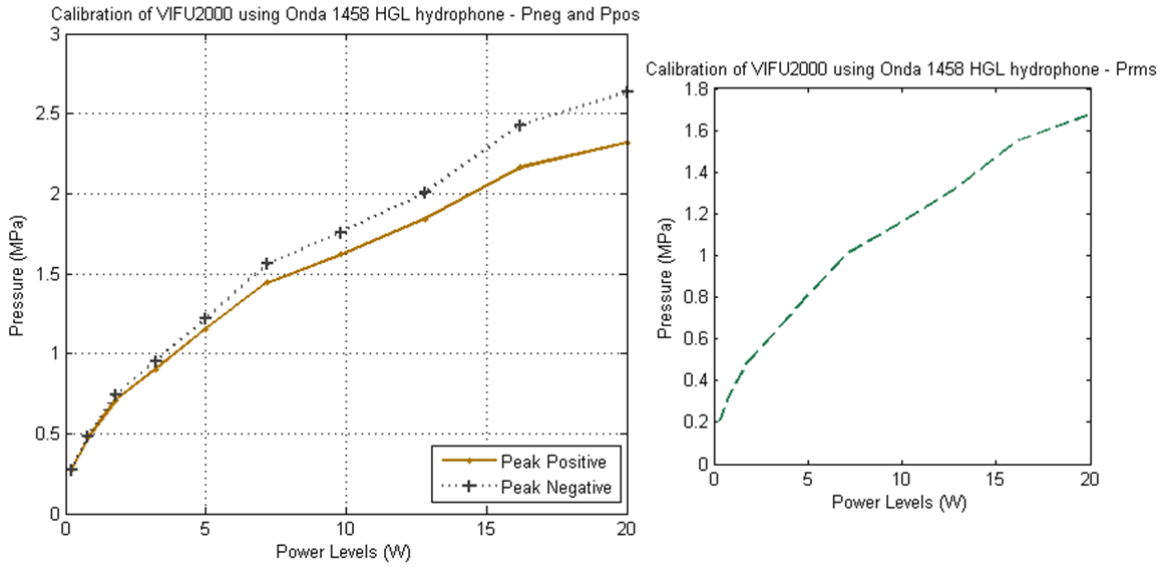

Figure 4.6. Data from VIFU2000 calibration at different power levels using an hydrophone and the micrometric gantry to positioning effects. Only one measurement was done due to lack of time so there are no error bars present. Specifications sheet from NPL sets the error of the hydrophone detection to 7% but a value of 10% of error in each measurement is considered to avoid underestimates

3. Treatment Planning

The results *in vitro* have been used as a starting point to test whether there was an effect of ultrasound on viable cells, but the results cannot be compared to what happens *in vivo* due different factors including the aborption in tissue, higher temperature and presence of vasculature.

As a starting point, a dummy experiment was made on a dead rat and the coupling was achieved using a water bag – see figure 4.7.A. The alignment of the cavitation detection system was aligned with the HIFU focal region prior to experiments. The exposures started at peak negative pressure of 0.6 MPa. The output was increased until some signal was detected by the PCD. After a number of exposures it was decided to group the experiments into two exposure levels – "low" and "high" pressure, i.e. the lowest pressure in which some reflections could be detected by the PCD and a higher level to test if there was a big difference in terms of viral uptake results. In the low pressure cohort, 6 rats were exposed at 50W (~7MPa peak negative pressure at the focus) and ... rats in the high pressure cohort, were treated with a 150W exposure (corresponding to ~10MPa peak negative pressure), with fixed parameters of 5% duty, 100 PRF and

ultrasound frequency of 1.5 MHz. Figure 4.7 shows a part of the experimental set up for *in vivo* experiments.

In this pilot study, 4 cohorts were defined as follows:

i. Standard ILP alone
ii. Cohort 1 (ILP + 10% MB + FUS at 50W with TNFα in perfusate)
iii. Cohort 2 (ILP + 10% MB + FUS at 150W with TNFα in perfusate)
iv. Cohort 3 (ILP + 10% MB + FUS at 150W)

In all the cohorts, 3 animals were euthanized 1h after treatment and the other 3, 72h after the treatment.

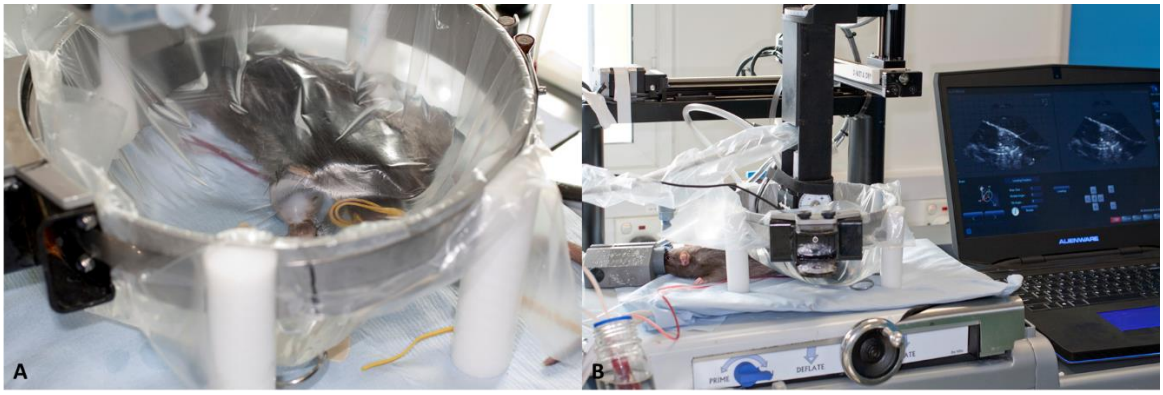

Figure 4.7. Photo showing the experimental arrangement, including the water bag used for effects of coupling. A - The leg of the rat is roughly centered under the plastic film which is transparent to ultrassound. B – A rat is positioned under the water bag, the VIFU transducer is positioned just above the leg and the computer on the right shows what the imaging probe is detecting. The computer contains a software that allows treatment planning.

The transducer used in the *in vivo* experiments is a single element HIFU transducer of nominal frequency 1.5 MHz, Focal Depth of 4 cm, Focal Width of 1 mm and Focal Height of 7 mm – see Figure 4.8. Acoustic Pressure data from manufacturer as a function of Software Input Power can be seen in Table 1. As it was expected, there is a big difference from what have been calibrated from Alpinion's calibration due to the fact that during calibration, the hidrophone was slightly out of focus and in a 1 mm point, any slightly displacement makes a big difference. Previous calibration on the wet system, made by a member of the therapeutic ultrasound team, proved that data from calibration is accurate when compared to in-house made calibration so, due to the impossibilty to perform an accurate measurement on the dry configuration and considering the fact that

the transducers are identical, the values of pressure for the power levels used will be according the manufacturer's calibration.

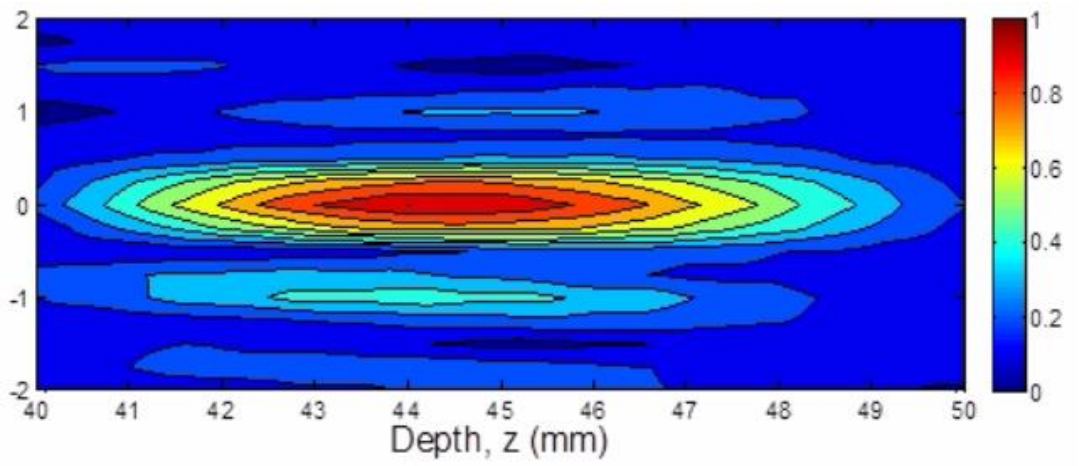

Figure 4.8. Alpinion's Focal Field Map in two orthogonal directions – x and z.

Table 1 – Acoustic Pressure Table

Software Input Power (W)	Acoustic Power (W)	Peak Positive Pressure (MPa)	Peak Negative Pressure (MPa)
10	5.9	5.41	-4.04
30	19.3	7.84	-5.25
50	31.1	12.35	-6.93
70	44.5	15.82	-8.13
90	59.3	20.67	-8.36
110	72.7	25.17	-9.40
130	86.0	29.67	-10.34
150	99.3	34.39	-10.85

Table 1. Acoustic Pressure Data from Alpinion's Calibration in two orthogonal directions – x and z.

4. *In Vivo* Experiments

Sample collection and storage

The animals were culled one hour and seventy-two hours following the procedure. The tumours were resected, weighed and snap frozen immediately. Tumour samples were homogenised with PBS and protease inhibitors using a Precellys homogeniser. Cell lysis was assisted by repeated freeze-thaw cycles. The samples were stored at -80°C.

Viral plaque assays

CV-1 cells were grown to confluence on 24 well plates. The samples were thawed and the supernatants were incubated on the CV-1 cells for 48 hours prior to viral detection. The cells were fixed with 2% formaldehyde/0.2%glutaraldehyde for 5 minutes then washed with PBS and stained for 4 hours with X-gal staining buffer, X-gal (1:100) and X-gal (1:1000). The cells were then washed with Ultra Filtered Water and dried.

Quantitative PCR

Expression of the A21L vaccinia gene was measured by qPCR using the Genelux GL-LC1 VV-A21L kit. DNA was prepared from the lysate of the tumour samples. A21L specific primers were used (forward: 5'-GTAAACTACAAACGTCTAAACAAGAA-3' and reverse: 5'-CCTGGTATATCGTCTCTATCTTTATCAC-3'). The viral copy number was then normalised by the weight of the tumour samples to give the number of viral copies per gram of tissue.

4.3. Results and Discussion of the *In Vivo* Study

Successful results, in terms of reduced tumor growth and increased rat survival time, using oncolytic virotherapy have highlighted the need to develop a treatment which increases viral uptake, in which invasiveness is reduced, and where post-treatment surgery would not be needed. In addressing this goal, this project focused on the study of the combination of ILP and FUS in the presence of microbubbles to increase viral penetration of tumour bulk efficiency in Brown Norwegian rats transfected with BN175 fibrosarcoma cells.

The rats were prepared for ultrasound exposure– see Figures 4.9-4.11, cavitation was detected during the experiments and then, the tumor tissue was analysed using histochemical, qPCR and VPA assays. Organs such as lungs, heart and liver were also collected to study the effectiveness of the tourniquet around the limb. Results from tumor tissue analysis and cavitation are presented below.

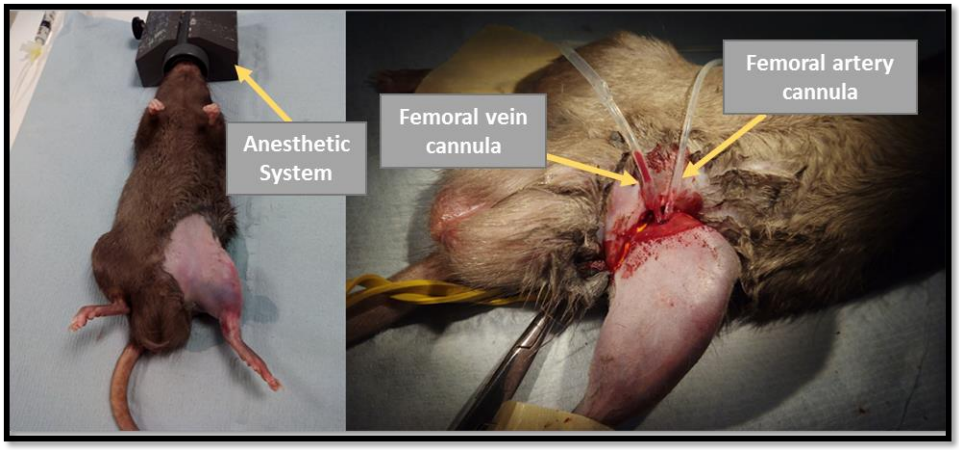

Figure 4.9. Brown Norwegian Rats were used for the in vivo experiments of the pilot study were anesthetized, operated in to cannulate the femoral artery and vessel

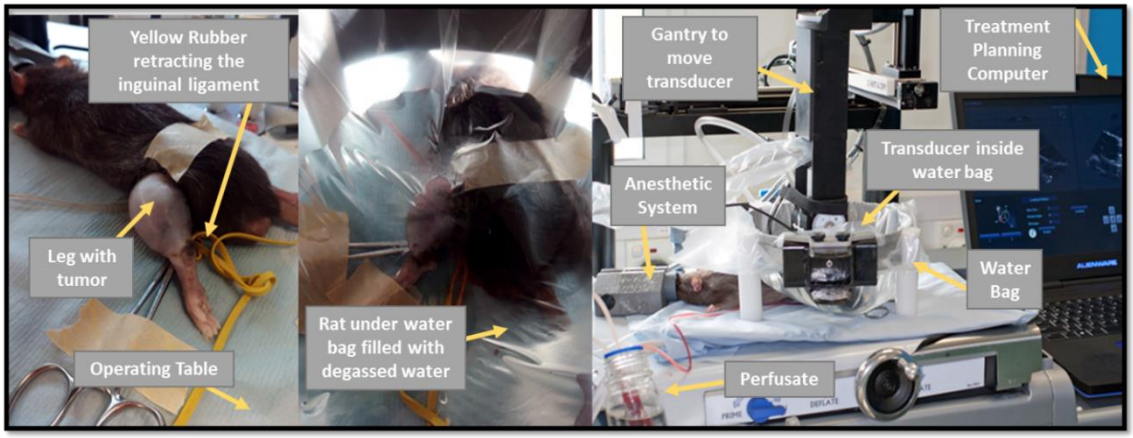

Figure 4.10. Brown Norwegian Rats used for the in vivo experiments of this pilot study were positioned on the VIFU 2000 operating table, a water bag filled in with degassed water was placed on top .

Figure 4.11. After the experiments, the rats were sutured, kept in a cage and medicated to minimise any suffering and either 1 or 72h post experiment, they were euthanized and the tumor and organs have been collected and stored to later analysis.

The results of the quantitative PCR for the tumour samples suggest that FUS has not added anything in terms of viral copy numbers – see Figure 4.12. Apart from the cohort without TNF-α, the viral copy number does not increase with time as was hoped. As there is a lack of information about how the virus responds to FUS, a possible explanation could be that the virus is being destroyed or damaged by the ultrasound. The viral copy number on PCR goes down from 1 hour to 72 hours in the HIFU cohorts, which may suggest that the virus is damaged, or at least not able to replicate. Overall it looks as if FUS may be having a negative effect. The viral plaque assays (VPAs) reveal live virus that is still able to replicate, rather than just the amount of viral DNA (which is measured by qPCR assesses).

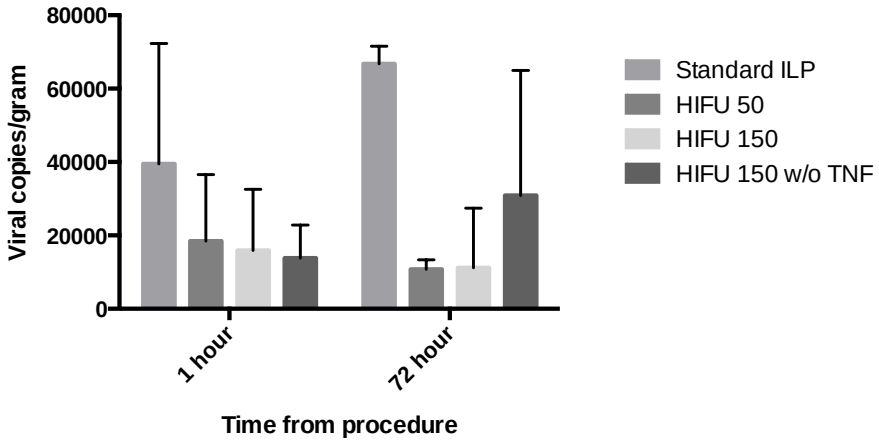

Figure 4.12. Expression of the A21L vaccinia gene as measured by qPCR using the Genelux GL-LC1 VV-A21L kit. The viral copy number was normalised using the weight of the tumour samples to give the number of viral copies per gram of tissue.

In this assay, cell monolayers are infected with a low ratio of virus, such that only sporadic cells become infected. Each group of infected cells is referred to as a plaque. Uninfected cells surround the plaques. After several infection cycles, the infected cells in the center of the plaques begin to lyse and the peripheral infected cells remain surrounded by uninfected cells. This phenomenon causes the light passing through the infected cells to refract differently from the surrounding uninfected cells, and the plaque can be visualized either by the naked eye or by light microscopy. Each plaque represents a single virus. Individual plaques obtained from different dilutions of a viral stock can be counted to determine the viral titer (pfu/ml) of a given transfection or virus stock. In this study, the viral plaques from the tumour samples have not grown any significant amount of

virus, and grew only from the viral stock used for the perfusions (used as a positive control for the plaques). Some pictures from the VPAs can be seen in figure 4.13.

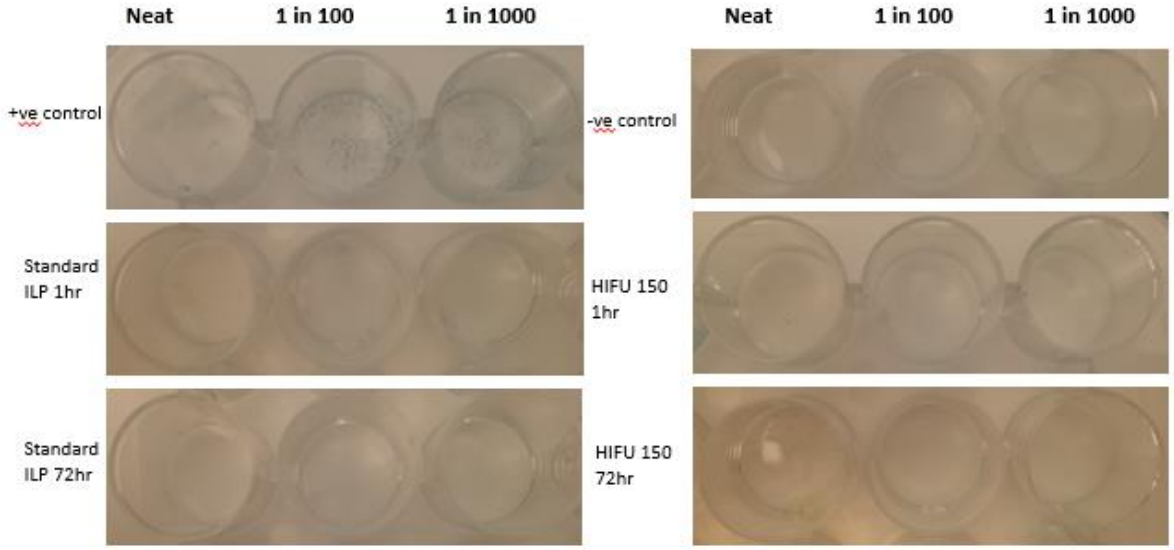

Figure 4.13. Pictures from the VPAs of two different cohorts – a cohort without exposure to ultrasound (Standard ILP) and a cohort with the combined treatment at 150W of exposure. There are three wells per sample. The first well is the undiluted lysate from the tumour (Neat) followed by 1 in 100 and 1 in 1000 dilutions of the lysate. The positive control is the stock of virus used at the same dilution for each perfusion.

As can be seen in Figure 4.13, plaques are only visible on the positive control. This suggests that the virus could be killed by the US or by other means, including lack of perfusion access into the limb and therefore lack of virus. The yield from the VPAs was too small for a comparison between cohorts, and so does not provide any usable data and . It would be good to have histology data to see whether there was ultrasound damage in the tissue but the staining for X-gal did not work either. X-gal staining is a rapid and convenient histochemical technique used to detect β-galactosidase activity - used in molecular biology as a reporter marker to monitor gene expression The presence of an active β-galactosidase produces a characteristic blue dye which provides a means of distinguishing the presence of an active/live virus.

For the purpose of this *in vivo* study and contrary to what has been done *in vitro*, pulsed exposures have been used to avoid the rise in temperature *in* situ. So, both in the low (50 W) and high (150W) cohort, the exposure duration has been 10 s in each point with a PRF of 100 Hz and 5% DC. This introduced an issue in terms of cavitation processing because the script used to process recorded data analysed in Chapter 2 was prepared to process continuous data. Using the same script for pulsed data would be a

problem because of the discontinuities in between pulses – off time data would be regarded as if a signal would have been acquired. The modifications in the processing script have been made with the help of Dr. John Civale, a member of the Therapeutic Ultrasound Team in the Institute of Cancer Research. The signal was divided into segments and in each segment, everytime the signal was above a defined threshold, the signal would be processed in consecutive segments until the signal would below the defined threshold.

The results from the cavitation detection have been summarized and can be seen in Tables 2-4, representing the results by cohort. In these tables, the first row identifies in which rat the experiment was made. A total of 23 rats have been used in a random way, i.e. the experiments started with rat 1 (rats 1-6 have been used to define the conditions to then start the main experiments) and in each day of experiments, it was tried to operate in rats from different cohorts to guarantee that the experience gained from experiment to experiment would not interfer in the results. All the tumors were exposed 45 times to 10 s of ultrasound in 5 grids of 9 points in different positions on the tumor, and cavitation data has been acquired during each exposure.

The summary present in Tables 2-4 show the percentage of exposures in each rat that allowed the detection of the effect described in each row. As it was already discussed, the term harmonic refers to frequencies that are integral multiples of the frequency of the transmitted pulse (which is also called the fundamental frequency or first harmonic). The presence of half or ultra harmonics is linked to nonlinear propagation and stable cavitation and the detection of these phenomena is present in the second and third rows of Tables 2-4. Forth and fifth columns have to due with the detection of inertial cavitation – a first look at recorded data in the time domain would be used to choose time points of highest amplitude compared to noise level (two or three point have been used to further analyses) and then through FFT on these time points, an elevation in FFT would be regarded as inertial cavitation everytime there was a broadband of signal above the threshold as defined in Chapter 2.

Table 2 - Summary of the information collected from cavitation data processing and analysis of Cohort 1

Rat	9	11	20	6	13	15
Half Harmonic (%)	20.0	95.6	20.0	4.44	55.6	4.44
Ultraharmonics (%)	11.1	66.7	13.3	0.00	22.2	4.44
Suspicious BB Level (%)	31.1	40.0	0.00	57.8	82.2	4.44
Elevation in FFT above threshold (%)	26.7	66.7	17.8	48.9	60.0	37.8

Table 2. Summary of the information collected from cavitation data processing and analysis of cohort 1 (ILP + 10% MB + FUS at 50W with TNFa in perfusate). In this cohort, all the tumors were exposed 45 times to 10s of ultrasound in 5 grids of 9 points in different positions on the tumor, and cavitation data hasbeen acquired during each exposure.

Table 3 - Summary of the information collected from cavitation data processing and analysis of Cohort 2

Rat	10	12	21	7	8	14
Half Harmonic (%)	25.6	100	25.0	27.3	13.3	55.6
Ultraharmonics (%)	25.6	100	11.4	13.6	13.3	37.8
Suspicious BB Level (%)	44.2	93.2	2.27	27.3	33.3	44.4
Elevation in FFT above threshold (%)	32.6	100	40.9	50.0	75.6	64.4

Table 3. Summary of the information collected from cavitation data processing and analysis of cohort 2 (ILP + 10% MB + FUS at 150W with TNFa in perfusate). In this cohort, all the tumors were exposed 45 times to 10s of ultrasound in 5 grids of 9 points in different positions on the tumor. Cavitation detection was performed during all the exposures but in rat 7 the data acquisition failed in two exposures and in rats 12 and 21 it failed once.

Table 4 - Summary of the information collected from cavitation data processing and analysis of Cohort 3

Rat	18	22	23	16	17	19
Half Harmonic (%)	47.7	24.4	11.4	100	23.1	17.8
Ultraharmonics (%)	43.2	31.1	4.55	100	19.2	17.8
Suspicious BB Level (%)	65.9	17.8	40.9	100	84.6	15.6
Elevation in FFT above threshold (%)	75.0	68.9	52.3	100	46.2	62.2

Table 4. Summary of the information collected from cavitation data processing and analysis of cohort 2 (ILP + 10% MB + FUS at 150W). In this cohort, all the tumors have been exposed 45 times to 10s of ultrasound in 5 grids of 9 points in different positions on the tumor. Cavitation detection was performed during all the exposures but in rats 18 and 16 it failed once and in rat 17 the cannula moved and only 3 grids were completed.

One of the first things to comment on when looking at Tables 2-4 is the huge variation between thenumber of exposures in which cavitation is detected. Data acquired required a close inspection to decide whether inertial cavitation **was present or not** – data was analysed both in the time and frequency domain as described in section 2.2.

In Table 2, there is a summary of the results of cavitation detection of cohort 1 in which the tumor was exposed at a peak negative pressure of approximately -7 MPa during Isolated Limb Perfusion with 10% SonoVue microbubbles in the perfusate containing TNF-α, Melphalan and Vaccinia Virus. A probable detection of broadband of 42.9 ±

19.0% is associated with this cohort. This cohort comprised in 3 rats in which the organs were collected 1h post-experiment, and 3 rats in which the collection was made 72h after exposure. The broadband detection in these two sub-groups is considered to be present in 37.1 ± 26.0% and 48.8 ± 11.1%, respectively. If we look at Figure 108, we see that the amount of virus detected in the 1h collection rats is higher than the amount detected in the 72h collection rats.

Table 2 summarizes the results of cavitation detection for cohort 2 in which the tumor was exposed at a peak negative pressure of approximately -11 MPa during Isolated Limb Perfusion with 10% SonoVue microbubbles in the perfusate containing TNF-α, Melphalan and Vaccinia Virus. In this cohort, there is a detection of broadband of 60.6 ± 24.8%. This cohort also comprises 3 rats with organ collection 1h post-experiment and 3 rats in which the organ collection was 72h post-experiment. The broadband detection is considered to be present in 57.8 ± 36.8% and 63.3 ± 12.8%, respectively. In Figure 108, we see that the amount of virus detected in the 1h collection rats is higher than that detected in the 72h collection rats.

In Table 3, there is information from cavitation detection for cohort 3 in which the tumor was exposed at a peak negative pressure of approximately -11 MPa under Isolated Limb Perfusion with 10% SonoVue microbubbles in the perfusate containing only Melphalan and Vaccinia Virus (without TNF-α). In the 6 rats of the cohort, there is a detection of broadband of 67.4 ± 19.1%. This cohort also comprises 3 rats of 1h collection post-experiment and 3 rats in which the collection was made 72h post-experiment. The broadband detection is in 65.4 ± 11.7% and 69.5 ± 27.6%, respectively, in these two groups. In Figure 108, we see that the amount of virus detected in the 1h collection rats is lower than the amount detected in the 72h collection rats.

The analysis Table by Table suggests that the higher probability of the occurence of inertial cavitation is directly associated with the amount of virus detected 1h post collection – see Figure 4.12 - but more experiments would be needed to have enough data for concrete conclusions, although there is a "trend". When it comes to the data from the 72h collection, this trend may also be found but there is a big difference between the cohorst with and without TNF-α present – is TNF-α toxic not only for the tumor but also for the virus? This is an important question that would be an advantage for a future clinical aplication – the increased efficacy of oncolytic virus in the absence of TNF-α would greatly reduce the toxicity of a combined therapy including, for example, FUS, Melphalan and Vaccinia Virus or only FUS and Vaccinia Virus.

Figures 4.14-4.16, show examples of the traces from processed cavitation data in which it is possible to detect broadband, half harmonic or ultra harmonics. These figures are representative of the figures that helped to decide wheter these effects were present or not at each exposure of each rat.

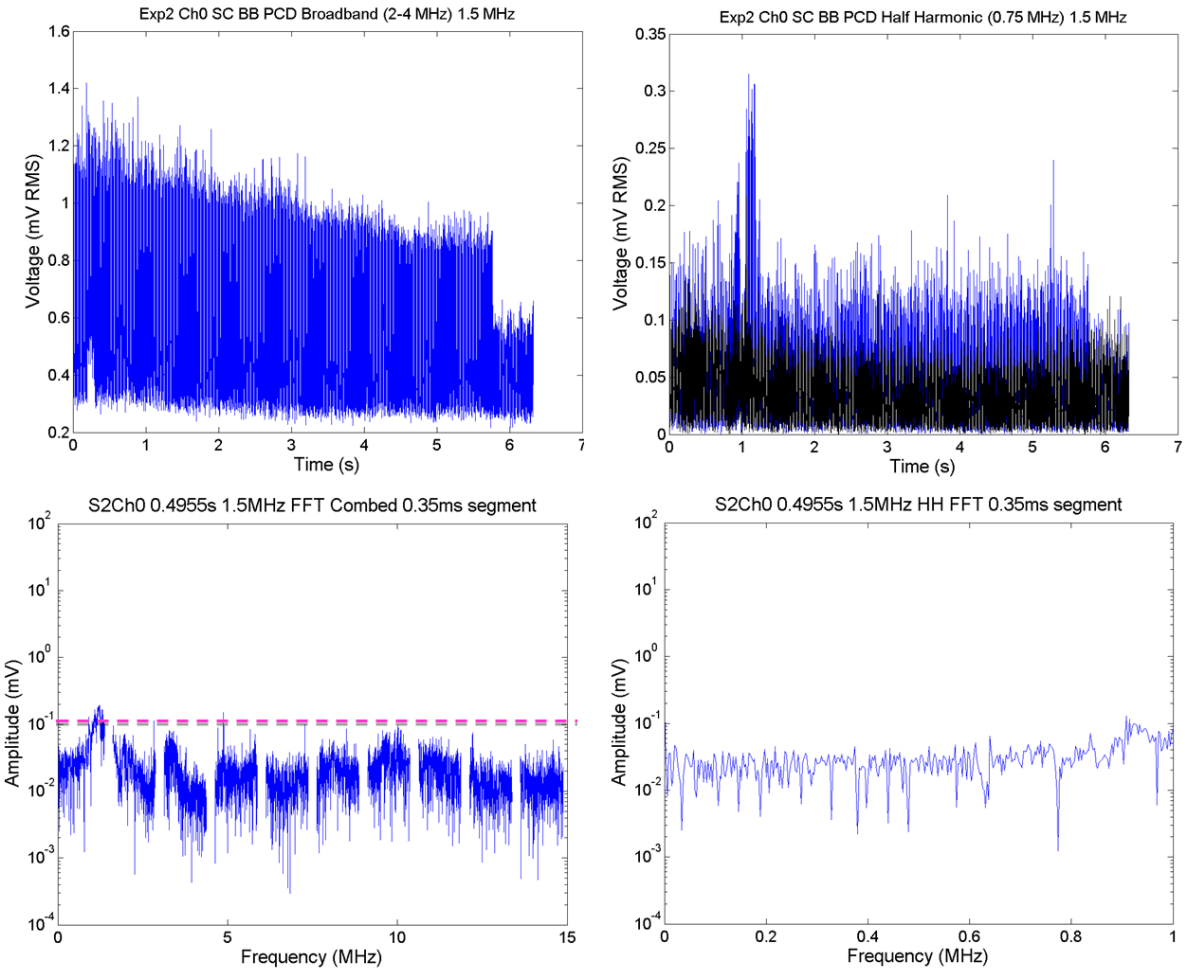

Figure 4.14. On top (left), PCD broadband signal (frequency-integrated over 3-10 MHz) and (on right) Half Harmonic signal (integrated around 0.75 MHz) as a function of time for a single 1.5 MHz, 10 s exposure of Brown Norwegian Rats at a peak negative pressure of ~7 MPa. The exposure lasts 10 s and there is cavitation detection during 6.3s. On bottom (left), combed FFTs from a single segment of PCD data at the time point 0.4955 s of the exposure. The FFTs show signal above the threshold for inertial cavitation as defined in Chapter 2. On bottom (right) half harmonic detection at 0.75 MHz with no half harmonic present. The title shows the exposure number (S2) and that data recorded channel 0 on the DAQ were processed.

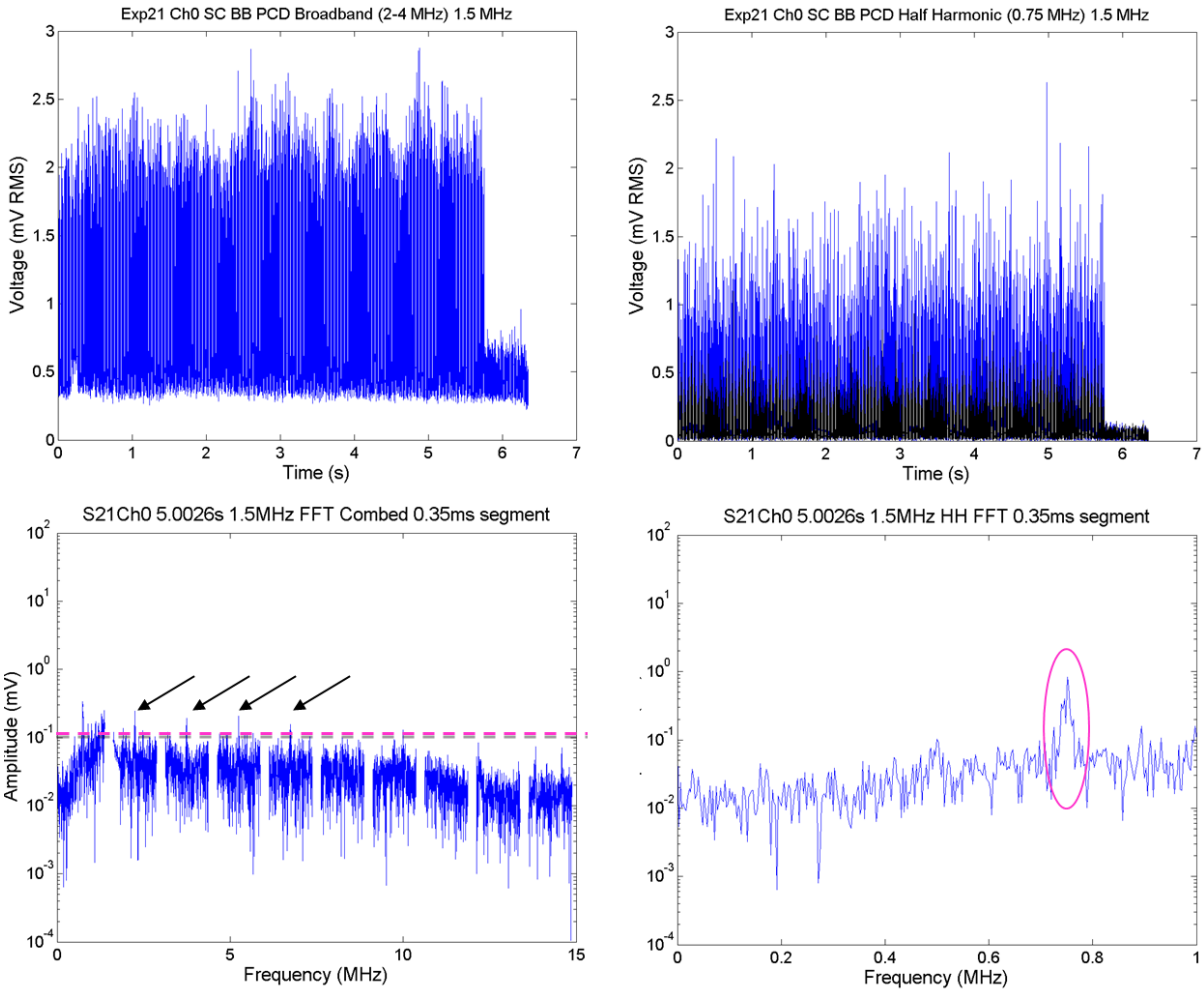

Figure 4.15. On top (left), PCD broadband signal (frequency-integrated over 3-10 MHz) and (on right) Half Harmonic signal (integrated around 0.75 MHz) as a function of time for a single 1.5 MHz, 10 s exposure of Brown Norwegian Rats at a peak negative pressure of ~10 MPa. The exposure lasts 10 s and there is cavitation detection during 6.3s. On bottom (left), combed FFTs from a single segment of PCD data at the time point 5.0026 s of the exposure. The FFTs show signal above the threshold for inertial cavitation as defined in Chapter 2 and black arrows point towards the spikes coming from ultra harmonics. On bottom (right) half harmonic detection at 0.75 MHz with half harmonic present and circled in red. The title shows the exposure number (S21) and that data recorded channel 0 on the DAQ were processed.

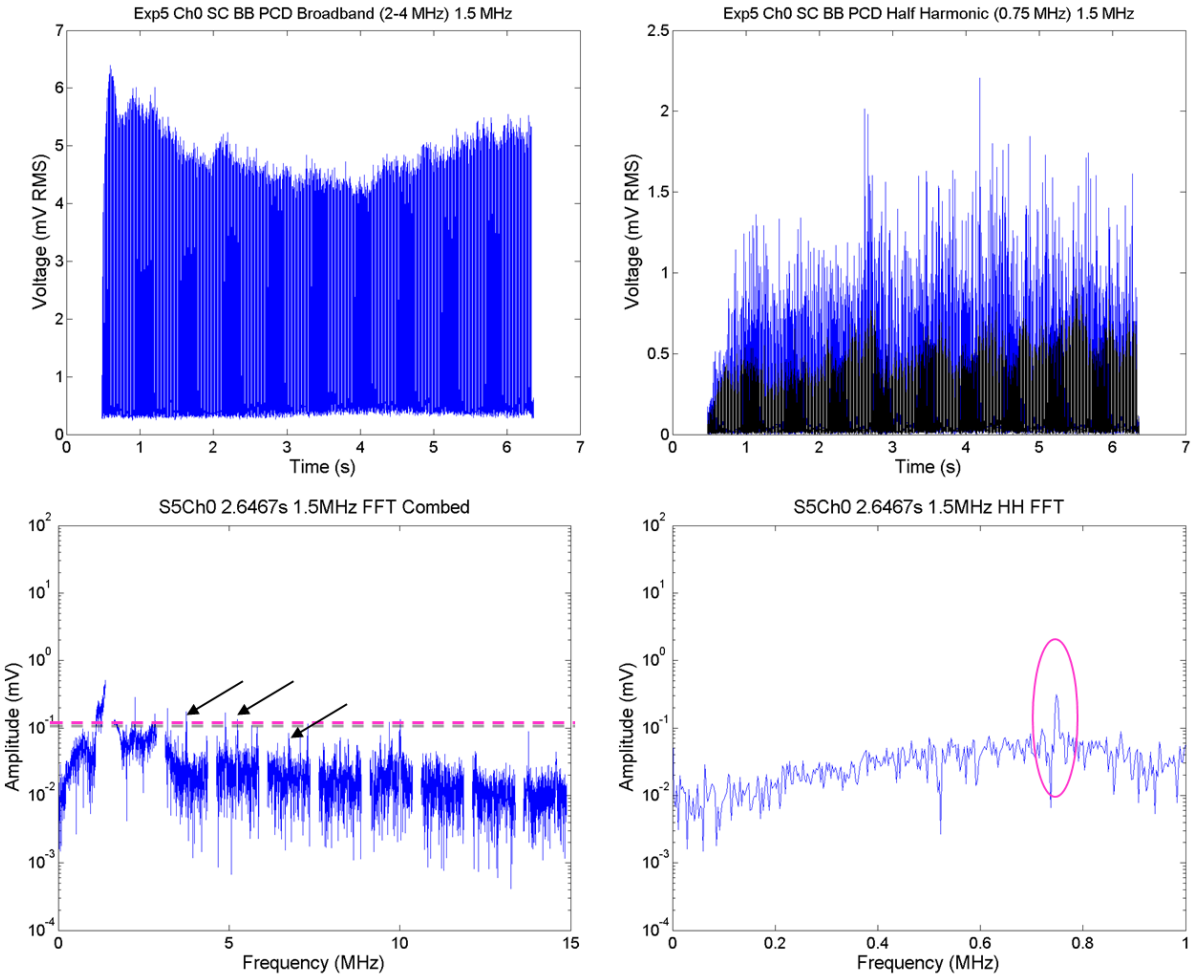

Figure 4.16. On top (left), PCD broadband signal (frequency-integrated over 3-10 MHz) and (on right) Half Harmonic signal (integrated around 0.75 MHz) as a function of time for a single 1.5 MHz, 10 s exposure of Brown Norwegian Rats at a peak negative pressure of ~10 MPa. The exposure lasts 10 s and there is cavitation detection during 6.3s. The graph title shows that this was exposure number two, with data acquired on Ch0 of the DAQ system. On bottom (left), combed FFTs from a single segment of PCD data at the time point 5.0026 s of the exposure. The FFTs show signal above the threshold for inertial cavitation as defined in Chapter 2 and black arrows point towards the spikes coming from ultra harmonics. On bottom (right) half harmonic detection at 0.75 MHz with half harmonic present and circled in red.

There was considerable difficulty in getting the cavitation detection system working properly – the PCD alignment was done with respect to the centre of the water bag used to "cover" the limb, and in which degassed water was used for coupling; then, it was not possible to trigger the cavitation detection system automatically and it was necessary for someone to start the data acquisition as the treatment started and for each point of the 5 grids chosen.

The size of the leg influences the quality of cavitation detection from rat to rat. This depends on the success of the surgery, i.e., on the time it takes to place the cannula and to get the perfusion working. This would also affect the distance traveled by the

ultrasound beam to reach the tumor; additionaly, different rats may have different vasculature distribution and this also influences not only the attenuation of the ultrasound beam, the amount of reflected signal heard by the PCD, but also the perfusion rate and number of microbubbles that get into the limb.

Another point to consider is the positioning of the rat was not fixed from experiment to experiment although a great effort was made to have each rat in a similar position; finally, the detection was allways dependent on the position of the PCD with respect to the tumor, and it is possible that the detection zone of the PCD was not allways able to hear the scatter from the tumor. It is important to remember that broadband detection only means that it was of sufficient amplitude for the system to hear it, but absence of a detected signal does not mean there was no cavitation. The deeper the ultrasound is fired into tissue, the less signal is detected. Conversely, if target is superficial, and there is cavitation in the water as it regassed and/or heated, significant amounts of cavitation activity can be detected, but may not come from within the tumour (imaging is good for showing cavitation in the water bath, but it had to be turned off because it interfered with cavitation detection when on). Imaging data acquired in the beginning and end of the exposure is of some help to compare how the depth of the target could have influenced the cavitation detection. Some of these images are shown in Figures 4.17-4.19.

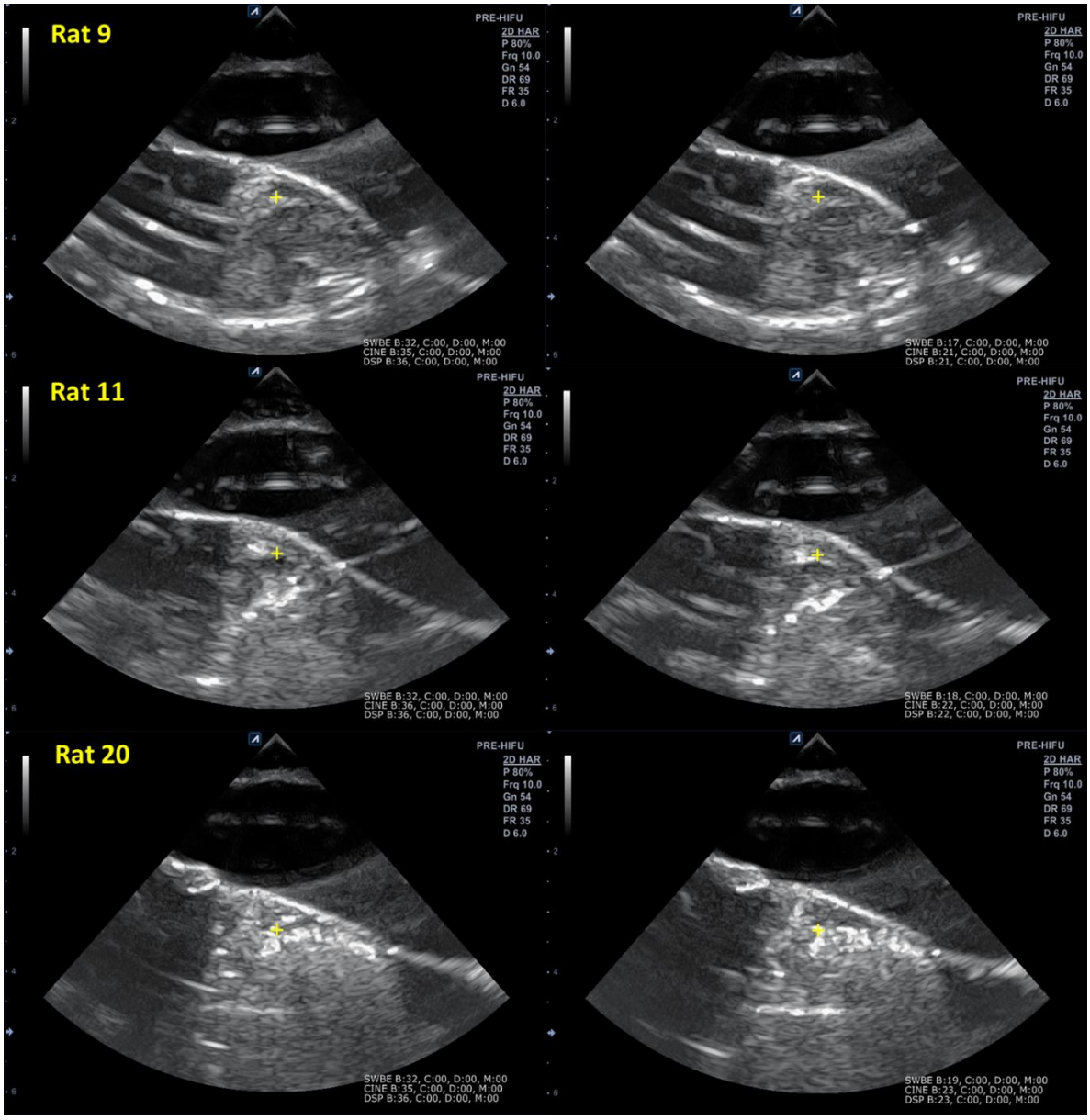

Figure 4.17. Ultrasound Imaging acquired in the prior (left) and post (right) exposure to ultrasound on rats 9 , 11 and 20 from cohort 1. The images were acquired using the E-Cube 9 provided with the VIFU system with a phased array transducer working at 10 MHz. The yellow cross marks the starting point of the treatment – the initial target. Then, a grid of 9 points centred on this point was exposed.. In each grid, the exposure were created from left to right in three rows of three points.

If the variability in cavitation detection could be explained by the differences in the depth of treatment in cohort 1, one would expect that rat 20 would give the poorer data because, , the treatment starting point is deeper than in rats 9 and 11. Similar results would be expected for rats 9 and 11 – see Figure 4.17. From Table 2, the detection of, for example, half harmonic in rats 9, 11 and 20 is of approximately 20, 95.6 and 20% and in terms of broadband detection the values at 26.7, 66.7 and 17.8%, respectively. This is counter to the hypothesis about the depth of treatment, and the same is true for the three

examples from cohort 2 – see Figure 4.18. For rats 10 and 12, the depth of treatment is similar and, as can be seen in Table 3, for these rats the half harmonic detection rates are of 25.6 and 100% and 32.6 and 100% for broadband. In cohort 3, from the three examples chosen, rat 22 should give the better results in terms of cavitation detection because the treatment is more superficial but this is also not the case – see Figure 4.19 and Table 4.

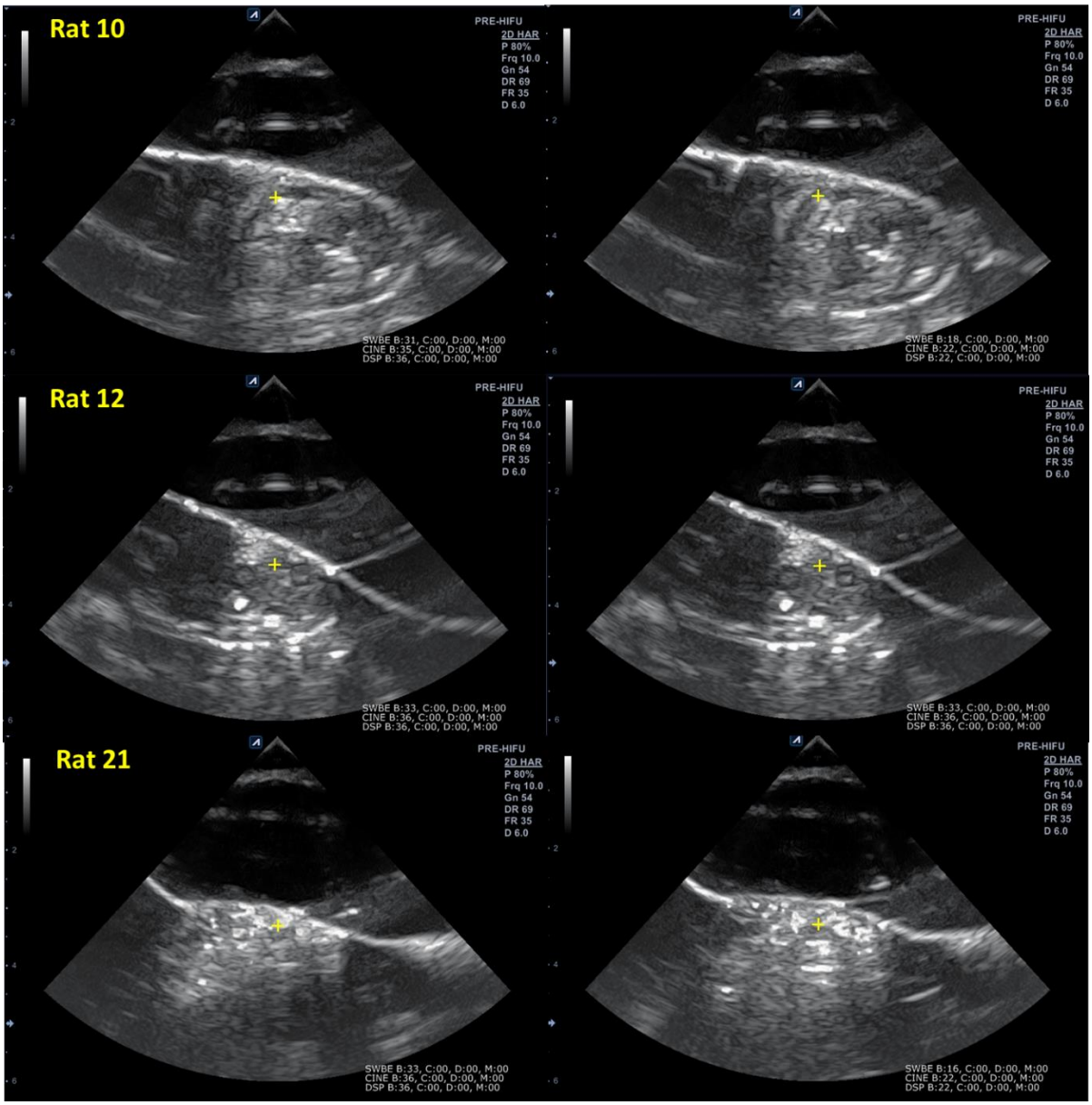

Figure 4.18. Ultrasound Imaging acquired in the prior (left) and post (right) exposure to ultrasound on rats 10, 12, 21 from cohort 2.. The images were acquired using E-Cube 9 system from Alpinion with a phased array transducer working at 10 MHz.

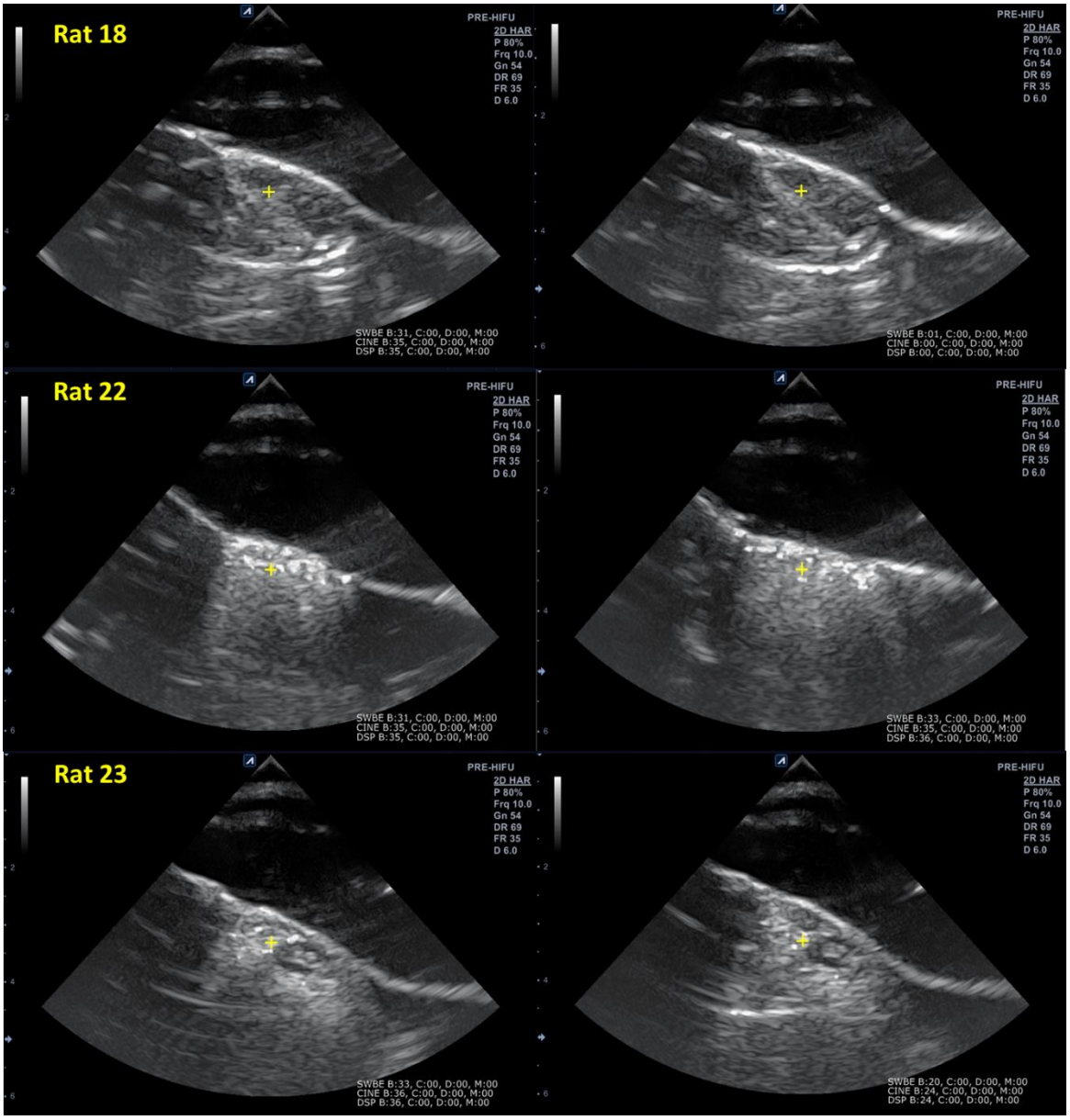

Figure 4.19. Ultrasound Imaging acquired in the prior (left) and post (right) exposure to ultrasound on rats 18, 22 and 23 from cohort 3. The images were acquired using E-Cube 9 system from Alpinion with a phased array transducer working at 10 MHz.

A general conclusion on these results is that, as the cavitation detection data of the three cohorts is higly variable and despite the fact that there is a possibility that the use of focused ultrasound at ~7 and 10 MPa could have been the cause to the death of virus, this is not possible to confirm. The assays available only detect the amount of live virus in the tumors and also because it was not possible to study *in vitro* the consequences of the exposure of Vaccinia Virus to ultrasound. The histochemical analysis would be needed to analyse the level of damage in the tissue, if there was any, and then, it could be proved if the virus did not replicate in the tumor because either the virus or the tissue have been destroyed.

5. Conclusions and Future Work

This project was a pilot study in which Focused Ultrasound and Microbubbles were added to a combined therapy, which includes Melphalan, TNF-α and Vaccinia Virus, to try to enhance the efficacy, and to reduce the toxicity of the treatment. This work involves the calibration of equipment, detection of cavitation thresholds, and *in vitro* and *in vivo* experiments with BN175 rat sarcoma line. The *in vitro* experiments were carried out to test the combined therapy in the presence or absence of (i) focused ultrasound and (ii) microbubbles, with different exposure parameters, such as peak rarefactional focal pressures, duty cycle, pulse repetition frequency, exposure duration and microbubble concentration. Finally, *in vivo* experiments in Brown Norwegian rats were conducted to help to determine the effectiveness of this combined therapy using Focused Ultrasound in the presence of Microbubbles, Melphalan, TNF-α and Vaccinia Virus, and Isolated Limb Perfusion. The main conclusions on the work carried out are summarised here.

The cavitation thresholds study was performed i) to study the difference in thresholds for different transducer frequencies, ii) to choose the levels of pressure for *in vitro* exposures, iii) to decide on the best frequency to use when microbubbles were present (that being the one closest to the resonant frequency of the microbubbles).

The main conclusions from this study are that the microbubbles resonate at a lower l evel of peak negative pressure at the frequency of 1.34 MHz than what happens at 1.66 MHz in the absence of microbubbles. This may be because of the condition of the medium at the time of exposure. Differences in the quantity of dissolved gases and temperature are the main things that could affect the results. The samples had to be prepared in a cell culture room and then transferred to a physics lab to be exposed. Another factor that could explain this result has to do with the resonant frequency of the microbubbles. A study of the SonoVue Microbubbles used reported its resonant frequency to be 1.6, 2.1 and 3.1 MHz for bubbles of 4.0, 3.2 and 2.6 μm, respectively. It is also stated that the mean diameter of the microbubbles is 2.5μm, 90% are smaller than 6μm and 99% smaller than 11μm. Looking at this data, we could say that bigger bubbles are resonant at lower frequencies and so, in the sample tested, a large number of bubbles could be bigger than 4.0 μm.

Interestingly, at each drive frequency, the cavitation threshold lay in the same pressure interval, and so a general conclusion could be made about the influence of the

microbubbles on the cavitation threshold – the percentage of microbubbles dissolved in a certain amount of medium does not seem to change the threshold to get cavitation. At the cavitation threshold, at any given frequency, in the presence of microbubbles, the amplitude of the cavitational events detected is similar for the three frequencies. As it was necessary to choose between 1.34 MHz and 1.66 MHz, in order to be closer to the frequency used *in vivo*, 1.66 MHz seemed to be a better choice because the data suggests that at this frequency, broadband was maximised and the main goal is to achieve inertial cavitation. Accurate measurements must be made if a quantitative rather qualitative analysis is required.

As appreciation summary of the *in vitro* study, it seems that treatment of the cells with ultrasound only, or of ultrasound with 1% microbubble concentration, has no effect. However, when a 10 % concentration of microbubbles is used there are two interesting things: i) there is a reduction in cell viability immediately after treatment irrespective of acoustic pressure used, ii) medium and high pressures with microbubbles kill the cells, but no cell killing is seen with low pressure and microbubbles. As a result, cells treated with low pressure and 10% microbubbles start proliferating again and by day 3 they reach control viability. The rest of the treatments do not seem to affect the cells, so the differences in between measurements can be regarded as experimental variation.

As most of these results are reproducible, they were useful for this study whose purpose is to open up cells and cell junctions without actually killing them. It shows that low pressure and high concentration of microbubbles will affect the cells immediately after treatment but not actually kill them.

The results from FACS analysis are important in that they allow a distinction to be drawn between populations with and without PI for unexposed, 'low' and 'high' exposure controls – the detection of PI inside the cells, in a living population, is increases as the exposure is raised. This could suggest that there is an increased permeabilization of the membranes that allow the PI to get inside the cells.

This project focused on the study of the combination of ILP and FUS, in the presence of microbubbles, to increase viral penetration efficiency in tumour bulk in Brown Norwegian rats transfected with BN175 fibrosarcoma cells.

The results of the quantitative PCR for the tumour samples suggest that FUS has added nothing in terms of viral copy numbers. As there is a lack of information of how the virus responds to FUS, a possible explanation could be that the virus is destroyed, or damaged by, the ultrasound. The results of the viral plaque assays should help to explain

this situation as this assay quantifies live virus that remains able to replicate, rather than just the amount of viral DNA (which is what qPCR assesses).

The VPAs showed that plaques could only be seen on the positive control. This suggests that the virus had been killed by the US, or by another mechanis), including a lack of perfusion access into the limb, and therefore lack of virus. The yield from the VPAs was too small too allow a comparison between cohorts, so does not provide any usable data. It would be good to have histology data to see whether there was ultrasound damage in the tissue, but the staining for X-gal did not work well.

The analysis of cavitation data shows a huge variation in terms of results both from different cohorts, and within the same cohort – this proves how unpredictable and unstable cavitation detection can be - more experiments are needed to have enough data to draw reliable conclusions. The difficulty found while trying to get the cavitation detection system working properly was definitely one of the main reasons for the poor results seen. As discussed before, the *in vivo* factors that could have reduced the quality of cavitation detection in different rats, could have been differences in the size of the legs, and in the time taken to place the cannula to get the perfusion working. Possible differences in vasculature, different positioning of the rat from experiment to experiment, and the fact that the detection was dependent on the position of the PCD relative to the tumor are factors that have a negative influence on the quality of cavitation detection. It is important to remember that detecting broadband just means there was enough for the system to "hear" it, but that its absence does not mean there was no cavitation.

"What could have been done better in this project?" or "What should be done next?" are important questions to ask when we are discussing a pilot project on any topic. One of the main issues on this project was the lack of time to learn, and put into practice all the new concepts needed to perform *in vitro* and *in vivo* experiments on such a new topic as ultrasound assisted oncolytic virotherapy.

A lot of burocracy is involved in getting authorization to experiment on viral samples, and this was not achieved during the project's timetable. Also, if there had been more time, it would have been important to do at least 5 repeats for each condition on test (PNP, PRF, DC and DE), instead of only 3, in order to be more certain about the reproducibility of the experiments. Adding to this, more levels in each condition should have been tested to have a better understanding of any trend that could have been present, but a choice of quality over quantity had to be made – during the project's timescale, it was crucial to have better, rather than more, data. Then, in terms of the experiment itself,

it would have been better to have a different well plate configuration to avoid the contamination of the sample due to the entrance of non-sterile degassed water through the channels around the wells. Although a big effort has been made to decontaminate the well plate prior to manipulation inside the hood, this could explain some of the variation present in the results. Another issue for the experiments *in vitro* is the fact that the transducer used was not being driven at the same drive frequency as the transducer used *in vivo*. Despite the differences between the two scenarios, it is allways important to have a means of comparison when we need to translate what we see *in vitro* to the experiments done *in vivo*.

There is need to find a way to have a fixed position for the rat for the *in vivo* experiments, to minimise the variation in the path travelled by the ultrasound beam until its target, and to re-design the cavitation detection system to guarantee detection in the same direction in any experiment. A ring passive cavitation detector would be a suitable option because it would allways be aligned with the ultrasound beam. More animals in each cohort are required for better quantitative analysis. Despite the poor detection in terms of cavitation detection, a lower value of peak negative pressure should have been used and must be tested to see if there are better results in terms of the enhanced uptake of virus into the tumor bulk.

It is worth repeating the experiments performed for the purpose of this thesis because the combined therapy including Melphalan, TNF-α and Vaccinia Virus seemed to have potential to increase efficacy and reduce toxicity of the treatment. The parameters of the ultrasound beam used seem to have no negative effect on cell viability even in the presence of microbubbles so there is the need to prove that this can also improve the permeability of cell membrane to virus with *in vitro* experiments. Once this is done, experiments *in vivo* must be repeated under different conditions to confirm that the efficacy of the combined therapy can be enhanced.

References

1. Jacob, D., et al, *Suppressing orthotopic pancreatic tumour growth with a fibermodified adenovector expressing the TRAIL gene from the human telomerase reverse transcriptase promoter.* Clin Cancer Res, 2004. **10**(10): p. 3535–3541.
2. Bauer, T.W., et al *A human melanoma xenograft in a nude rat responds to isolatedlimb perfusion with TNF plus melphalan.* Surgery, 2003. **133**(4): p. 420–428.
3. Djeha, A.H., et al, *Combined adenovirus-mediated nitroreductase gene delivery and CB1954 treatment: a well-tolerated therapy for established solid tumors.* Mol Ther, 2001. **3**(2): p. 233–240.
4. Reid, T., et al., *Intra-arterial administration of a replication-selective adenovirus (dl1520) in patients with colorectal carcinoma metastatic to the liver: a phase I trial.* Gene Ther, 2001. **8**(21): p. 1618-26.
5. Vile, R., D. Ando, and D. Kirn, *The oncolytic virotherapy treatment platform for cancer: unique biological and biosafety points to consider.* Cancer Gene Ther, 2002. **9**(12): p. 1062-7.
6. Liu, T.C., E. Galanis, and D. Kirn, *Clinical trial results with oncolytic virotherapy: a century of promise, a decade of progress.* Nat Clin Pract Oncol, 2007. **4**(2): p. 101-17.
7. Buijs, P.R., et al., *Oncolytic viruses: From bench to bedside with a focus on safety.* Hum Vaccin Immunother, 2015: p. 0.
8. Huang, Y., et al., *Development of viral vectors for gene therapy for chronic pain.* Pain Res Treat, 2011. **2011**: p. 968218.
9. Zitvogel, L., et al., *The anticancer immune response: indispensable for therapeutic success?* J Clin Invest, 2008. **118**(6): p. 1991-2001.
10. Wolfert, M.A.e.a., *Characterization of vectors for gene therapy formed by self-assembly of DNA with synthetic block copolymers.* Hum Gene Ther, 1996. **7**: p. 2123-2133.
11. Fukazawa T., M.Y., Durbin M.L., et al, *Pulmonary adenocarcinoma-targeted gene therapy by a cancer and tissue specific promoter system.* Mol Cancer Ther, 2007. **6**(1): p. 244-252.
12. Fukazawa, T.e.a., *Adenovirus-mediated cancer gene therapy and virotherapy.* International Journal of Molecular Medicine, 2010. **3**: p. 3-10.
13. Pencavel, T.D., et al., *Isolated limb perfusion with melphalan, tumour necrosis factor-alpha and oncolytic vaccinia virus improves tumour targeting and prolongs survival in a rat model of advanced extremity sarcoma.* Int J Cancer, 2015. **136**(4): p. 965-76.
14. Kennedy, J.E., G.R. Ter Haar, and D. Cranston, *High intensity focused ultrasound: surgery of the future?* Br J Radiol, 2003. **76**(909): p. 590-9.

15. Ter Haar, G.R., *Therapeutic applications of ultrasound.* Prog Biophys Mol Biol, 2007. **93**((1-3)): p. 111–129.
16. O'Brien, W.D., *Ultrasound—biophysics Mechanisms.* Progress in biophysics and molecular biology, 2014. **93**((1-3)): p. 212–255.
17. Mason, T.J., *Therapeutic ultrasound an overview.* Ultrason Sonochem, 2011. **18**(14): p. 847–852.
18. Ter Haar G.R., *Biological effects of ultrasound in clinical applications*. 1988, New York: VCH Publishers Inc.
19. Kitchen S. S., P.C.J., *A review of therapeutic ultrasound.* Physiotherapy, 1990. **76**: p. 593–600.
20. Johns, L.D., *Nonthermal effects of therapeutic ultrasound: the frequency resonance hypothesis.* J Athl Train, 2002. **37**(3): p. 293-9.
21. Qin, S., C.F. Caskey, and K.W. Ferrara, *Ultrasound contrast microbubbles in imaging and therapy: physical principles and engineering.* Phys Med Biol, 2009. **54**(6): p. R27-57.
22. van Wamel, A., et al., *Vibrating microbubbles poking individual cells: drug transfer into cells via sonoporation.* J Control Release, 2006. **112**(2): p. 149-55.
23. Liang, H.D., J. Tang, and M. Halliwell, *Sonoporation, drug delivery, and gene therapy.* Proc Inst Mech Eng H, 2010. **224**(2): p. 343-61.
24. Pinto de Carvalho, L., et al., *Hydrodynamics- and ultrasound-based transfection of heart with naked plasmid DNA.* Hum Gene Ther, 2007. **18**(12): p. 1233-43.
25. Taniyama, Y., et al., *Plasmid DNA-based gene transfer with ultrasound and microbubbles.* Curr Gene Ther, 2011. **11**(6): p. 485-90.
26. Lauterborn, W., Kurz, T., Mettin, R., and Ohl, C. D., *Experimental and theoretical bubble dynamics.* Advanced in Chemical Physics, 1999. **110**: p. 295–380.
27. Zhou, S.J., et al., *High-intensity focused ultrasound combined with herpes simplex virus thymidine kinase gene-loaded ultrasound-targeted microbubbles improved the survival of rabbits with VX(2) liver tumor.* J Gene Med, 2012. **14**(9-10): p. 570-9.
28. Wang, G., et al., *Investigation into the impact of diagnostic ultrasound with microbubbles on the capillary permeability of rat hepatomas.* Ultrasound Med Biol, 2013. **39**(4): p. 628-37.
29. Ebbini, E.S. and G. ter Haar, *Ultrasound-guided therapeutic focused ultrasound: current status and future directions.* Int J Hyperthermia, 2015. **31**(2): p. 77-89.
30. Fry, F.J., *Precision high intensity focusing ultrasound machines for surgery.* Am J Phys Med, 1958. **37**: p. 152–156.
31. Fry, W.J., et al., *Ultrasonic lesions in the mammalian central nervous system.* Science, 1955. **122**(3168): p. 517-8.
32. Burov, A.K., *High intensity ultrasonic vibrations for action on animal and human malignant tumours.* Dokl Akad Nauk SSR, 1956. **106**: p. 239–241.
33. Polat, B.E., et al., *Ultrasound-mediated transdermal drug delivery: mechanisms, scope, and emerging trends.* J Control Release, 2011. **152**(3): p. 330-48.
34. Huber P.E., P.P., *In vitro and in vivo transfection of plasmid DNA in the Dunning prostate tumor Rss27-AT1 is enhanced by focused ultrasound.* Gene Ther, 2000. **7**(17): p. 1516-25.
35. ter Haar G.R. and C.C. Coussios, *High intensity focused ultrasound: Physical principles and devices.* Int J Hyperthermia, 2007. **23**((2)): p. 89-104.
36. Hill, C.R., *Optimum acoustic frequency for focused ultrasound surgery.* Ultrasound Med Biol, 1994. **20**(3): p. 271-7.
37. Coussios, C.C., et al., *Role of acoustic cavitation in the delivery and monitoring of cancer treatment by high-intensity focussed ultrasound.* Int J Hyperthermia, 2007.
38. Dubinsky, T.J., et al., *High-intensity focused ultrasound: current potential and oncologic applications.* AJR Am J Roentgenol, 2008. **190**(1): p. 191-9.

39. Hu, Z., et al., *Release of endogenous danger signals from HIFU-treated tumor cells and their stimulatory effects on APCs.* Biochem Biophys Res Commun, 2005. **335**(1): p. 124-31.
40. Yu, A., et al. *Cellular and subcellular impact of low-intensity ultrasound: stimulus or stress*. in *International Congress on Ultrasonics*. 2013. Singapore: The Society of Acoustics.
41. Bourke, M.G., et al., *The emerging role of viruses in the treatment of solid tumours.* Cancer Treat Rev, 2011. **37**(8): p. 618-32.
42. Coleman, A.J. and J.E. Saunders, *A review of the physical properties and biological effects of the high amplitude acoustic field used in extracorporeal lithotripsy.* Ultrasonics, 1993. **31**(2): p. 75-89.
43. Coleman, A.J., et al., *The cavitation threshold of human tissue exposed to 0.2-MHz pulsed ultrasound: preliminary measurements based on a study of clinical lithotripsy.* Ultrasound Med Biol, 1995. **21**(3): p. 405-17.
44. Deng, C.X., et al., *In vitro measurements of inertial cavitation thresholds in human blood.* Ultrasound Med Biol, 1996. **22**(7): p. 939-48.
45. Miller D.L., S.J., *Lithotripter shockwaves with cavitation nucleation agents produce tumor growth reduction and gene transfer in vivo.* Ultrasound Med Biol, 2002. **28**(10): p. 1343–1348.
46. Miller, D.L., et al., *Cavitation nucleation agents for nonthermal ultrasound therapy.* J Acoust Soc Am, 2000. **107**(6): p. 3480-6.
47. Miller, D.L., et al., *Ultrasonic enhancement of gene transfection in murine melanoma tumors.* Ultrasound Med Biol, 1999. **25**(9): p. 1425-30.
48. Song, J., et al, *Combined shockwave and immunogene therapy of mouse melanoma and renal carcinoma tumors.* Ultrasound Med Biol, 2002. **28**(7): p. 957-64.
49. Bao, S., et al., *In vivo transfection of melanoma cells by lithotripter shock waves.* Cancer Res, 1998. **58**(2): p. 219-21.
50. Miller, D.L., C. Dou, and J. Song, *Lithotripter shockwave-induced enhancement of mouse melanoma lung metastasis: dependence on cavitation nucleation.* J Endourol, 2004. **18**(9): p. 925-9.
51. Oosterhof, G.O.N., et al, *The influence of high-energy shock waves on the development of metastases.* Ultrasound Med Biol, 1996. **22**(3): p. 339-44.
52. Miller, D.L. and J. Song, *Tumor growth reduction and DNA transfer by cavitation-enhanced high-intensity focused ultrasound in vivo.* Ultrasound Med Biol, 2003. **29**(6): p. 887-93.
53. Mehier-Humbert, S., et al., *Plasma membrane poration induced by ultrasound exposure: implication for drug delivery.* J Control Release, 2005. **104**(1): p. 213-22.
54. Rahim, A., et al, *Spatial and acoustic pressure dependence of microbubble-mediated gene delivery targeted using focused ultrasound.* J Gene Med, 2006. **8**(11): p. 1347-57.
55. Rahim, A., et al., *Physical parameters affecting ultrasound/microbubble-mediated gene delivery efficiency in vitro.* Ultrasound Med Biol, 2006. **32**(8): p. 1269-79.
56. Taylor, S.L., et al, *Targeted retroviral gene delivery using ultrasound.* J Gene Med, 2007. **9**(2): p. 77-87.
57. Shintani, M., et al., *Effect of ultrasound on herpes simplex virus infection in cell culture.* Virol J, 2011. **8**: p. 446.
58. Bazan-Peregrino, M., et al., *Ultrasound-induced cavitation enhances the delivery and therapeutic efficacy of an oncolytic virus in an in vitro model.* J Control Release, 2012. **157**(2): p. 235-42.
59. Kemeny, N., et al., *Phase I, open-label, dose-escalating study of a genetically engineered herpes simplex virus, NV1020, in subjects with metastatic colorectal carcinoma to the liver.* Hum Gene Ther, 2006. **17**(12): p. 1214-24.

60. Mace, A.T., et al., *Potential for efficacy of the oncolytic Herpes simplex virus 1716 in patients with oral squamous cell carcinoma.* Head Neck, 2008. **30**(8): p. 1045-51.
61. Mansfield, D., et al., *Oncolytic Vaccinia virus and radiotherapy in head and neck cancer.* Oral Oncol, 2013. **49**(2): p. 108-18.
62. Mineta, T., et al, *Attenuated multimutated herpes simplex virus-1 for the treatment of malignant gliomas.* Nat Med, 1995. **1**: p. 938 - 943.
63. Saggar, J.K., et al., *The tumor microenvironment and strategies to improve drug distribution.* Front Oncol, 2013. **3**: p. 154.
64. Tredan, O., et al., *Drug resistance and the solid tumor microenvironment.* J Natl Cancer Inst, 2007. **99**(19): p. 1441-54.
65. Shannon, A.M., et al., *Tumour hypoxia, chemotherapeutic resistance and hypoxia-related therapies.* Cancer Treat Rev, 2003. **29**(4): p. 297-307.
66. Wilson, W.R. and M.P. Hay, *Targeting hypoxia in cancer therapy.* Nat Rev Cancer, 2011. **11**(6): p. 393-410.
67. Agrawal, V.K., et al., *Microvascular free tissue transfer for gene delivery: in vivo evaluation of different routes of plasmid and adenoviral delivery.* Gene Ther, 2009. **16**(1): p. 78-92.
68. Eisenberg, D.P., et al, *Hyperthermia potentiates oncolytic herpes viral killing of pancreatic cancer through a heat shock protein pathway.* Surgery, 2010. **148**(2): p. 325-34.
69. Arvanitis, C.D., et al., *Cavitation-enhanced extravasation for drug delivery.* Ultrasound Med Biol, 2011. **37**(11): p. 1838-52.
70. Bazan-Peregrino, M., et al, *Cavitation-enhanced delivery of a replicating oncolytic adenovirus to tumors using focused ultrasound.* J Control Release, 2013. **169**(1-2): p. 40-47.
71. Carlisle, R., et al, *Enhanced Tumor Uptake and Penetration of Virotherapy Using Polymer Stealthing and Focused Ultrasound.* J Natl Cancer Inst, 2013. **105**(22): p. 1701-10.
72. Chen, H.H., et al, *Active adenoviral vascular penetration by targeted formation of heterocellular endothelial-epithelial syncytia.* Mol Ther, 2011. **19**(1): p. 67-75.
73. Graham, S.M., et al., *Inertial cavitation to non-invasively trigger and monitor intratumoral release of drug from intravenously delivered liposomes.* J Control Release, 2014. **178**: p. 101-7.
74. Civale, J., I. Rivens, and G. ter Haar, *Quality assurance for clinical high intensity focused ultrasound fields.* Int J Hyperthermia, 2015. **31**(2): p. 193-202.
75. Huber P., et al., *In vivo detection of ultrasonically induced cavitation by a fibre-optic technique.* Ultrasound Med Biol, 1994. **20**(8): p. 811-25.
76. Staudenraus, J. and W. Eisenmenger, *Fibre-optic probe hydrophone for ultrasonic and shock-wave measurements in water.* Ultrasonics, 1993. **31**(4): p. 267-273.
77. Koch, C. and K.V. Jenderka, *Measurement of sound field in cavitating media by an optical fibre-tip hydrophone.* Ultrason Sonochem, 2008. **15**(4): p. 502-9.
78. Connolly W. and F.F. E., *Ultrasonic Cavitation Thresholds in Water.* Acoust Soc Am, 1954. **26**.
79. Emmer, M., et al., *The onset of microbubble vibration.* Ultrasound Med Biol, 2007. **33**(6): p. 941-9.
80. Chen, W.-S., et al., *Inertial cavitation dose and hemolysis produced in vitro with or without Optison®.* Ultrasound in Medicine & Biology, 2003. **29**(5): p. 725-737.
81. Hallow, D.M., et al., *Measurement and correlation of acoustic cavitation with cellular bioeffects.* Ultrasound Med Biol, 2006. **32**(7): p. 1111-22.
82. Hwang, J.H., et al., *Correlation between inertial cavitation dose and endothelial cell damage in vivo.* Ultrasound Med Biol, 2006. **32**(10): p. 1611-9.
83. Chen, C., et al., *Effect of ethanol injection on cavitation and heating of tissues exposed to high-intensity focused ultrasound.* Phys Med Biol, 2012. **57**(4): p. 937-61.

84. Kyriakou, Z., et al., *HIFU-induced cavitation and heating in ex vivo porcine subcutaneous fat.* Ultrasound Med Biol, 2011. **37**(4): p. 568-79.
85. Maxwell, A.D., et al., *Probability of cavitation for single ultrasound pulses applied to tissues and tissue-mimicking materials.* Ultrasound Med Biol, 2013. **39**(3): p. 449-65.
86. Ferrara, K., R. Pollard, and M. Borden, *Ultrasound microbubble contrast agents: fundamentals and application to gene and drug delivery.* Annu Rev Biomed Eng, 2007. **9**: p. 415-47.
87. VanBavel, E., *Effects of shear stress on endothelial cells: possible relevance for ultrasound applications.* Prog Biophys Mol Biol, 2007. **93**(1-3): p. 374-83.
88. van Wamel, A., et al., *Micromanipulation of endothelial cells: ultrasound-microbubble-cell interaction.* Ultrasound Med Biol, 2004. **30**(9): p. 1255-8.
89. Meijering, B.D., et al., *Ultrasound and microbubble-targeted delivery of macromolecules is regulated by induction of endocytosis and pore formation.* Circ Res, 2009. **104**(5): p. 679-87.
90. Postema, M., et al., *High-speed photography during ultrasound illustrates potential therapeutic applications of microbubbles.* Medical Physics, 2005. **32**(12): p. 3707.
91. Zhou, Y., et al., *Controlled permeation of cell membrane by single bubble acoustic cavitation.* J Control Release, 2012. **157**(1): p. 103-11.